Statistical Analysis of Sum-of-Sinusoids Fading Channel Simulators

by

Marius Pop

A thesis submitted to the
Department of Electrical and Computer Engineering
in conformity with the requirements for the degree of
Master of Science (Engineering)

Queen's University

February 1999

Abstract

Multipath propagation leading to Rayleigh fading in wireless channels can be adequately modelled through the use of sum-of-sinusoids simulators. We present a quick overview of the work carried out thus far in this area, culminating with the development of Clarke's model [3]. A popular sum-of-sinusoids fading channel simulator is derived from this model by Jakes [23]. In general, in order to assess the performance of channel simulators one needs to determine the statistics of the fading channel. A common way of accomplishing this is sending a sine wave across the channel and then determining the statistics of the output signal; even this simplified problem may not always be tractable. In the case of sum-of-sinusoids simulators, however, we are able to derive the envelope and phase probability density functions of the fading signal produced by the simulator, given that a sine wave was sent. In addition, we determine the autocorrelation function.

Once the statistics of the sum-of-sinusoids simulators are developed, we apply them to Clarke's model and Jakes' fading channel simulator in order to determine whether the simplifications made by Jakes are justified. We find they are not. In particular, while the signal produced by Clarke's model is wide-sense stationary, the signal produced by Jakes' simulator is not. We attempt to improve the performance of Jakes' simulator and find that introduction of random phase shifts in the low-frequency oscillators does produce a wide-sense stationary signal. However, the phase shifts of the resulting fading signal are only uncorrelated; they are not independent, as in the signal generated by Clarke's model. Therefore, we do not solve the underlying problem with Jakes' simulator.

Also presented in this thesis are quality measures of the fading signal produced by sum-of-sinusoids simulators. These measures are based on the results developed for the envelope probability density functions, envelope distribution function, as well as the autocorrelation function. We present examples of how such quality measures may be derived and how they may aid in the proper choice of the number of low-frequency oscillators, or equivalently, sinusoids, which need to be incorporated in the simulators.

Acknowledgments

I would like to express my gratitude and appreciation to my supervisor, Dr. Norm Beaulieu, for making this work possible. As well, I would like to thank Dr. Jon Davis for help with some of the material in Chapter 3. Ed Chow's encouragement and help with various statistics topics is also much appreciated. I would also like to thank Dave Young for numerous hours of conversation on the topic of fading channel simulators, Chris Tan for expert help with computer problems, and Dave Paranchych for supplying the template upon which this thesis is based.

I would like to thank all the other members of the wireless laboratory, Phil Boll, Xiaodai Dong, Andrew Toms, and Phil Vigneron, as well as my classmates, Kareem Baddour, Kim Edwards, Mike Hubbard, Shafique Jamal, and Serge Mister for the countless hours of entertainment and support.

Last but not least, I would like to thank my best friend in the whole wide world, Leissa Smith, for her patience and support during the completion of this thesis.

Contents

List of Figures

List of Abbreviations and Symbols

Symbol	Definition
cdf	cumulative distribution function
i.i.d.	independent and identically distributed
jpdf	joint probability density function
pdf	probability density function
rv	random variable
$\langle \cdot \rangle$	time average operator
$E\{\cdot\}$	statistical expectation operator
$\mathscr{F}\{\cdot\}$	Fourier transform operator
$\Re\{\cdot\}$	real part operator
$Var\{\cdot\}$	variance operator
α_n	angle of arrival of nth arriving ray
β_n	gain of nth low-frequency oscillator
$\mu_R(t)$	mean function of stochastic process R(t)
$\Phi_n(\omega_1, \omega_2)$	characteristic function corresponding to the joint probability density function describing the nth random vector in the sum of N two-dimensional independent random vectors
ϕ_n	phase shift of nth arriving ray, in radians
ψ_n	random offset phase of the nth low-frequency oscillator
ω	radian frequency, in radians/s
ω_c	carrier frequency, in radians/s

ω_m	maximum Doppler frequency shift, in radians/s
ω_n	Doppler frequency shift of nth arriving ray, in radians/s
τ	time lag
Θ_n	random variable representing the direction from the positive x-axis of the nth random vector in the sum of N independent random vectors
c_n	path attenuation coefficient for nth arriving ray
E_0	amplitude of transmitted signal
f	frequency, in Hertz
$F_X(x)$	cumulative distribution function of the random variable X
$f_X(x)$	probability density function of the random variable X
$f_{R,\Theta}(r,\theta)$	joint probability density function of the sum of N independent two-dimensional random vectors, in polar coordinates
$f_{R_n,\Theta_n}(r_n,\theta_n)$	joint probability density function of the nth random vector in the sum of N independent two-dimensional random vectors, in polar coordinates
$f_{X,Y}(x,y)$	joint probability density function of the sum of N independent two-dimensional random vectors, in Cartesian coordinates
$f_{X_n,Y_n}(x_n,y_n)$	joint probability density function of the nth random vector in the sum of N independent two-dimensional random vectors, in Cartesian coordinates
$J_k(x)$	Bessel function of the first kind of order k
$M+1$	number of low-frequency oscillators in simplified fading simulator, or equivalently, the number of distinct Doppler frequency shifts
N	number of low-frequency oscillators in fading simulator, $N = 4M+2$ in Jakes' case

R_n	random variable representing the length of the nth random vector in the sum of N independent random vectors
$\mathscr{R}_{RR}(t_1, t_2)$	statistical autocorrelation of stochastic process $R(t)$
$\mathscr{R}_R(\tau)$	statistical autocorrelation of stationary stochastic process $R(t)$
$R(t)$	stochastic process representing the received signal
$\tilde{R}(t)$	reduced realization of the stochastic process $R(t)$
$S_R(\omega)$	power spectral density of stochastic process $R(t)$
$T(t)$	transmitted signal
t	time
$X_c(t)$	stochastic process representing the in-phase received signal
$\tilde{X}_c(t)$	reduced realization of the stochastic process $X_c(t)$
$X_s(t)$	stochastic process representing the quadrature received signal
$\tilde{X}_s(t)$	reduced realization of the stochastic process $X_s(t)$

Chapter 1

Introduction

Humans communicate. The need to transmit information reliably has been around for as long as humans have existed. Smoke signals, postal couriers, and telephones, are just a few of the ways humans have tried to satisfy the need to communicate. Each step, brought on by the human impetus to push the boundaries of knowledge further, was met with its unique set of challenges. Today, most would agree the next step in this evolution is wireless communication. Instant communication to and from anywhere on Earth is an impressive goal, and it too, presents a daunting set of challenges to be met before the goal is reached.

Unlike the examples mentioned above, where the effects of the medium through which messages are exchanged are relatively well known, the same can not be said about wireless communication. The message, in our case a sine wave, is sent through the wireless channel as electromagnetic radiation. The geography between the transmitter and receiver leads to the electromagnetic signal being scattered and reflected, such that upon reception, it appears as a superposition of waves. In addition, natural elements such as clouds, moisture in the air, and precipitation, further impair the reception by unequally attenuating waves arriving from different directions at the receiver. Furthermore, these component waves experience varying degrees of Doppler shift arising from the motion of the mobile receiver. To make matters worse, the characteristics of the channel vary from hour to hour, from day to day. Thus, the problem the wireless engineer must solve is that of reliably transmitting voice or data over a geographically diverse and time-varying channel.

In order to design reliable systems and to assess the performance of existing systems, the wireless engineer tests them. An obvious approach would be to test the system once it is built. However, there are some drawbacks to this method. First, it is not cost-effective. Building prototypes is usually expensive and they are not guaranteed to work upon first trial. Second, the time-varying nature of the channel would make it hard to distinguish the shortcomings of a certain design from the impediments of the channel.

Fortunately, one may derive a model for the wireless channel, then implement it in software, say. The engineer could then test the communication system under study without leaving the laboratory, or even having to manufacture a prototype. In addition, the effects of the channel on the system are easier to control because the time-varying nature of the channel may be removed. One inherent drawback to models, in general, is that they are only approximations to naturally occurring phenomena. As such, the results obtained by using these models are close to those measured directly, but not exactly the same. Of course, the results obtained with a particular model are valid only insofar as the model represents the natural phenomenon, in our case fading.

Models of fading wireless channels are readily derived from physical considerations of the fading phenomenon. It should be noted that many types of models exist. They vary in complexity, time domain implementation, i.e., discrete time vs. continuous time, and underlying design, i.e., deterministic vs. stochastic. The application at hand will dictate the complexity of the model, what time domain the model will be implemented in, and whether it will be deterministic or stochastic. For example, one may generate an approximation to the Rayleigh fading signal by using uniform phase modulation or quadrature amplitude modulation, i.e., amplitude modulate the in-phase and quadrature components of a carrier with a lowpass filtered Gaussian noise source [23], [24]. The main problem with the first model is that the power spectrum is hard to compute. The second model's main drawback is that only rational forms of the fading spectrum may be obtained, whereas the fading spectra encountered in practice are often non-rational. Other approaches include generation of

Rayleigh random variates via the Fourier transform [13], [22], [25]. The main difficulty with this lies in the fact that the entire fading waveform needs to be generated before the simulation is run. In this thesis, we look at sum-of-sinusoids models of the Rayleigh flat fading narrowband wireless channel. The sum-of-sinusoids model is simple and may be implemented in either discrete or continuous time. Another advantage is that the Rayleigh fading signal is generated in real-time, i.e., as it is needed, in contrast with Fourier transform methods. Most often, these models are described as deterministic, to emphasize that once the parameters of the model are chosen they do not change over the duration of the simulation.

A simulator based on one such model, which has received attention lately, is Jakes' fading channel simulator. The simulator is attractive for a number of reasons. Among these are its simplicity, making it easily implementable in either software or hardware. Also, the model parameters are closely related to those of the physical channel, and thus the effects of the channel parameters on the simulator are easily identifiable. This would lead us to expect that the results obtained with such simulators would closely approximate those observed in nature. However, as mentioned above, models approximate real phenomena. It would be useful to know how well the results obtained with sum-of-sinusoids simulators characterize the fading channel.

One objective of this thesis is to take an in-depth look at the statistical properties of sum-of-sinusoids models of the Rayleigh flat fading narrowband wireless channel, in general, and Jakes' fading channel simulator, in particular. Another objective is to derive some quantitative measures of the inaccuracies introduced by the limitations inherent in the sum-of-sinusoids models.

1.1 Outline of the thesis

The thesis is organized as follows. Chapter 2 presents an overview of the development of sum-of-sinusoids flat fading channel models born from a physical consideration of the fad-

ing phenomenon. In particular, we look at Clarke's work because it is from Clarke's model that Jakes derives his simulator. We show the steps Jakes follows to obtain the fading channel simulator from Clarke's model. This development culminates with the presentation of the simulator in both block diagram and equation form. Recently, there has been much attention devoted to determining the properties of sum-of-sinusoids simulators. In particular, the works of Pätzold et al. [7], Pätzold et al. [8], and Pätzold et al. [9] are of relevance; Pätzold's analysis, as it applies to the topic of this thesis, is also summarized in this chapter.

Chapter 3 determines the statistical properties of Clarke's model, the reference model, and those of Jakes' fading channel simulator, such as the envelope and phase probability density functions (pdf's), and the autocorrelation functions. The pdf's are computed using a well-known theorem from statistics relating to the computation of the pdf of the sum of independent random variables. It is found that the signal produced by Clarke's model is wide-sense stationary. In addition, it exhibits ergodicity of the mean and autocorrelation, i.e., the statistical mean is equal to the time average mean and the statistical autocorrelation is equal to the time average autocorrelation. The signal produced by Jakes' fading channel simulator is not wide-sense stationary, and therefore, it does not possess ergodicity of the mean and autocorrelation.

In Chapter 4, we look at two methods of improving the performance of Jakes' simulator. The improvement is measured in terms of whether the fading signal generated by the simulator has the same statistical properties as that produced by Clarke's model, i.e., if the signal is wide-sense stationary. The first improvement proposes the insertion of $\sin(\cdot)$ terms. It is found that this does not result in the generation of a wide-sense stationary signal. The second approach proposes the insertion of random phases in the low-frequency oscillators. This does result in the generation of a wide-sense stationary signal. However, the phase shifts of the components of the resulting fading signal are still dependent. This may pose problems when higher order statistics are computed.

It is noted that, in general, Clarke's model can not be simplified, as in the procedure

outlined by Jakes, i.e., by reducing the degrees of freedom corresponding to the phase shifts. In certain cases, where the angles of arrival exhibit symmetry, the number of Doppler frequency shifts[1] observed is reduced. Hence, the number of low-frequency oscillators is reduced as well, leading to a simplification of the structure of the simulator. In reducing the number of oscillators, however, we must include the phase shifts of all waves experiencing the same Doppler frequency shift as appropriate gains for the corresponding low-frequency oscillator.

Chapter 5 analyzes the errors introduced by the inherent limitations of Clarke's model. We illustrate how the formulae derived in Chapter 3 can be used to derive quality measures which may be used to assess the performance of simulators derived from Clarke's model. In particular, we look at how the maximum absolute error between the envelope pdf of the simulator signal and the desired envelope pdf varies with the number of low-frequency oscillators. The same is done for the envelope cumulative distribution function (cdf). Also, we seek an explanation to the deviation of the autocorrelation function from its desired value at large lags. We develop a formula for computing the point beyond which this deviation becomes large, i.e., relate the breakpoint to the number of distinct Doppler frequency shifts and the maximum error allowed in the autocorrelation function.

Finally, Chapter 6 presents some concluding remarks and suggestions for further study.

1.2 Contributions of the thesis

In analyzing the statistical properties of Clarke's model and Jakes' simulator, we have discovered previously known and unknown results that may be useful to the engineer modelling the Rayleigh flat fading narrowband wireless channel.

- In Chapter 3, we apply a well-known approach, that of computing the pdf of the sum of independent random variables via the characteristic function domain, to the

[1] Throughout this thesis, the use of the word "shift" includes both positive and negative Doppler frequencies, unless otherwise noted.

computation of the envelope pdf of the fading signal. Using this technique, and reasonable assumptions, we derive the exact envelope pdf, rather than an approximation. We also show the phase is uniformly distributed over $[0, 2\pi]$.

- In Chapter 3, we show that the fading signal produced by Jakes' simulator is not wide-sense stationary. Previously, it was assumed to be stationary and to exhibit ergodicity of the mean and autocorrelation.

- In Chapter 4, we show that introduction of random phases in the low-frequency oscillators of Jakes' simulator leads to the generation of a wide-sense stationary signal. This method has been previously used to improve the simulator's operation. However, the phase shifts of the resulting multipath fading signal are dependent; they are not independent as in Clarke's model.

- In Chapter 5, we show how the formulae of Chapter 3 can be used to derive quality measures, which in turn can be used to analyze the performances of sum-of-sinusoids simulators.

- In Chapter 5, we present a method for determining the time lag beyond which the autocorrelation function deviates significantly from the desired value. We relate the magnitude of this time point to the number of low-frequency oscillators used in the model or simulator.

1.3 Thesis notation

To aid the reader, the following notational conventions will be followed in this thesis. The conventions herein follow those of the literature. In cases where authors use different notation, that notation has been changed to meet these conventions, in order to ease comparisons between others' work and this thesis.

Random variables are denoted by capital letters. Values taken by random variables are

denoted by the corresponding lowercase letter. That is, $x_1, x_2, \ldots, x_n$ are the observed values of the random variables $X_1, X_2, \ldots, X_n$.

Stochastic processes are also denoted by capital letters, indexed by a time variable, such as $R(t)$. Corresponding sample functions are denoted by lowercase letters, such as $r(t)$. Thus, $r(t)$ is an sample function of the stochastic process $R(t)$.

The calligraphic $\mathscr{R}_R$ denotes statistical (ensemble) autocorrelation. The subscript indicates the stochastic process whose autocorrelation is under study, in our case $R(t)$. We use angle brackets $\langle \cdot \rangle$ to denote time averages, in particular the time-average autocorrelation.

Probability density functions are denoted by the lowercase f indexed by the appropriate random variable. Thus, $f_X(x)$ is the pdf of the random variable X. Furthermore, $f_R(r,t)$ is the pdf of the stochastic process $R(t)$, in particular the envelope pdf of $R(t)$. Note that, in general, this pdf may also be time-varying; this is emphasized through the inclusion of time t in the pdf. Similarly, cumulative distribution functions are denoted by the uppercase F.

Characteristic functions are denoted by the uppercase Greek Φ. Thus, the characteristic function of a scalar random variable is $\Phi(\omega)$, and the characteristic function of a two-dimensional random vector (X,Y) is $\Phi(\omega_1, \omega_2)$. Note that phase shifts are also denoted by the uppercase Greek Φ. However, the context should make it clear whether Φ refers to a characteristic function or a phase shift. In particular, when Φ is used to denote a characteristic function, it will always be followed by an argument in parentheses, as above.

More particular to the topic of sum-of-sinusoids models of fading channels, we will use N to denote the number of waves making up the received fading signal. We use M to denote the number of distinct Doppler frequency shifts in the modelled signal, i.e., the number of rays in the reduced realization of the modelled fading signal. It is always the case that $M \leq N$. We note that in cases where the angles of arrival are symmetric about the x-axis, as in Jakes' case, the number of distinct Doppler frequency shifts is given by $M+1$ if the maximum Doppler frequency shift ω_m is included, and M if it is not.

Finally, we use the tilde to denote reduced realizations. Thus $\tilde{R}(t)$ is a reduced realiza-

tion of the stochastic process $R(t)$. In other words, $\tilde{R}(t)$ may be a more efficient realization of $R(t)$, i.e., $\tilde{R}(t)$ contains fewer sinusoids than $R(t)$.

Chapter 2

Jakes' Simulator and Pätzold's Analysis

In this chapter, we will present a brief review of the work that led to the development of Jakes' simulator. While many have contributed to the theory upon which the simulator is based, Clarke [3], in particular, has collected most of the relevant information in one paper. We present the equations which he developed because it is with these equations that Jakes started. We present some of the development here, together with the structure which implements Jakes' simulator. Finally, we conclude the chapter with a presentation of Pätzold's work [8], [9] relating to sum-of-sinusoids simulators, and in particular, Jakes' simulator.

2.1 Previous work

The general problem in communications consists of sending a message through an imperfect channel. The channel may introduce noise, fade, or otherwise distort the original message, such that the output signal is not identical to the input signal. Most often, the effect of the channel can be quantified through the channel impulse response. In some cases, however, determination of the impulse response may not be tractable. This is especially true in the case of fading channels, where the impulse response is usually time-variant. A common approach for determining the effects of the channel on a message is channel sounding. This method consists of sending a known signal across the channel and observing statistically the output signal. To simplify the problem, it is almost always the case that

the sounding signal is a cosine wave. This is certainly true of the work summarized below.

Ossanna [1] was one of the first to attempt to model the fading phenomena observed in mobile wireless channels via sum-of-sinusoids models. The simplest model, Ossanna's work is based upon a mobile receiver moving through a standing wave pattern due to a single reflector. For simplicity, he assumed the transmitted signal is vertically polarized. The model allowed Ossanna to compute theoretical power spectra, which he then verified against recorded fading waveforms. Although the model could not account for a rise in the demodulated power spectra at low frequencies in urban areas, it worked well in suburban areas.

Gilbert [2] expanded on Ossanna's work. In Gilbert's model, there are N arriving waves uniformly spaced around the unit circle about the mobile. The amplitudes of the N arriving waves are chosen independently from a Rayleigh distribution, while the phases are chosen independently from a uniform distribution over $[0, 2\pi]$. Like Ossanna, Gilbert also assumed the transmitted wave is vertically polarized. Although he was mainly interested in antenna diversity reception systems, Gilbert developed expressions for the energy density distribution function, correlation coefficients, and the power spectrum of the energy density observed at the mobile.

Much like Gilbert, Clarke [3] also assumed that the received signal is made up of a superposition of waves. Clarke generalized Gilbert's work in that the angles of arrival of the N waves are independent and are allowed to follow some arbitrary pdf; simplified answers are obtained in the case where this pdf is uniform over $[0, 2\pi]$, i.e., the angles of arrival are uniform independent, identically distributed (i.i.d.) over $[0, 2\pi]$. The amplitudes of the N arriving waves are assumed to be constant and equal. Clarke also assumed the transmitted wave is vertically polarized. He writes expressions for the three fields, i.e., the electric field in the z-direction E_z, the magnetic field in the x-direction H_x, and the magnetic field in the y-direction H_y. From these equations, Clarke derives expressions for the autocorrelations of the three fields, as well as expressions for the cross-correlations of

the possible combinations. Clarke also determines a simple relation between the power spectral density of the signal at the receiver, and the product of the antenna's azimuthal power gain and the pdf of the angles of arrival of the N waves. This relation is further analyzed by Gans [4].

The general setup is depicted in Figure 2.1. The transmitter sends a continuous wave, i.e., a cosine. At the receiver we observe the interference pattern generated by the superposition of N arriving cosine waves. The equations for the three fields, as given by Clarke, are

$$E_z = E_0 \sum_{n=1}^{N} e^{j\Phi_n},, \tag{2.1a}$$

$$H_x = -\frac{E_0}{\eta} \sum_{n=1}^{N} \sin A_n e^{j\Phi_n}, \tag{2.1b}$$

and

$$H_y = \frac{E_0}{\eta} \sum_{n=1}^{N} \cos A_n e^{j\Phi_n}, \tag{2.1c}$$

where

- E_0 is the common real amplitude of the N arriving waves,
- η is the intrinsic impedance of free space,
- Φ_n is the random variable (rv) describing the phase shift of the nth arriving wave,
- A_n is the rv describing the angle the nth arriving wave makes with the positive x-axis, and
- j is the complex constant, $j^2 = -1$.

Note that the attenuation along all of the N paths is assumed to be the same. As well, the time variation in the above equations is suppressed and understood to be of the form $e^{j\omega_c t}$. Also note that the possible time dependence of the phase shifts Φ_n is not explicitly included, i.e., the Doppler effect is not explicitly written.

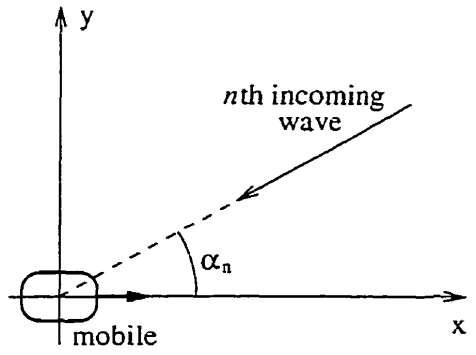

Figure 2.1. A typical component wave (after [3, p. 961]). Note that the mobile receiver is moving in the direction of the positive x-axis.

In the remainder of this thesis we will only concern ourselves with the electric field E_z. The justification for this lies in the fact that we are interested in evaluating the performance of Jakes' simulator. Jakes limits himself to simulating only the electric field of the received signal; hence, our choice to restrict our study to the electric field E_z. Furthermore, Jakes' development can be readily extended to model each of the two magnetic fields H_x and H_y.

It should be mentioned here, that when computing the first order statistics of the fading signal, such as the envelope and phase pdf's, none of the authors mentioned thus far provide a solution, save to mention that in the limiting case, i.e., as N becomes large, the envelope pdf is Rayleigh, while the phase pdf is uniform.

From equation (2.1a), Clarke then develops an expression for the autocorrelation function of the electric field E_z,

$$\mathscr{R}_{E_z}(x) = NE_0^2 \int_{-\pi}^{\pi} f_A(\alpha) e^{jkx\cos\alpha} d\alpha, \tag{2.2}$$

where

- $f_A(\alpha)$ is the pdf of the angle of arrival of the component waves,
- $k = \frac{2\pi}{\lambda_c}$ is the free-space phase constant, with λ_c representing the wavelength of the transmitted signal, and
- x is distance in the direction of the motion of the mobile, i.e., the distance along the x-axis.

If the N waves can arrive from any direction with equal probability, i.e., if $f_A(\alpha) = 1/2\pi$ for $-\pi \leq \alpha \leq \pi$, then equation (2.2) simplifies to

$$\mathscr{R}_{E_z}(x) = NE_0^2 J_0(kx), \tag{2.3}$$

where $J_0(\cdot)$ is the Bessel function of the first kind of order zero.

A more general class of sum-of-sinusoids channel models was introduced by Bello [11]. These fading channel models are characterized by the wide-sense stationary nature of the fading signal, at least in the short term. In addition, the channel may be modelled as a continuum of uncorrelated scatterers. Hence, a channel of this class is commonly referred to as the wide-sense stationary uncorrelated scattering (WSSUS) channel. In general, the WSSUS channel impulse response at time t, given that an impulse was applied at time $t - \tau$, may be written as

$$h(\tau; t) = \lim_{N \to \infty} \sum_{n=1}^{N} C_n e^{j(\Omega_n t + \Phi_n)} \cdot \delta(\tau - T_n), \tag{2.4}$$

where

- C_n is the rv describing the attenuation along the nth path,
- Ω_n is the rv describing the Doppler frequency shift along the nth path, due to the motion of the receiver,
- Φ_n is the rv describing the phase shift along the nth path, and
- T_n is the rv describing path delay along the nth path.

Note that the Doppler effect is made explicit by the inclusion of the Ω_n terms.

We pause here to note that the phase shifts Φ_n arise due to the reflection and refraction of the electromagnetic waves from obstructions. The path delays T_n arise because of the finite velocity with which the waves travel. Different path delays may arise due to the fact that different paths followed by different rays of the multipath fading signal have different lengths. Observe that at least in the case of Rayleigh flat fading channel Φ_n and T_n have

no influence upon each other; in fact, they arise from unrelated considerations. It might be that in the case of line-of-sight channels the phase shifts Φ_n might be related to the path delays T_n; however, we are not concerned with such channels here.

The next step of complexity and corresponding improvement in fading channel modelling via sum-of-sinusoids was taken by Aulin [6]. Whereas authors previous to him assumed the transmitted waves travelled only horizontally, Aulin allowed for non-horizontal travelling waves. He argued that in urban centers, where tall buildings dominate, horizontally travelling waves would not reach mobile users at street level. Therefore, it must be that the tops of buildings scatter these horizontal waves such that they travel at different angles of elevation. In other words, Aulin introduced a third dimension to the fading channel model.

2.2 Jakes' fading channel simulator

Jakes' fading channel simulator attempts to model the fading phenomenon present in radio mobile channels. A detailed description of the model is presented in [23]. Here we give a quick overview of this development.

To determine the effects of fading on a particular channel, suppose we transmit an unmodulated carrier

$$T(t) = E_0 \cos \omega_c t. \tag{2.5}$$

Then, at the receiver we will observe the interference pattern produced by N arriving waves. Following Clarke, but slightly more general than his equation [3, eq. (1)], i.e., equation (2.1a) here, the received signal can be written as,

$$R(t) = \Re\{E_0 \sum_{n=1}^{N} C_n e^{j(\omega_m t \cos A_n + \Phi_n)} e^{j\omega_c t}\}, \tag{2.6}$$

where,

- E_0 is the common real amplitude of the N arriving waves, i.e., the amplitude of the transmitted signal,

- C_n is the rv describing the attenuation along the nth path,
- $\omega_m = \frac{2\pi V}{\lambda_c}$ is the maximum Doppler frequency shift, with V representing the speed of the mobile, and λ_c representing the wavelength of the transmitted wave,
- A_n is the rv describing the direction the nth arriving wave makes with the positive x-axis,
- Φ_n is the rv describing the phase shift along the nth path, and
- ω_c is the radian frequency of the transmitted wave.

Note that since the C_n's are real, we may re-write the fading signal of equation (2.6) as

$$R(t) = E_0 \sum_{n=1}^{N} C_n \cos(\omega_c t + \omega_m t \cos A_n + \Phi_n). \tag{2.7}$$

Without loss of generality, we set $E_0 = \sqrt{2}$, i.e., normalize the power transmitted. This will hold true for the remainder of this thesis, unless otherwise indicated. Then, equation (2.5) simplifies to

$$T(t) = \sqrt{2}\cos\omega_c t,$$

and equation (2.7) simplifies to

$$R(t) = \sqrt{2}\sum_{n=1}^{N} C_n \cos(\omega_c t + \omega_m t \cos A_n + \Phi_n).$$

It should be obvious at this point why simulators which produce signals of the form of equation (2.1a), or equivalently equation (2.7), are called sum-of-sinusoids simulators. The distinguishing feature of this type of simulator is that it contains a low-frequency oscillator for each Doppler shift $\Omega_n = \omega_m \cos A_n$, i.e., is made up of N oscillators. We are interested in analyzing the performance of simulators which contain fewer than N oscillators. One such example is Jakes' simulator, to be introduced shortly. The model represented by equation (2.6) is slightly more general than that of Clarke, through the inclusion of the path attenuations C_n and Doppler shifts Ω_n. As well, the time variation is explicitly indicated,

unlike Clarke's model. Actually, equation (2.6) is closer to Bello's formula of equation (2.4); it is obtained from the latter by setting $T_n = 0$ for $n = 1, 2, \ldots, N$.

A general relation between the C_n's and the pdf of the angles of arrival is supplied by Jakes, [23, p. 68]

$$c_n^2 = f_{A_n}(\alpha_n) d\alpha_n \quad n = 1, 2, \ldots, N, \tag{2.8}$$

where $f_{A_n}(\alpha_n)$ is the pdf of the nth angle of arrival α_n. The c_n's may be interpreted as the power ratio received within the small arc $d\alpha_n$ about the angle of arrival α_n.

The first step taken by Jakes is to restrict the angles of arrival from being uniform i.i.d., i.e., $f_{A_1}(\alpha_1) = \ldots = f_{A_n}(\alpha_N) = 1/2\pi$, to being uniformly spaced, i.e., $d\alpha_n = \alpha_{n+1} - \alpha_n = 2\pi/N$, and fixed according to

$$\alpha_n = \frac{2\pi n}{N}, \quad n = 1, 2, \ldots, N. \tag{2.9}$$

This, in turn, leads to the attenuation along the N paths being equal, i.e., equation (2.8) becomes

$$c_n = 1/\sqrt{N} \tag{2.10}$$

This amounts to observing that since the pdf of the angles of arrival $f_{A_n}(\alpha_n)$ is uniform, the power received in each arc $d\alpha_n$ is the same, as long as the α_n are uniformly spaced.

Next, Jakes forces N to be of the form $4M + 2$, for some integer M. This restriction imposes a certain symmetry upon the directions of the arriving waves at the mobile; this symmetry lies at the heart of the reduction performed by Jakes. This scenario is illustrated in Figure 2.2 for $N = 10$. The choice of N, and hence A_n reduces the number of distinct Doppler shifts from N to $M + 1$. Therefore, instead of needing N oscillators to generate N Doppler shifts, we now need only $M + 1$ oscillators to generate the smaller number $M + 1$ of Doppler shifts. It should be noted that while some form of symmetry is required to reduce the number of terms in equation (2.6), the choice made by Jakes is not unique. For another choice, see [5].

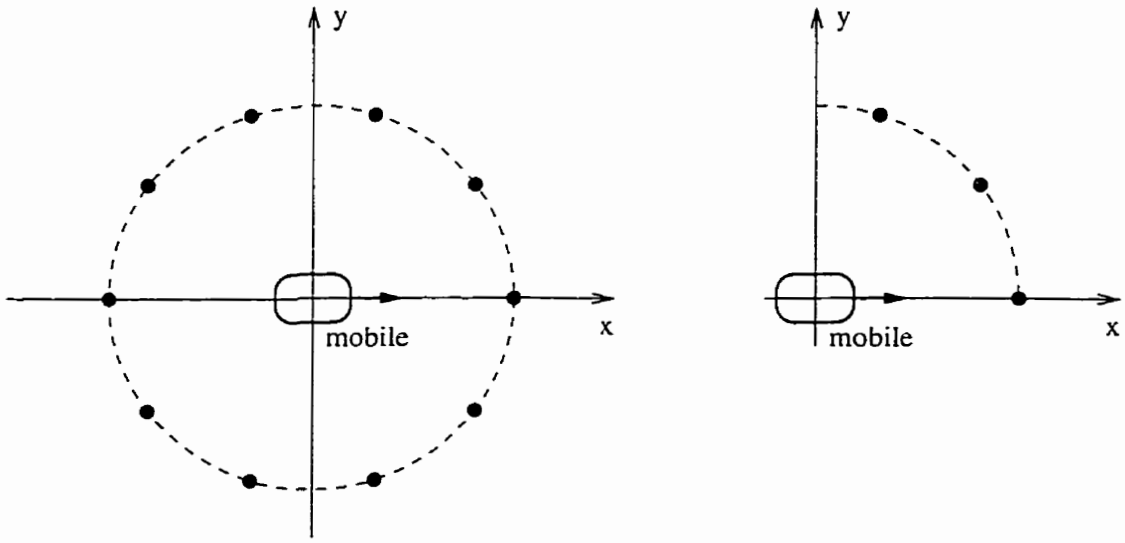

Clarke model
N = 10

Jakes' model
M = 2

Figure 2.2. Symmetry imposed by Jakes on the angles of arrival and the number of rays following the reduction.

For the mathematical details of the reduction from N to $M+1$ oscillators, the reader is referred to [23, pp. 68-69]. The form of the simulator is now apparent from Figure 2.2, i.e., the simulator contains $M+1$ low-frequency oscillators properly weighted and summed to produce the fading signal. We reproduce this in Figure 2.3.

From Figure 2.3, the fading signal can be readily written in terms of quadrature components as[1]

$$\tilde{R}(t) = \tilde{X}_c(t)\cos\omega_c t + \tilde{X}_s(t)\sin\omega_c t, \tag{2.11}$$

where $\tilde{X}_c(t)$ and $\tilde{X}_s(t)$ are given by[2]

$$\tilde{X}_c(t) = \frac{2}{\sqrt{N}}\left(\sqrt{2}\cos B_{M+1}\cos\omega_m t + 2\sum_{n=1}^{M}\cos B_n\cos\omega_n t\right), \tag{2.12a}$$

and

$$\tilde{X}_s(t) = \frac{2}{\sqrt{N}}\left(\sqrt{2}\sin B_{M+1}\cos\omega_m t + 2\sum_{n=1}^{M}\sin B_n\cos\omega_n t\right), \tag{2.12b}$$

[1]The tilde "~" is used to emphasize that the signal produced by Jakes' simulator $\tilde{R}(t)$ may, in general, differ from that produced by Clarke's model $R(t)$. In other words, Jakes' simulator is a reduced version of Clarke's model; we have not shown the two to be statistically identical yet.

[2]Jakes does not include the constant $\frac{2}{\sqrt{N}}$. They are included here to normalize the power in $\tilde{R}(t)$, similar to the normalization of the power in $R(t)$ earlier.

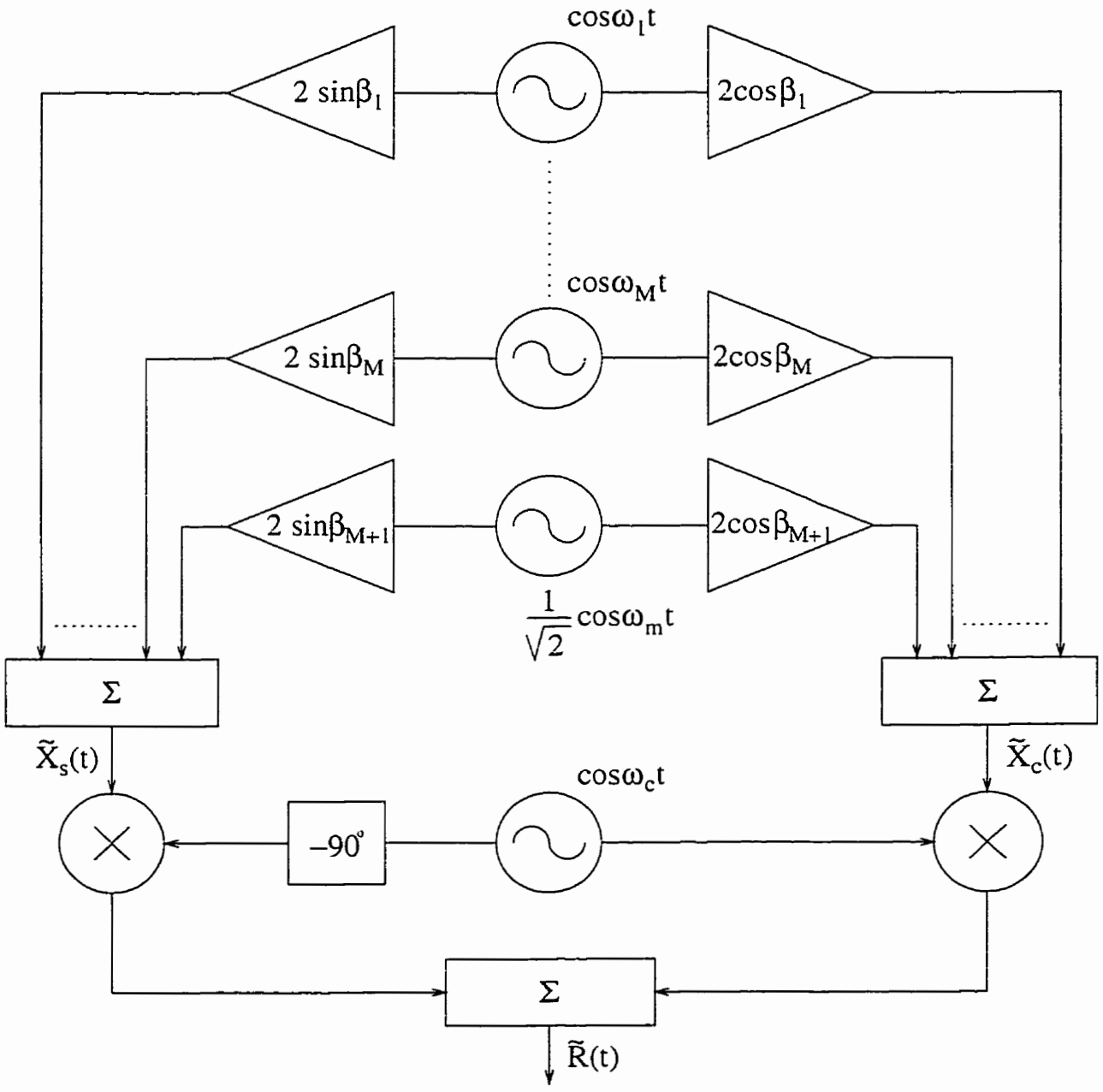

Figure 2.3. Jakes' fading channel simulator (after [23, p. 70]).

where ω_n is the radian Doppler frequency shift undergone by the nth arriving wave, and is given by

$$\omega_n = \omega_m \cos\alpha_n = \omega_m \cos\frac{2\pi n}{N}.$$

The terms $\cos B_n$ and $\sin B_n$ are termed oscillator gains; the term is also applied directly to B_n, however. The values for β_n, $n = 1,2,\ldots,M+1$ are chosen such that the phase of the signal $\tilde{R}(t)$ is uniformly distributed over $[0,2\pi]$. Jakes points out that there are several choices for $B_1,\ldots,B_{M+1}$. The values chosen by him are

$$B_{M+1} = 0, \qquad B_n = \frac{\pi n}{M+1} \quad n = 1,\ldots,M. \tag{2.13}$$

For other sets of values see [23, Figure 1.7-2] or [24, p. 78].

The structure of Figure 2.3 together with the choices made in equation (2.13) is commonly referred to as *Jakes' fading channel simulator* [5], [9], [10], [12], [24].

A final note on the value of N, or equivalently M. As mentioned before, for large enough values of N the envelope pdf is Rayleigh. Jakes [23] quotes the works of Slack [20] and Bennett [21] to justify that a value of $M \geq 6$ is sufficient [23, p. 69]. He points out that deviations from the Rayleigh distribution are confined mostly to the extreme peaks. Other considerations stemming from, for example, the autocorrelation function, result in other choices of N. Jakes indicates that a value of $N = 34$, or equivalently $M = 8$, is sufficient (see [23, p. 69]) to assure required accuracy in the autocorrelation function.

2.2.1 A note on the pdf of B_n

In this subsection, we determine the relationship between the oscillator gains $B_1,\ldots,B_{M+1}$ of Jakes' simulator and the phase shifts $\Phi_1,\ldots,\Phi_N$ of Clarke's model. We should mention here that Jakes [23] does not describe how $B_1,\ldots,B_{M+1}$ are obtained, or how the oscillator gains of his simulator are related to the phase shifts of Clarke's model.

Re-writing the signal generated by Jakes' simulator under the constraint that it have

unit power, we have

$$\begin{aligned}\tilde{R}(t) &= \cos\omega_c t\sqrt{\frac{2}{N}}\left(2\cos B_{M+1}\cos\omega_m t + 2\sqrt{2}\sum_{n=1}^{M}\cos B_n\cos\omega_n t\right)\\ &\quad + \sin\omega_c t\sqrt{\frac{2}{N}}\left(2\sin B_{M+1}\cos\omega_m t + 2\sqrt{2}\sum_{n=1}^{M}\sin B_n\cos\omega_n t\right)\\ &= \sqrt{\frac{2}{N}}\left[2\cos\omega_m t\cos(\omega_c t - B_{M+1}) + 2\sqrt{2}\sum_{n=1}^{M}\cos\omega_n t\cos(\omega_c t - B_n)\right], \quad (2.14)\end{aligned}$$

where we have used the well-known trigonometric identity

$$\cos x\cos y + \sin x\sin y = \cos(x-y).$$

Substituting another well-known trigonometric identity,

$$2\cos x\cos y = \cos(x-y) + \cos(x+y),$$

in equation (2.14) yields

$$\begin{aligned}\tilde{R}(t) &= \sqrt{\frac{2}{N}}\left[\cos(\omega_c t - \omega_m t - B_{M+1}) + \cos(\omega_c t + \omega_m t - B_{M+1})\right]\\ &\quad + \frac{2}{\sqrt{N}}\sum_{n=1}^{M}\left[\cos(\omega_c t - \omega_n t - B_n) + \cos(\omega_c t + \omega_n t - B_n)\right]. \quad (2.15)\end{aligned}$$

Recall that $\tilde{R}(t)$ is meant to be a more efficient realization of $R(t)$,

$$R(t) = \sqrt{\frac{2}{N}}\sum_{n=1}^{N}\cos(\omega_c t + \omega_n t + \Phi_n).$$

To determine the relation between the B_n's and the Φ_n's, we equate cosines of the same frequency. Recalling that $\omega_n = \omega_m\cos\frac{2\pi n}{N}$, we have for $n = 2M+1$

$$\cos(\omega_c t - \omega_m t + \Phi_{2M+1}) = \cos(\omega_c t - \omega_m t - B_{M+1}).$$

Clearly,

$$B_{M+1} = -\Phi_{2M+1}. \quad (2.16a)$$

Similarly, for $n = N = 4M+2$, we obtain

$$\cos(\omega_c t + \omega_m t + \Phi_{4M+2}) = \cos(\omega_c t + \omega_m t - B_{M+1}),$$

from which we infer

$$B_{M+1} = -\Phi_{4M+2}. \tag{2.16b}$$

Comparing equations (2.16a) and (2.16b), we must have

$$B_{M+1} = -\Phi_{2M+1} = -\Phi_{4M+2}. \tag{2.17}$$

From equation (2.17) it follows that Jakes forces $\Phi_{2M+1} = \Phi_{4M+2}$; these phase shifts are no longer independent, as assumed in Clarke's model.

We can obtain a similar result for $B_1, \ldots, B_M$. Equating components of equal frequency, we have

$$\cos(\omega_c t + \omega_n t + \Phi_n) + \cos(\omega_c t + \omega_n t + \Phi_{4M+2-n}) = \sqrt{2}\cos(\omega_c t + \omega_n t - B_n). \tag{2.18}$$

Equation (2.18) may be simplified by combining the two cosines on the left side, i.e.,

$$\sqrt{2+2\cos(\Phi_n - \Phi_{4M+2-n})}\cos\left(\omega_c t + \omega_n t + \frac{\Phi_n + \Phi_{4M+2-n}}{2}\right) = \sqrt{2}\cos(\omega_c t + \omega_n t - B_n). \tag{2.19}$$

Comparing the amplitudes of the cosines in equation (2.19), we have

$$\cos(\Phi_n - \Phi_{4M+2-n}) = 0. \tag{2.20}$$

Equation (2.20) gives an implicit relationship between Φ_n and Φ_{4M+2-n}, for $n = 1, \ldots, M$. We can make the relationship between the two phase shifts explicit by observing that they must satisfy one of the four equalities

$$\Phi_n = \Phi_{4M+2-n} - \frac{3\pi}{2}, \tag{2.21a}$$

$$\Phi_n = \Phi_{4M+2-n} - \frac{\pi}{2}, \tag{2.21b}$$

$$\Phi_n = \Phi_{4M+2-n} + \frac{\pi}{2}, \tag{2.21c}$$

$$\Phi_n = \Phi_{4M+2-n} + \frac{3\pi}{2}, \tag{2.21d}$$

for each $n = 1, \ldots, M$. Again, we note that the phase shifts are no longer independent as in Clarke's model.

Similarly, we may obtain that the phases Φ_{2M+1-n} and Φ_{2M+1+n} must satisfy one of the four equalities

$$\Phi_{2M+1-n} = \Phi_{2M+1+n} - \frac{3\pi}{2}, \tag{2.22a}$$

$$\Phi_{2M+1-n} = \Phi_{2M+1+n} - \frac{\pi}{2}, \tag{2.22b}$$

$$\Phi_{2M+1-n} = \Phi_{2M+1+n} + \frac{\pi}{2}, \tag{2.22c}$$

$$\Phi_{2M+1-n} = \Phi_{2M+1+n} + \frac{3\pi}{2}, \tag{2.22d}$$

Returning to equations (2.19), we now determine the relationship of $B_1,\ldots,B_{M+1}$ to $\Phi_1,\ldots,\Phi_{4M+2}$. Equating the phases of the two cosines, we have

$$B_n = -\frac{\Phi_n + \Phi_{4M+2-n}}{2}. \tag{2.23}$$

Substituting equations (2.21a) – (2.21d) in equation (2.23) we observe that $B_1,\ldots,B_M$ and $\Phi_1,\ldots,\Phi_M$ must satisfy one of the four equalities

$$B_n = -\Phi_n + \frac{3\pi}{4}, \tag{2.24a}$$

$$B_n = -\Phi_n + \frac{\pi}{4}, \tag{2.24b}$$

$$B_n = -\Phi_n - \frac{\pi}{4}, \tag{2.24c}$$

$$B_n = -\Phi_n - \frac{3\pi}{4}. \tag{2.24d}$$

Similarly, we may obtain

$$B_n = -\frac{\Phi_{2M+1-n} + \Phi_{2M+1+n}}{2} \tag{2.25}$$

and we observe that B_n and Φ_{2M+1-n} must satisfy one of the four equalities

$$B_n = -\Phi_{2M+1-n} + \frac{3\pi}{4}, \tag{2.26a}$$

$$B_n = -\Phi_{2M+1-n} + \frac{\pi}{4}, \tag{2.26b}$$

$$B_n = -\Phi_{2M+1-n} - \frac{\pi}{4}, \tag{2.26c}$$

$$B_n = -\Phi_{2M+1-n} - \frac{3\pi}{4}. \tag{2.26d}$$

From equations (2.23) and (2.25), we conclude that the four-tuple of phase shifts Φ_n, Φ_{2M+1-n}, Φ_{2M+1+n}, Φ_{4M+2-n} for $n = 1,\ldots,M$, are no longer independent as in Clarke's model.

Returning to equations (2.24a) – (2.24d), we note that $B_1,\ldots,B_M$ depend directly on $\Phi_1,\ldots,\Phi_M$. Also, because $\Phi_1,\ldots,\Phi_M$ are uniform i.i.d. over $[0,2\pi]$, we conclude that $B_1,\ldots,B_M$ are also independent and uniformly distributed over some interval of length 2π. However, since the B_n's appear only as arguments to either $\cos(\cdot)$ or $\sin(\cdot)$, we may take the B_n as uniform i.i.d. over $[0,2\pi]$ without loss of generality.

2.3 Pätzold's analysis

One author who has done extensive research on the topic of deterministic fading channel simulators is Pätzold (see, for example, [7] – [9]). The word *deterministic*, as used by Pätzold, is meant to emphasize that the simulator parameters, once chosen, remain unchanged for the duration of the simulation run. Thus, simulators of the form given in equation (2.6) fall in this category. In particular, Jakes' simulator is a deterministic model because once the C_n, A_n, and B_n are chosen they do not change for the duration of the simulation. We note that this is strictly a choice of nomenclature, and does not affect the analysis of the model.

Returning to Pätzold's work, we note that he has computed the statistics of the Jakes' fading channel simulator [9]. He obtained analytical expressions for the autocorrelation and cross-correlation functions of the in-phase $\tilde{X}_c(t)$ and quadrature $\tilde{X}_s(t)$ components, as well as the envelope and phase pdf's of the resulting fading signal $\tilde{R}(t)$.

To derive the results mentioned above, Pätzold notes that the signal produced by the simulator is deterministic, and thus its properties can be analyzed on the basis of time averages instead of statistical averages. However, substituting time averages for statistical averages is meaningful only in the case of (at least) wide-sense stationary and ergodic signals; Pätzold does not verify that the fading signal $\tilde{R}(t)$ possesses either property. It

should be pointed out that in [8] Pätzold justifies this approach by observing that for a single random-phased sine process the time average does indeed equal the statistical average. To connect this step to the final answer would require the same to be true of sums of such processes. This is easily shown to be false through the following counterexample.

Suppose we have the signal

$$R(t) = \cos(t+\Theta) + \cos(2t+\Theta),$$

where Θ is a random variable uniformly distributed over $[0, 2\pi]$. It is easily shown that for each of the signals $\cos(t+\Theta)$ and $\cos(2t+\Theta)$ the time average equals the statistical average. For example, one may note that both processes are wide-sense stationary and ergodic, and hence the two averages are equal. Conversely, one may directly compute the two averages.

Now, we compute the statistical autocorrelation of $R(t)$. It is

$$\begin{aligned}
&E\{R(t_1)R(t_2)\} \\
&\quad = E\left\{\left[\cos(t_1+\Theta)+\cos(2t_1+\Theta)\right] \times \left[\cos(t_2+\Theta)+\cos(2t_2+\Theta)\right]\right\} \\
&\quad = E\left\{\cos(t_1+\Theta)\cos(t_2+\Theta)\right\} + E\left\{\cos(t_1+\Theta)\cos(2t_2+\Theta)\right\} \\
&\qquad + E\left\{\cos(2t_1+\Theta)\cos(t_2+\Theta)\right\} + E\left\{\cos(2t_1+\Theta)\cos(2t_2+\Theta)\right\} \\
&\quad = \frac{1}{2}\left[\cos(t_2-t_1)+\cos 2(t_2-t_1)\right] + \frac{1}{2}\left[\cos(2t_2-t_1)+\cos(t_2-2t_1)\right]. \qquad (2.27)
\end{aligned}$$

Clearly, the statistical average function is not a function of only the time difference $t_2 - t_1$, as is obvious from looking at the second term of the sum in equation (2.27).

Next, we compute the time-average autocorrelation of $R(t)$. For a particular value of Θ, it is

$$\begin{aligned}
&\langle R(t)R(t+\tau)\rangle \\
&\quad = \lim_{T\to\infty}\frac{1}{2T}\int_{-T}^{T}\left[\cos(t+\Theta)+\cos(2t+\Theta)\right] \times \left[\cos(t+\tau+\Theta)+\cos(2t+2\tau+\Theta)\right]dt \\
&\quad = \lim_{T\to\infty}\frac{1}{2T}\int_{-T}^{T}\left[\cos(t+\Theta)\cos(t+\tau+\Theta)+\cos(t+\Theta)\cos(2t+2\tau+\Theta)\right.
\end{aligned}$$

$$+\cos(2t+\Theta)\cos(t+\tau+\Theta)+\cos(2t+\Theta)\cos(2t+2\tau+\Theta)]\,dt$$

$$= \frac{1}{2}(\cos\tau+\cos 2\tau). \tag{2.28}$$

Comparing equations (2.27) and (2.28), it is clear that the statistical average autocorrelation does not equal the time average autocorrelation. Hence, we conclude that, in general, sums of wide-sense stationary processes may not be wide-sense stationary, thus removing the possibility that the sum may exhibit any ergodicity properties.

It is also interesting to note that, in general, the statistical autocorrelation is a function of two variables, t_1 and t_2 in our case, while the time average correlation is a function of only one variable, usually the time difference $\tau = t_2 - t_1$. In the case of wide-sense stationary processes the statistical autocorrelation depends only on the time difference $\tau = t_2 - t_1$. It is no surprise, then, that one prerequisite for equating time averages with statistical ones requires the stochastic process to be at least wide-sense stationary.

Furthermore, the computation of the envelope and phase pdf's rests on the assumption that the in-phase and quadrature components are independent, and thus uncorrelated. In [8], Pätzold notes $\tilde{X}_c(t)$ and $\tilde{X}_s(t)$ are uncorrelated if the sets of frequencies used to generate the quadrature components are disjoint. With the assumption that the two sets of frequencies are disjoint, i.e., that $\tilde{X}_c(t)$ and $\tilde{X}_s(t)$ are independent, Pätzold develops expressions for the envelope and phase pdf's. He then applies these results to Jakes' simulator in [9]. However, the assumption required to validate the answer, namely that the two sets of frequencies are disjoint, is violated. This is readily obvious from [9, eq. (11)]. One has to conclude the results obtained in [9] are unsupported in this sense.

For the sake of completeness, we include below the results derived by Pätzold in [9]. The notation is changed from the original, so that it matches that of this thesis. Also, we set $2\sigma_0^2 = 1$, i.e., we normalize the average signal power, much like before when we set $E_0 = \sqrt{2}$. Another difference from the work presented until now lies in the fact that Pätzold uses lowpass equivalent forms, whereas Jakes uses bandpass forms. The results presented

below also use the lowpass equivalent forms. It should be noted that this is of relevance only in the case of the autocorrelation and cross-correlation functions. The interested reader is directed to [9] for details.

The envelope and phase pdf's of the fading signal $\tilde{R}(t)$ are given by

$$f_{\tilde{R}}(r) = r\int_{-\pi}^{\pi} f_{\tilde{X}_s}(r\cos\theta) f_{\tilde{X}_c}(r\sin\theta)d\theta, \quad r \geq 0,$$
$$f_{\tilde{\Theta}}(\theta) = \int_0^{\infty} r f_{\tilde{X}_s}(r\cos\theta) f_{\tilde{X}_c}(r\sin\theta)dr, \quad |\theta| \leq \pi,$$

where,

$$f_{\tilde{X}_s}(x) = 2\int_0^{\infty}\left[J_0\left(\frac{2\pi\nu}{\sqrt{2M+1}}\right)\prod_{n=1}^{M} J_0\left(\frac{4\pi\nu}{\sqrt{2M+1}}\sin\frac{\pi n}{M}\right)\right]\cos(2\pi\nu x)d\nu,$$
$$f_{\tilde{X}_c}(x) = 2\int_0^{\infty}\left[J_0\left(\frac{2\pi\nu}{\sqrt{2M+1}}\right)\prod_{n=1}^{M} J_0\left(\frac{4\pi\nu}{\sqrt{2M+1}}\cos\frac{\pi n}{M}\right)\right]\cos(2\pi\nu x)d\nu.$$

Note that in order to obtain the envelope and phase pdf's one has to compute at least double integrals.

As mentioned above, the time-average autocorrelations and cross-correlation functions are given in lowpass equivalent form. To obtain the corresponding bandpass forms, such as those used by Jakes, multiply the equations below by $\cos(\omega_c t)$. In the limit, as N becomes large, the time-average lowpass equivalent in-phase and quadrature autocorrelation functions are, respectively,

$$\langle \tilde{X}_s(t)\tilde{X}_s(t+\tau)\rangle^{LP} = \frac{1}{2}[J_0(\omega_m\tau) - J_4(\omega_m\tau)], \tag{2.29a}$$

and

$$\langle \tilde{X}_c(t)\tilde{X}_c(t+\tau)\rangle^{LP} = \frac{1}{2}[J_0(\omega_m\tau) + J_4(\omega_m\tau)], \tag{2.29b}$$

where the superscript LP is used to emphasize we are using lowpass equivalent forms. Pätzold notes that neither of these time-average autocorrelations matches the desired, statistical one, i.e.,

$$\mathscr{R}_{X_s}^{LP}(\tau) = \mathscr{R}_{X_c}^{LP}(\tau) = \frac{1}{2}J_0(\omega_m\tau).$$

However, the time-average autocorrelation function of the complex Gaussian fading signal, given by the sum of the time-average autocorrelations of the in-phase and quadrature components, matches the expected one, i.e.,

$$\langle \tilde{R}(t)\tilde{R}(t+\tau)\rangle^{LP} = \langle \tilde{X}_s(t)\tilde{X}_s(t+\tau)\rangle^{LP} + \langle \tilde{X}_c(t)\tilde{X}_c(t+\tau)\rangle^{LP} = J_0(\omega_m \tau).$$

The time-average autocorrelations given in equations (2.29a) and (2.29b) hold true only in the limit, as $N \to \infty$. For finite N, the reader is directed to [9]. However, it is worthwhile mentioning that in this case the time-average autocorrelation of the fading signal $\langle \tilde{R}(t)\tilde{R}(t+\tau)\rangle$ matches the expected autocorrelation closely over the interval $[0, (M+1)/(2f_m)]$ only.

In [9], the expression for the time-average cross-correlation of the in-phase and quadrature components is left in integral form,

$$\langle \tilde{X}_s(t)\tilde{X}_c(t+\tau)\rangle^{LP} = \frac{1}{\pi}\int_0^{\pi/2} \sin(4z)\cos(\omega_m \tau \cos z)dz.$$

Note that in general the time-average cross-correlation is non-zero.

Pätzold concludes that Jakes' approach is useful in the design of fading channel simulators. In fact, he uses this approach to derive a number of similar simulators. The structure is essentially the same for all of the models derived. The differences lay in the method chosen to compute the simulator parameters, such as the path attenuation coefficients C_n, the radian Doppler frequency shifts $\Omega_n = \omega_m \cos A_n$, and the phase shifts Φ_n. For these other types of simulators, the reader is referred to [7] and [8]. However, the conclusions drawn herein will apply equally to all simulators derived by Pätzold, with perhaps minor modifications.

2.4 Problems with the simulator

Despite the simplicity and widespread use of Jakes' simulator, there are some drawbacks to its employ. We point out below some of the problems inherent in the simulator.

A potentially serious problem lies in the assumption that the fading signal produced by Jakes' simulator is wide-sense stationary. Gilbert [2] noted that choosing the N phases

independently from a uniform distribution over $[0, 2\pi]$ for the N arriving waves, leads to models generating wide-sense stationary signals. Certainly, in equation (2.6) this condition is met. However, this condition is not readily verified by analyzing Figure 2.3.

Another drawback to Jakes' simulator is that there is no obvious relationship between the gains $B_1, \ldots, B_M$, and the parameters of the model of equation (2.6), in particular the phase shifts Φ_n, $n = 1, \ldots, N$. One of the advantages of the model of equation (2.6) is that it relates in a straightforward manner to the physical world. This obvious relationship is lost in the derivation leading to Jakes' simulator. Note that we have already addressed this problem in Section 2.2.1.

An inherent drawback to fading channel models is that signals generated based on them are only approximations to the fading phenomena observed over mobile radio channels. The obvious analogy is that just as representing an analog signal by a digital one introduces quantization errors, so simulation in our case introduces errors. These errors arise from the resolution of the continuum of paths present between transmitter and receiver into N waves. There has been some work done in trying to estimate the errors introduced by this quantization process, most notably that of Pätzold et al. [7], Pätzold et al. [8], and Pätzold et al. [9]. Conversely, one might be interested in how many low-frequency oscillators one needs in an implementation, software or hardware, to reduce the error to an acceptable level. Many authors have provided unsubstantiated answers to this question; for example, Jakes [23] suggests that more than 6 oscillators are sufficient, while Pätzold [9] suggests that 10 are enough. However, when modelling channels some authors resort to using a much higher number; for example Hoeher [12] uses 500. We need some means of relating the error introduced during the quantization process to the number of oscillators used in the simulator.

Finally, two important properties which may be used to advantage by the wireless engineer are stationarity and ergodicity. While there is little known about whether flat fading channels are indeed ergodic, some models do exhibit this property. A useful property

of ergodic and stationary channels is that time averages and statistical averages are interchangeable. This is useful when the wireless engineer wants to estimate certain statistical averages and has a limited number of sample functions to work with. It still remains to verify that the given stochastic process is both stationary and ergodic. Usually this is a difficult task; an unfortunate solution to the problem is to carry out calculations under the assumption that the signal under study is both ergodic and stationary. For example, Jakes [23] implicitly assumes the fading signal is both ergodic and stationary when he computes the time-average autocorrelation. Pätzold [9] states that (pseudo)random processes can be studied via time averages. However, without verifying that the fading signal is both ergodic and stationary, there is no guarantee that substitution of time averages for statistical ones is warranted, or even meaningful.

A commonly cited problem [5], [9] of Jakes' simulator is that the in-phase and quadrature components of the simulator are correlated. Pätzold [9], for example, shows that the time-average cross-correlation of the in-phase and quadrature components is generally non-zero[3]. The problem with this approach is that use of time-averages, instead of statistical ones, assumes ergodicity of the autocorrelation, i.e., that the two averages are equal. We will see in Subsection 3.2.3 that the signal produced by Jakes' simulator is not wide-sense stationary, and therefore does not possess the required ergodicity property. Hence, we can not justify using the time-average cross-correlation as an estimate to the statistical average.

While the basic idea of simulating the fading signal as a sum of randomly phased cosines of different frequencies is correct, the simplifications made by Jakes may lead to a statistically incorrect model. Such simplifications may have been warranted in the past because of limited computer power and suboptimal receiver and system designs, but such restrictions do not exist today. However, it would be of great benefit if there were an efficient method of generating flat fading signals, and thus Jakes' approach may still be useful.

[3]It is well known that when two independent, zero-mean Gaussian rv's are added in quadrature, the resulting amplitude rv is Rayleigh distributed, with the obvious extension to stochastic processes. To start, then, we need two uncorrelated Gaussian stochastic processes.

To this end, this thesis tries to answer the question of whether the number of oscillators can be reduced from N, while still generating a statistically correct fading signal.

Chapter 3

Statistical Properties of Sum-of-Sinusoids Simulators

In this chapter, we analyze the statistical properties of sum-of-sinusoids simulators, of which Jakes' simulator is a special case. We start with the development of some theory relating to the computation of the pdf of the sum of independent random vectors. We then use the results to compute the pdf's of the envelope of the signal generated by Clarke's model and of the envelope of the signal generated by Jakes' simulator. As well, we obtain the phase pdf's in the two cases mentioned above. We continue by computing the auto-correlation function of each of the two signals. It will be shown that while the signal of equation (2.6) is at least wide-sense stationary, the signal produced by Jakes' simulator is not. We conclude the chapter with a discussion of the ergodic properties of the signals generated by Clarke's model and Jakes' simulator.

3.1 First-order statistics

In this section, we develop some theory to be used in the calculation of the envelope and phase pdf's of the signals produced by sum-of-sinusoids simulators. The approach most often followed when computing these pdf's is to observe that the fading signal can be written in terms of quadrature terms, as in equation (2.11). Each of the in-phase and quadrature terms is shown to be approximately a zero-mean Gaussian random process; hence the en-

velope resulting after combining the two independent random processes in quadrature will be approximately Rayleigh distributed. There is a considerable body of literature relating to the computation of the pdf resulting from adding randomly-phased sine waves. See, for example, the works of Slack [20] and Bennett [21]. As well, Rice has contributed through his classical papers [14] and [15], as well as [16] and [18]. More recently, see the works of Pätzold [8] and Helstrom [19].

There are very few results pertaining to the direct computation of the envelope and phase pdf's. One such result is presented by Goldman [17]. However, he does not present a proof of the result. Here we give a simple proof, hoping to gain additional insight into the problem. We attempt to solve the problem by noting we are adding independent two-dimensional random variables. We already know that the pdf of the sum of independent (scalar) random variables can be obtained by the convolution of the pdf's of the random variables. In the Fourier transform domain, this amounts to multiplying the characteristic functions of the random variables. The pdf of the sum is then obtained by taking the inverse Fourier transform of the product of characteristic functions. A similar approach is followed here.

We denote the nth random vector in the sum by (X_n, Y_n), for $n = 1, \ldots, N$. Here, we may interpret (X_n, Y_n) as a vector in the plane, with X_n the increment in position along the x-axis and Y_n the increment in position along the y-axis. In general, X_n and Y_n are correlated.

Alternatively, we could use polar coordinates (R_n, Θ_n) to represent the same random vector. In this case, R_n can be interpreted as a length, while Θ_n as a direction measured from the positive x-axis.

In what follows, we assume R_n is independent of Θ_n; this is saying precisely that the length of the random vector bears no relation to its direction. When applying the results obtained herein, we must make sure that the above assumption is justified; this justification may be provided by the nature of the problem. Moreover, the pdf's of R_n and Θ_n are easily obtainable from the description of the problem. In particular, when all directions are

equally likely, the angle pdf is

$$f_{\Theta_n}(\theta_n) = \frac{1}{2\pi} \quad 0 \le \theta_n \le 2\pi. \tag{3.1}$$

The independence of R_n and Θ_n will make it much easier to work in polar coordinates. Observe that the N random vectors $(X_1, Y_1), \ldots, (X_N, Y_N)$ or $(R_1, \Theta_1), \ldots, (R_N, \Theta_N)$ are independent of each other; the representation, Cartesian or polar, is irrelevant.

Geometrically, we are interested in determining the joint probability density function (jpdf) of the resultant vector sum, i.e., the jpdf of the length and direction from the positive x-axis. Ultimately, however, we want to determine the pdf of the magnitude of the sum R of the N random vectors, and the pdf of the angle Θ the final point makes with the positive x-axis. i.e., the pdf's of the random variables[1]

$$R = \sqrt{X^2 + Y^2} \quad \text{and} \quad \Theta = \arctan(X, Y), \tag{3.2}$$

where X and Y are defined by

$$X = \sum_{n=1}^{N} X_n = \sum_{n=1}^{N} R_n \cos\Theta_n, \tag{3.3a}$$

and

$$Y = \sum_{n=1}^{N} Y_n = \sum_{n=1}^{N} R_n \sin\Theta_n. \tag{3.3b}$$

We assumed above that R_n and Θ_n are independent. It is not obvious from this assumption that R and Θ are also independent; we will see that they are indeed independent below.

Figure 3.1 and Figure 3.2 illustrate the summation process with one, and two random vectors, respectively. For the purposes of illustration, we have restricted $R_n = 1$. The circles represent the sets of reachable points after one and two steps, respectively, i.e., one can not reach the shaded area.

The technique we will be using to arrive at the desired answer is outlined next. As mentioned above, the vectors being added are independent. Therefore the characteristic

[1] The arctan(x, y) function returns the proper angle, i.e., includes quadrantal information.

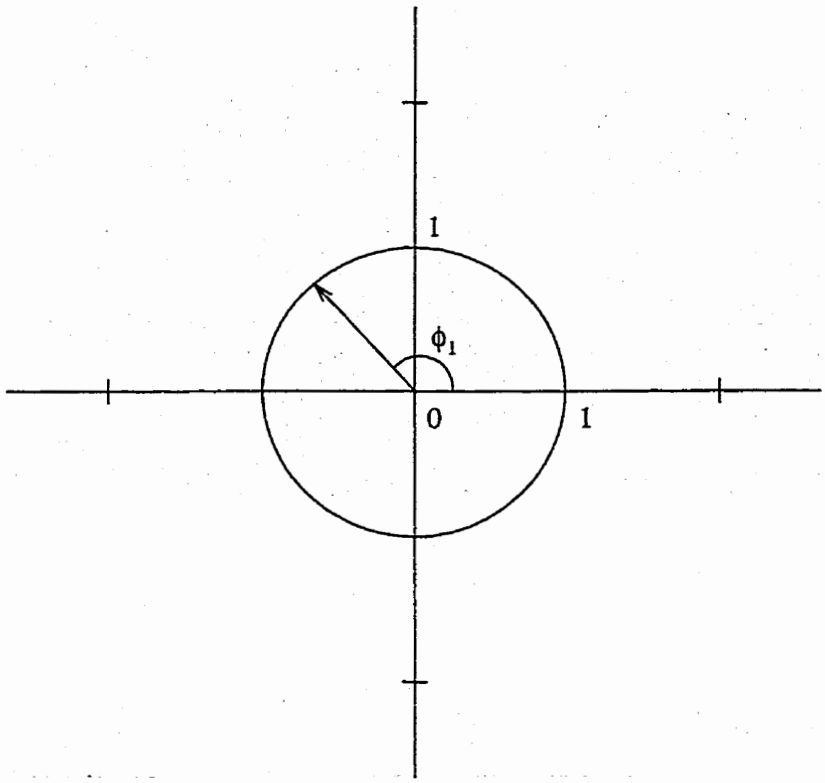

Figure 3.1. First step in summing two-dimensional independent random vectors of unit length. Note that only points on the unit circle can be reached.

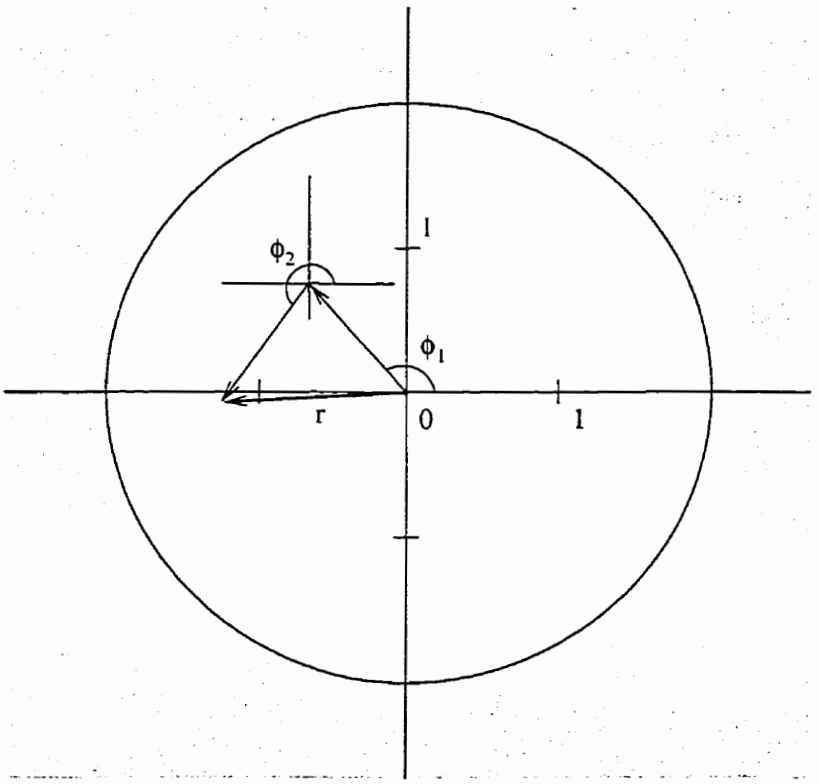

Figure 3.2. First two steps in summing two-dimensional independent random vectors of unit length.

function of the sum is the product of characteristic functions of the random vectors being added. This result follows readily from the definition of the characteristic function [29, eq. (7-25)] and the independence of the N random vectors. With the notation of equations (3.3a) and (3.3b) we have

$$\begin{aligned}\Phi(\omega_1,\omega_2) &= E\{e^{j(\omega_1 X+\omega_2 Y)}\} \\ &= E\{e^{j(\omega_1 X_1+\omega_2 Y_1)}\times\ldots\times e^{j(\omega_1 X_N+\omega_2 Y_N)}\}. \end{aligned} \tag{3.4}$$

Because the random vectors $(X_1,Y_1),\ldots,(X_N,Y_N)$ are independent, we can break up the expectation operator of equation (3.4) and

$$\begin{aligned}\Phi(\omega_1,\omega_2) &= E\{e^{j(\omega_1 X_1+\omega_2 Y_1}\}\times\ldots\times E\{e^{j(\omega_1 X_N+\omega_2 Y_N}\} \\ &= \Phi_1(\omega_1,\omega_2)\times\ldots\times\Phi_N(\omega_1,\omega_2) \\ &= \prod_{n=1}^{N}\Phi_n(\omega_1,\omega_2), \end{aligned} \tag{3.5}$$

as claimed.

From [29, Sec. 7-2] we note that either the jpdf or the joint characteristic function is sufficient to describe a random vector. In fact, the two are Fourier transform pairs. Thus, we seek to determine the characteristic function of (X,Y) and then, via the inverse Fourier transform, we obtain the jpdf of (X,Y). Next, we will perform a transformation to polar coordinates to obtain the jpdf of (R,Θ). From this, the envelope and phase pdf's $f_R(r)$, and $f_\Theta(\theta)$ respectively, are obtained by integrating over the other random variable.

We begin by determining the characteristic function of a typical random vector (X_n,Y_n). The definition of the characteristic function for a two-dimensional random vector is [29, eq. (7-23)],

$$\Phi_n(\omega_1,\omega_2)=\int_{-\infty}^{\infty}\int_{-\infty}^{\infty}f_{X_nY_n}(x_n,y_n)e^{j(\omega_1 x_n+\omega_2 y_n)}dx_n dy_n. \tag{3.6}$$

The subscript n is used to emphasize that this is the characteristic function of one random vector, the nth one in the sum. As observed above, when expressed in polar coordinates, the random variables involved, R_n and Θ_n, are independent. Thus, we perform the double

integration in (3.6) by converting to polar coordinates. To perform the change of variables we use [29, eq. (6-72)]

$$f_{R\Theta}(r,\theta) = r f_{XY}(r\cos\theta, r\sin\theta), \quad r > 0. \tag{3.7}$$

Performing the change to polar coordinates in equation (3.6) yields

$$\begin{aligned}\Phi_n(\omega_1,\omega_2) &= \int_0^{\infty}\int_0^{2\pi} f_{X_nY_n}(r_n\cos\theta_n, r_n\sin\theta_n) e^{jr_n(\omega_1\cos\theta_n+\omega_2\sin\theta_n)} d\theta_n r_n dr_n \\ &= \int_0^{\infty}\int_0^{2\pi} f_{R_n\Theta_n}(r_n,\theta_n) e^{jr_n(\omega_1\cos\theta_n+\omega_2\sin\theta_n)} d\theta_n dr_n. \end{aligned} \tag{3.8}$$

Next, we use the independence of R_n and Θ_n to separate the jpdf $f_{R_n\Theta_n}(r_n,\theta_n)$, and obtain

$$\begin{aligned}\Phi_n(\omega_1,\omega_2) &= \int_0^{\infty}\int_0^{2\pi} f_{R_n}(r_n) f_{\Theta_n}(\theta_n) e^{jr_n(\omega_1\cos\theta_n+\omega_2\sin\theta_n)} d\theta_n dr_n \\ &= \int_0^{\infty} f_{R_n}(r_n)\left[\int_0^{2\pi}\frac{1}{2\pi}\exp\left\{jr_n\sqrt{\omega_1^2+\omega_2^2}\cos(\theta_n-\psi_n)\right\}d\theta_n\right] dr_n, \end{aligned} \tag{3.9}$$

where $\psi_n = \arctan(\omega_1,\omega_2)$. To evaluate the integral inside the square brackets, we use [36, eq. 8.411.7] to obtain the equality

$$J_0(x) = \frac{1}{2\pi}\int_0^{2\pi} e^{jx\cos\beta} d\beta. \tag{3.10}$$

Performing the substitution $\beta = \theta_n - \psi_n$ in equation (3.9) and using equation (3.10), we obtain

$$\Phi_n(\omega_1,\omega_2) = \int_0^{\infty} f_{R_n}(r_n) J_0(r_n\sqrt{\omega_1^2+\omega_2^2}) dr_n. \tag{3.11}$$

Observe that the characteristic function of equation (3.11) is circularly symmetric, i.e., it depends only on the length of the vector (ω_1,ω_2). Integrals of the form of equation (3.11), i.e., in which we integrate against the Bessel function $J_0(\cdot)$, are referred to in the literature as *Hankel transforms*. The Hankel transform is useful in other areas of study, such as optics, in which circular symmetry is inherent. For more on two-dimensional Fourier transforms and the Hankel transform see [35][2].

[2]This would be useful in the event one wanted to perform the integration of equation (3.11); [35] contains a table of Hankel transforms.

We are now in a position to compute the characteristic function of the sum of independent random vectors

$$\begin{bmatrix} X \\ Y \end{bmatrix} = \begin{bmatrix} X_1 \\ Y_1 \end{bmatrix} + \begin{bmatrix} X_2 \\ Y_2 \end{bmatrix} + \cdots + \begin{bmatrix} X_N \\ Y_N \end{bmatrix}. \tag{3.12}$$

Substituting equation (3.11) in equation (3.5) yields

$$\begin{aligned} \Phi(\omega_1, \omega_2) &= \prod_{n=1}^{N} \Phi_n(\omega_1, \omega_2) \\ &= \prod_{n=1}^{N} \left[\int_0^\infty f_{R_n}(r_n) J_0(r_n \sqrt{\omega_1^2 + \omega_2^2}) dr_n \right]. \end{aligned} \tag{3.13}$$

To obtain the jpdf of (X, Y) we take the inverse Fourier transform of $\Phi(\omega_1, \omega_2)$ according to [29, eq. (7-24)]

$$f_{XY}(x,y) = \frac{1}{4\pi^2} \int_{-\infty}^{\infty} \int_{-\infty}^{\infty} \Phi(\omega_1, \omega_2) e^{-j(\omega_1 x + \omega_2 y)} d\omega_1 d\omega_2. \tag{3.14}$$

We choose to perform the double integration of equation (3.14) by changing to polar coordinates

$$\omega_1 = q\cos\theta, \quad \omega_2 = q\sin\theta. \tag{3.15}$$

Substituting equation (3.15) in equation (3.14), yields

$$\begin{aligned} & f_{XY}(x,y) \\ &= \frac{1}{4\pi^2} \int_0^\infty \int_0^{2\pi} \prod_{n=1}^{N} \left[\int_0^\infty f_{R_n}(r_n) J_0(r_n q) dr_n \right] e^{-jq(x\cos\theta + y\sin\theta)} d\theta q dq \\ &= \frac{1}{4\pi^2} \int_0^\infty \prod_{n=1}^{N} \left[\int_0^\infty f_{R_n}(r_n) J_0(r_n q) dr_n \right] \left[\int_0^{2\pi} \exp\left\{ -jq\sqrt{x^2+y^2}\cos(\theta - \psi) \right\} d\theta \right] q dq, \end{aligned} \tag{3.16}$$

where $\psi = \arctan(x,y)$. The negative sign in the exponential may be absorbed by the cosine via a shift of π. We now use equation (3.10) to evaluate the integral in the right set of square brackets. We thus have

$$f_{XY}(x,y) = \frac{1}{2\pi} \int_0^\infty \prod_{n=1}^{N} \left[\int_0^\infty f_{R_n}(r_n) J_0(r_n q) dr_n \right] J_0(q\sqrt{x^2+y^2}) q dq. \tag{3.17}$$

Next, we convert the jpdf of equation (3.17) to polar coordinates to obtain the jpdf of the random vector (R, Θ). Letting

$$X = R\cos\Theta, \quad Y = R\sin\Theta \tag{3.18}$$

in equation (3.17) and substituting in equation (3.7) gives

$$\begin{aligned} f_{R\Theta}(r,\theta) &= r f_{XY}(r\cos\theta, r\sin\theta) \\ &= \frac{1}{2\pi} r \int_0^\infty \prod_{n=1}^{N} \left[\int_0^\infty f_{R_n}(r_n) J_0(r_n q) dr_n \right] J_0(qr) q dq. \end{aligned} \tag{3.19}$$

Note that we can separate the jpdf of R and Θ as

$$f_{R\Theta}(r,\theta) = f_R(r) \times f_\Theta(\theta), \tag{3.20}$$

proving that, indeed, R and Θ are independent random variables. Furthermore, $f_{R\Theta}(r,\theta)$ in equation (3.19) does not depend on θ. From this we conclude that Θ is uniformly distributed over $[0, 2\pi]$

$$f_\Theta(\theta) = \frac{1}{2\pi}, \quad \text{for } 0 \le \theta \le 2\pi, \tag{3.21}$$

regardless of the number N of random vectors added.

To obtain the pdf of the magnitude of the sum of N random vectors $f_R(r)$, we may integrate the jpdf $f_{R\Theta}(r,\theta)$ over the variable θ. Integrating equation (3.19) with respect to θ, we obtain

$$f_R(r) = r \int_0^\infty \prod_{n=1}^{N} \left[\int_0^\infty f_{R_n}(r_n) J_0(r_n q) dr_n \right] J_0(qr) q dq, \quad r \ge 0. \tag{3.22}$$

For the purpose of illustration, we show how to use equation (3.22) in a simple case. We restrict $R_n = \sqrt{2/N}$, i.e., a deterministic pdf as in Figure 3.1 and Figure 3.2. The pdf corresponding to this choice is

$$f_{R_n}(r_n) = \delta\left(r_n - \sqrt{\frac{2}{N}} \right), \tag{3.23}$$

where $\delta(\cdot)$ is the Dirac delta function. The random vector length is normalized such that the variance of the rv's X and Y is always one.

Note that other choices of $f_{R_n}(r_n)$ are possible, depending on the problem at hand. We chose the pdf of equation (3.23) as this provides the simplest answers. For other applications, such as modelling hardware errors, the lengths might follow a uniform distribution over some interval $[a,b]$, or Gaussian, whichever is a better model. One could then compute the pdf of R to determine whether errors in the hardware will have an effect on the generation of Rayleigh distributed random variables, i.e., Rayleigh fading signal.

Inserting the pdf of equation (3.23) in equation (3.22) yields

$$f_R(r) = r\int_0^\infty J_0^N\left(q\sqrt{\frac{2}{N}}\right) J_0(rq)qdq, \quad r \geq 0. \tag{3.24}$$

An alternative answer can be obtained by performing the substitution $u = q\sqrt{2/N}$ in equation (3.24). We obtain

$$f_R(r) = \frac{N}{2}r\int_0^\infty J_0^N(q)J_0\left(qr\sqrt{\frac{N}{2}}\right) qdq.$$

This last form of the answer may be more suitable for numerical implementation. Figure 3.3 shows the pdf $f_R(r)$ obtained for selected values of N.

In some situations, however, one is interested in obtaining the cdf of the magnitude of the sum of N random vectors, i.e., $F_R(r)$. One approach to computing $F_R(r)$ would be to integrate the result of equation (3.22) with respect to r. This would require the computation of a double integral to arrive at the final answer. Although there are numerical routines available for evaluating such double integrals, the precision one can expect is much less than in the case of single integrals. Therefore, if we could determine an expression for $F_R(r)$ in terms of a single integral, its computation would be faster and more accurate.

In the case in which the random vector lengths are deterministic, i.e., whose pdf's are expressible in terms of the Dirac-delta function $\delta(\cdot)$ as above, we may turn to a result in Watson [26, Sec. 13-48]. The result is due to Kluyver, and is obtained in the context of random walks in the plane. He obtained

$$F_R(r) = r\int_0^\infty \prod_{n=1}^{N} \left[J_0(r_n q)\right] J_1(rq)dq, \tag{3.25}$$

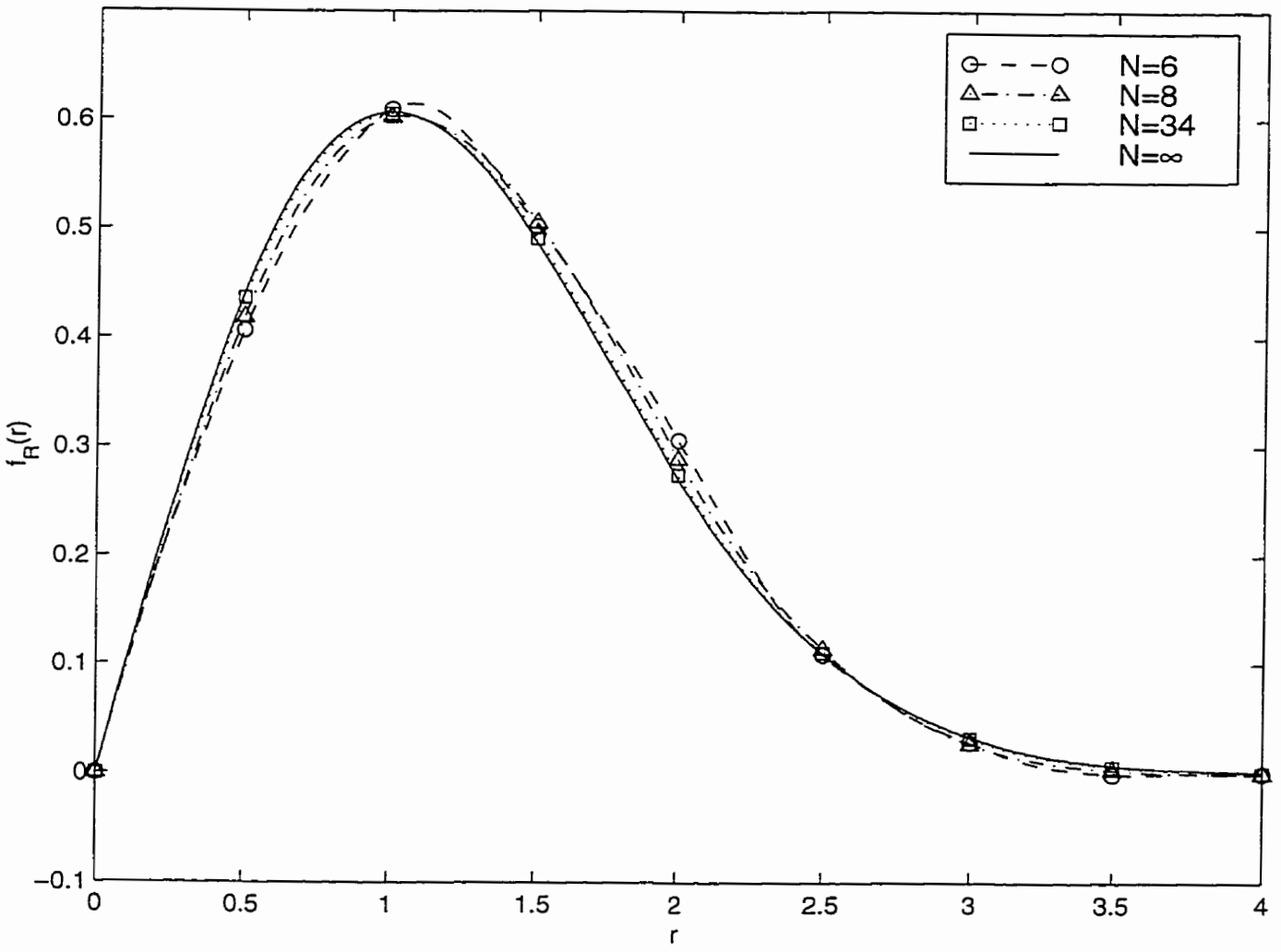

Figure 3.3. Envelope pdf of the signal generated by Clarke's model for various numbers of low-frequency oscillators.

where the r_n represent the lengths of the individual steps. It should be noted that such a case does occur; Clarke's model with constant c_n's would be an immediate example. The result of equation (3.25) is used later, in Section 5.1.

Unfortunately, there seems to be no such result in the more general case, where the R_n are allowed to follow any distribution. For these cases we are forced to perform the double integration as mentioned above.

3.1.1 The envelope and phase pdf's of Clarke's model

We presented in Section 3.1 a method for computing the jpdf of the random vector representing the sum of N independent random vectors in the plane. Here we will apply this method to compute the envelope and phase pdf's of the signal produced by Clarke's model. Of course, to be able to apply the results of Section 3.1, we must first recast the problem in terms of a sum of independent vectors, i.e., in the form of equations (3.3a) and (3.3b). Also, we must justify the assumption that R_n and Θ_n are independent. In addition, we must verify that the Θ_n's follow the pdf of equation (3.1).

Recall that we are trying to simulate the fading signal of equation (2.6). Here, we re-write this signal split into in-phase and quadrature components,

$$R(t) = \cos\omega_c t \sum_{n=1}^{N} \sqrt{\frac{2}{N}}\cos(\omega_n t + \Phi_n) - \sin\omega_c t \sum_{n=1}^{N} \sqrt{\frac{2}{N}}\sin(\omega_n t + \Phi_n). \tag{3.26}$$

By comparing equation (3.26) to equations (3.3a) and (3.3b), we note,

$$R_n = \sqrt{\frac{2}{N}}, \quad n = 1,\ldots,N \tag{3.27}$$

and

$$\Theta_n = \omega_n t + \Phi_n, \quad n = 1,\ldots,N. \tag{3.28}$$

To justify the independence [3] of R_n and Θ_n we turn to the model of equation (2.6). In this equation, the parameters C_n, A_n, and Φ_n are all independent. From equation (3.27) we

[3] One may also note that R_n constant is sufficient to guarantee R_n and Θ_n are independent.

note R_n is a function of C_n only. From equation (3.28) we note Θ_n is, in general, a function of A_n and Φ_n. From the independence of C_n, A_n, and Φ_n, it follows that R_n and Θ_n are also independent.

From equation (3.27), the length pdf of the nth random vector is given by the pdf of equation (3.23), i.e.,

$$f_{R_n}(r_n) = \delta(r_n - \sqrt{\frac{2}{N}}).$$

In equation (3.28) we have a deterministic component $\omega_n t$ and a random one Φ_n. Therefore, the pdf of Θ_n will be the same as that of Φ_n, except that it will be shifted by an amount equal to $\omega_n t$. Recall that the pdf of Φ_n is uniform over some interval of length 2π. However, due to the periodicity of the functions involved, i.e., $\cos(\cdot)$ and $\sin(\cdot)$, this is sufficient and we may take the Θ_n to be uniform i.i.d. over $[0, 2\pi]$. This satisfies the requirement of equation (3.1). We now proceed with the computation of the envelope pdf of the signal produced by Clarke's model.

To determine the envelope pdf, we need to substitute the appropriate pdf $f_{R_n}(r_n)$ in equation (3.22). We note the required result appears in the worked example at the end of Section 3.1. From equation (3.24), we have

$$f_R(r) = r \int_0^\infty J_0^N \left(q\sqrt{\frac{2}{N}} \right) J_0(rq) q dq, \quad r \geq 0. \tag{3.29}$$

We note that the envelope pdf of the signal produced by Clarke's model is independent of time t. We plot the result in Figure 3.4.

The phase pdf is given by equation (3.21)

$$f_\Theta(\theta) = \frac{1}{2\pi} \quad \text{for } 0 \leq \theta \leq 2\pi. \tag{3.30}$$

3.1.2 The envelope and phase pdf's of Jakes' simulator

In this subsection, we determine the envelope and phase pdf's of the signal produced by Jakes' simulator.

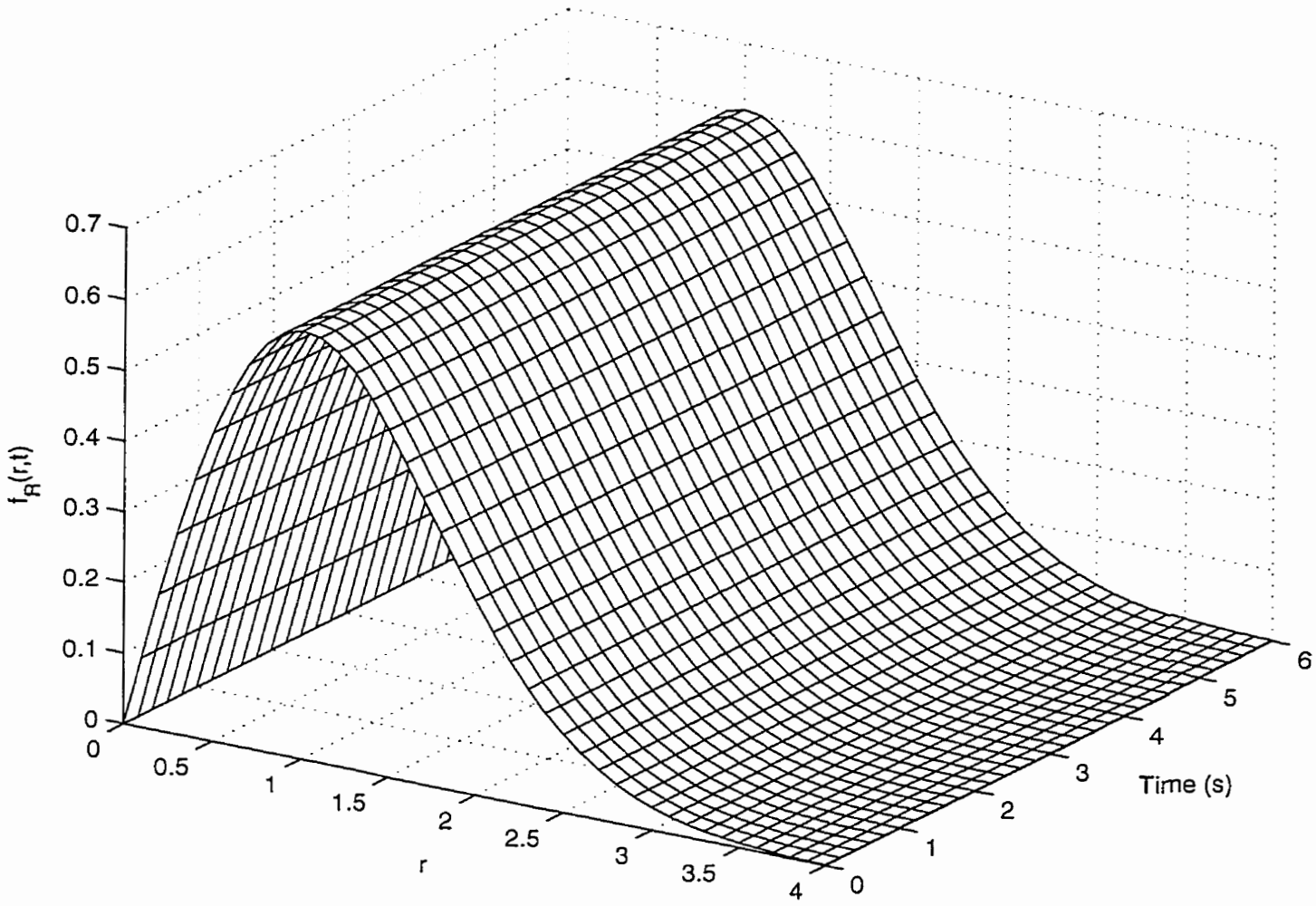

Figure 3.4. Variation with time of the envelope pdf of the signal produced by Clarke's model, for $N = 34$.

As in the case of Clarke's model, our first task is to recast the fading signal produced by Jakes' simulator in terms of the sum of $M+1$ independent random variables. We re-write the signal of equation (2.11) in terms of quadrature components

$$\begin{aligned}\tilde{R}(t) &= \cos\omega_c t \frac{2}{\sqrt{N}}\left(\sqrt{2}\cos B_{M+1}\cos\omega_m t + 2\sum_{n=1}^{M}\cos B_n \cos\omega_n t\right) \\ &\quad + \sin\omega_c t \frac{2}{\sqrt{N}}\left(\sqrt{2}\sin B_{M+1}\cos\omega_m t + 2\sum_{n=1}^{M}\sin B_n \cos\omega_n t\right). \end{aligned} \tag{3.31}$$

Similar to the procedure in the previous section, we compare equation (3.31) to equations (3.3a) and (3.3b). We see that the random vector lengths are described by the random variables

$$\begin{aligned} R_n &= \frac{4}{\sqrt{N}}\cos\omega_n t, \quad n = 1,\ldots,M, \\ R_{M+1} &= \frac{2\sqrt{2}}{\sqrt{N}}\cos\omega_m t. \end{aligned} \tag{3.32}$$

The corresponding random vector directions are described by the random variables

$$\Theta_n = B_n, \quad n = 1,\ldots,M+1. \tag{3.33}$$

As done in the previous section, we must first verify that R_n is independent of Θ_n. We note that R_n is, in general, a function of C_n and A_n. Θ_n, on the other hand, is a function of B_n, and hence, Φ_n only. We have already argued that C_n, A_n, and Φ_n are independent from physical considerations in Section 2.1. It follows, then, that R_n and Θ_n are also independent.

From equation (3.32), the pdf's of the random vector lengths are given by

$$f_{R_n}(r_n) = \delta\left(r_n - \frac{4}{\sqrt{N}}\cos\omega_n t\right), \quad n = 1,\ldots,M \tag{3.34a}$$

and

$$f_{R_{M+1}}(r_{M+1}) = \delta\left(r_{M+1} - \frac{2\sqrt{2}}{\sqrt{N}}\cos\omega_m t\right). \tag{3.34b}$$

Recall from Subsection 2.2.1 that we may take the rv's $B_1,\ldots,B_{M+1}$ uniform i.i.d. over $[0,2\pi]$. Thus, the rv's $\Theta_1,\ldots,\Theta_{M+1}$ are uniform i.i.d. over $[0,2\pi]$, satisfying equation (3.1).

Thus, substituting equations (3.34a) and (3.34b) in equation (3.11) yields

$$\Phi_n(\omega_1,\omega_2) = J_0\left(\frac{4\cos\omega_n t\sqrt{\omega_1^2+\omega_2^2}}{\sqrt{N}}\right), \quad n=1,\ldots,M, \tag{3.35a}$$

and

$$\Phi_{M+1}(\omega_1,\omega_2) = J_0\left(\frac{2\sqrt{2}\cos\omega_m t\sqrt{\omega_1^2+\omega_2^2}}{\sqrt{N}}\right). \tag{3.35b}$$

Next, following a procedure similar to that in Section 3.1 we obtain

$$f_{\tilde{R}}(r) = r\int_0^\infty \left[J_0\left(\frac{2q\cos\omega_m t}{\sqrt{2M+1}}\right)\prod_{n=1}^{M} J_0\left(\frac{4q\cos\omega_n t}{\sqrt{4M+2}}\right)\right] J_0(qr)qdq. \tag{3.36}$$

We note that the pdf of the envelope of the signal produced by Jakes' simulator is a function of both the envelope level r as well as time t. We plot the result of equation (3.36) in Figure 3.5. Analyzing Figure 3.5 we note that the variance of the fading process is time-variant. That is, the signal produced by Jakes' simulator is not stationary, nor even wide-sense stationary. The non-stationary character of the signal will be observed in a different form in Section 3.2.2.

The phase pdf is given by equation (3.21)

$$f_{\tilde{\Theta}}(\theta) = \frac{1}{2\pi} \quad \text{for } 0 \le \theta \le 2\pi. \tag{3.37}$$

It is interesting to note that this result contradicts Pätzold's development in [9]. Pätzold derives his results based on time averages. Here, we have computed a statistical average. We have also shown that the first-order pdf of $\tilde{R}(t)$ is time-variant, and thus suspect the random process $\tilde{R}(t)$ is not wide-sense stationary; we will show this directly later. This point further illustrates that one may not readily substitute time averages for statistical ones; such substitutions are meaningful only for random processes which satisfy some ergodic theorem, i.e., which exhibit ergodicity of the mean and autocorrelation.

3.2 Second order statistics

In this section, we compute the statistical mean and autocorrelation functions of the signals produced by Clarke's model and Jakes' simulator. We find that the signal produced

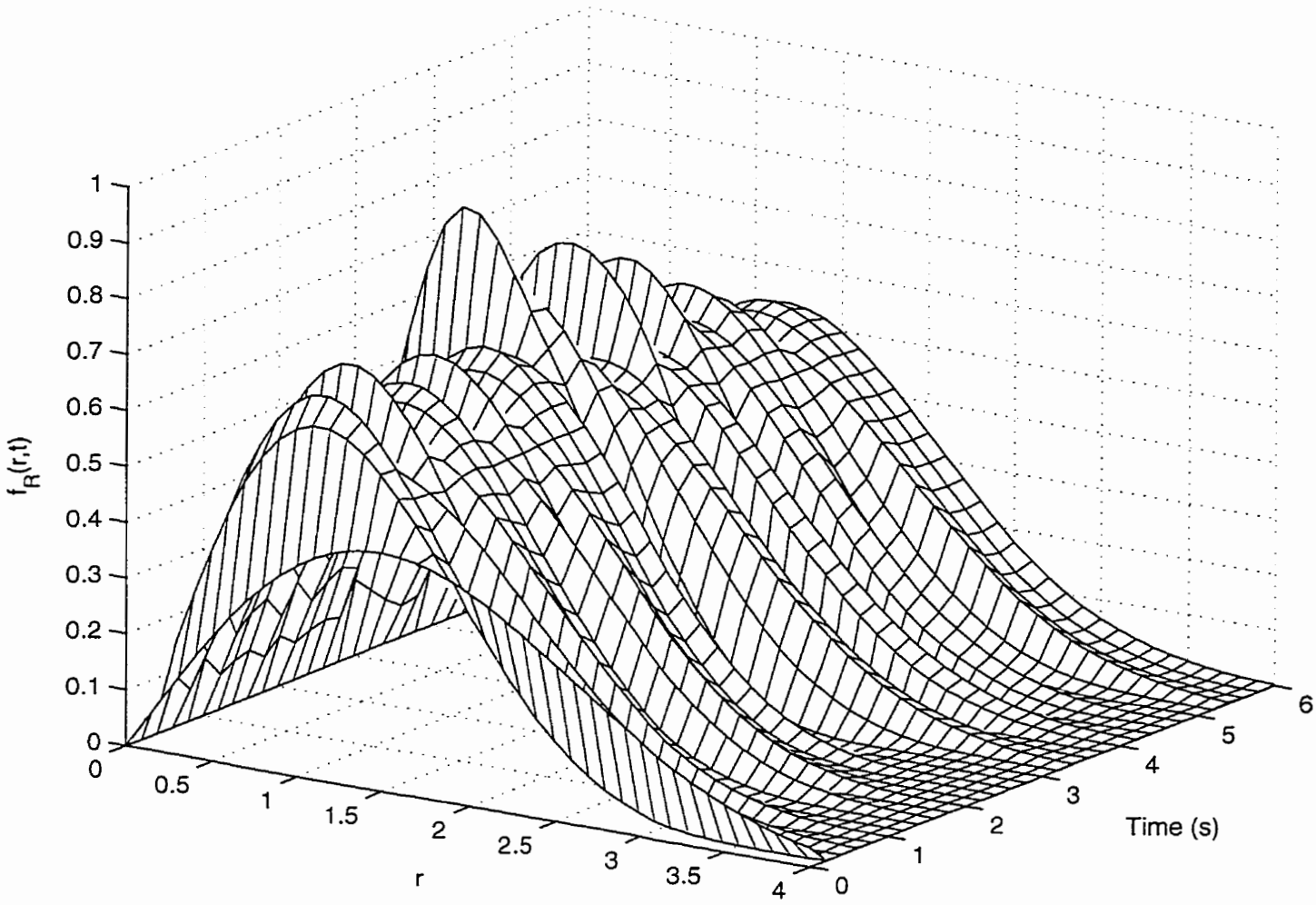

Figure 3.5. Variation with time of the envelope pdf of the signal produced by Jakes' simulator. Here, the value of $M = 8$ corresponds to $N = 34$ in Figure 3.4.

by Clarke's model is wide-sense stationary, while that produced by Jakes' simulator is not wide-sense stationary. As well, we determine the time-average mean and autocorrelation functions. These computations are readily carried out from appropriate definitions of the mean and autocorrelation functions. Comparisons of the two sets of averages, i.e., statistical and time-average, are made in the general framework of ergodicity. We find that in the case of Clarke's model, the statistical mean and autocorrelation functions are equal to the corresponding time-average functions. In the case of Jakes' model, this is true of only the mean function.

3.2.1 Clarke's model

In this subsection, we determine the autocorrelation $\mathscr{R}_{RR}(t_1, t_2)$ of the stochastic process $R(t)$ represented in equation (2.6), a second order statistical property. For the sake of completeness, we also compute the mean function $\mu_R(t)$. Recall that the fading signal $R(t)$ can be written as

$$R(t) = \sqrt{\frac{2}{N}} \sum_{n=1}^{N} \cos(\omega_c t + \omega_n t + \Phi_n), \tag{3.38}$$

where $\omega_n = \omega_m \cos(2\pi n/N)$. This re-formulation is equation (2.6) with the c_n and α_n as given by equations (2.9) and (2.10) in Section 2.2. In other words, the only rv's are the Φ_n, which we recall are uniform i.i.d. over $[0, 2\pi]$. This simplifies the computation of the mean and autocorrelation functions of the fading signal $R(t)$.

Applying the definition of the mean function as defined in [29, eq. (10-7)], we obtain successively

$$\begin{aligned}
\mu_R(t) &= E\{R(t)\} \\
&= E\left\{ \sqrt{\frac{2}{N}} \sum_{n=1}^{N} \cos(\omega_c t + \omega_n t + \Phi_n) \right\} \\
&= \sqrt{\frac{2}{N}} \sum_{n=1}^{N} E\{\cos(\omega_c t + \omega_n t + \Phi_n)\} \\
&= \sqrt{\frac{2}{N}} \sum_{n=1}^{N} \int_0^{2\pi} \cos(\omega_c t + \omega_n t + \phi_n) \frac{1}{2\pi} d\phi_n
\end{aligned}$$

$$= 0, \tag{3.39}$$

where we have used the linearity of the expectation operator, and the fact that the integral of a sine wave over one wavelength is zero.

To compute the autocorrelation function, we also start from the definition [29, eq. (10-8)]. We obtain successively

$$\begin{aligned}
\mathscr{R}_{RR}(t_1,t_2) &= E\left\{R(t_1)R(t_2)\right\} \\
&= \frac{2}{N} E\left\{\sum_{n=1}^{N}\sum_{k=1}^{N} \cos(\omega_c t_1 + \omega_m t_1 \cos\alpha_n + \Phi_n)\cos(\omega_c t_2 + \omega_m t_2 \cos\alpha_k + \Phi_k)\right\} \\
&= \frac{1}{N} E\left\{\sum_{n=1}^{N}\sum_{k=1}^{N} \left\{\cos\left[\omega_c(t_1+t_2) + \omega_m(t_1\cos\alpha_n + t_2\cos\alpha_k) + \Phi_n + \Phi_k\right]\right.\right. \\
&\quad \left.\left. + \cos\left[\omega_c(t_1-t_2) + \omega_m(t_1\cos\alpha_n - t_2\cos\alpha_k) + \Phi_n - \Phi_k\right]\right\}\right\}.
\end{aligned} \tag{3.40}$$

The first line in the development of equation (3.40) comes from substituting the definition of $R(t)$. To obtain the next line, we use the well-known trigonometric identity,

$$2\cos x\cos y = \cos(x+y) + \cos(x-y). \tag{3.41}$$

Taking advantage of the fact the Φ_n are uniform i.i.d. rv's over $[0, 2\pi]$ we obtain the following results,

$$\begin{aligned}
E\{\cos(\Phi_n + \Phi_k)\} &= 0, \quad 1 \le k,n \le N, \\
E\{\cos(\Phi_n - \Phi_k)\} &= \begin{cases} 0 & \text{if } n \ne k, \\ 1 & \text{if } n = k, \end{cases} \\
E\{\sin(\Phi_n \pm \Phi_k)\} &= 0, \quad 1 \le k,n \le N.
\end{aligned}$$

This allows us to further simplify equation (3.40) to

$$\mathscr{R}_{RR}(t_1,t_2) = \frac{1}{N}\sum_{n=1}^{N} \cos\left[\omega_c(t_1-t_2) + \omega_m(t_1-t_2)\cos\alpha_n\right]. \tag{3.42}$$

We observe that upon expanding $\cos[\omega_c(t_1-t_2) + \omega_m(t_1-t_2)\cos\frac{2\pi n}{N}]$ we should have two quadrature terms. The in-phase one corresponds to $\cos(\omega_c t)$, while the quadrature one

corresponds to $\sin(\omega_c t)$. We observe, however, that for N even

$$\sum_{n=1}^{N} \sin\left[\omega_m(t_1 - t_2)\cos\frac{2\pi n}{N}\right] = 0. \tag{3.43}$$

To prove the result of equation (3.43), we observe that

$$\begin{aligned}\cos\frac{2\pi\left(\frac{N}{2}+n\right)}{N} &= \cos\left(\pi + \frac{2\pi n}{N}\right) \\ &= -\cos\frac{2\pi n}{N}.\end{aligned} \tag{3.44}$$

Therefore,

$$\sin\left[\omega_m(t_1 - t_2)\cos\frac{2\pi\left(\frac{N}{2}+n\right)}{N}\right] = -\sin\left[\omega_m(t_1 - t_2)\cos\frac{2\pi n}{N}\right]. \tag{3.45}$$

For N even, we can re-write the summation of equation (3.43) as

$$\begin{aligned}&\sum_{n=1}^{N} \sin\left[\omega_m(t_1 - t_2)\cos\frac{2\pi n}{N}\right] \\ &= \sum_{n=1}^{N/2} \sin\left[\omega_m(t_1 - t_2)\cos\frac{2\pi n}{N}\right] + \sin\left[\omega_m(t_1 - t_2)\cos\frac{2\pi\left(\frac{N}{2}+n\right)}{N}\right].\end{aligned} \tag{3.46}$$

Upon substitution of equation (3.45) in equation (3.46), the result of equation (3.43) is obvious.

For N odd, the approximation

$$\sum_{n=1}^{N} \sin\left[\omega_m(t_1 - t_2)\cos\frac{2\pi n}{N}\right] \approx 0 \tag{3.47}$$

holds true for $0 \leq \omega_m(t_1 - t_2) \leq \frac{N}{2}$. This result can be verified graphically, or by using a method introduced later in Section 5.2.

Thus, in general, equation (3.42) can be approximated by

$$\mathscr{R}_{RR}(t_1, t_2) \approx \frac{1}{N}\cos[\omega_c(t_1 - t_2)] \sum_{n=1}^{N} \cos[\omega_m(t_1 - t_2)\cos\frac{2\pi n}{N}], \tag{3.48}$$

for $0 \leq t_1 - t_2 \leq \frac{N}{2\omega_m}$. It should be noted that most sum-of-sinusoids simulators use an even number of oscillators N, and thus the approximation of equation (3.48), with no restriction on $t_1 - t_2$, becomes exact.

As an aside, we relax the assumption that the α_n, $n = 1,\ldots,N$ are uniformly spaced around the unit circle, as in Section 2.2. However, we still maintain that the A_n are uniform i.i.d. random variables over $[0, 2\pi]$. Furthermore, the A_n are independent of the Φ_n, as assumed by Clarke [3] and Jakes [23], for example. This assumption seems physically reasonable as it states that the phase shift is independent of the angle of arrival. Recall that the angle of arrival is affected by the position of the obstacles between transmitter and receiver, whereas the phase shift depends on the material characteristics of the obstacles. Because of the independence of the two sets of rv's, the statistics computed thus far still apply; we only need to average the results obtained over the pdf of A_n. Thus, we still have

$$\begin{aligned}\mu_R(t) &= E\left\{\frac{2}{\sqrt{N}}\sum_{n=1}^{N}\cos(\omega_c t + \omega_m t\cos\alpha_n + \Phi_n)\right\}\\ &= 0.\end{aligned}$$

We turn our attention now to the re-computation of the autocorrelation function. We know from Gans [4] that the power spectral density[4] of the fading signal of equation (2.6) is given by

$$S(\omega) = \frac{3E_0^2}{2}\frac{2}{\sqrt{\omega_m^2 - (\omega - \omega_c)^2}}, \quad \omega_c - \omega_m < \omega < \omega_c + \omega_m. \tag{3.49}$$

The autocorrelation of the signal can then be computed by taking the inverse Fourier transform of the power spectral density $S(\omega)$,

$$\mathscr{R}_R(\tau) = \frac{3E_0^2}{2}\cos(\omega_c\tau)J_0(\omega_m\tau). \tag{3.50}$$

In our case, $E_0 = \sqrt{2}$, and equation (3.50) simplifies to

$$\mathscr{R}_R(\tau) = 3\cos(\omega_c\tau)J_0(\omega_m\tau). \tag{3.51}$$

Here we present a time-domain derivation, starting with the fading signal $R(t)$ as given in equation (3.38). Because A_n and Φ_n are independent, the derivation is identical to that

[4]This also appears in Jakes [23, eq. (1.2-11)].

presented above. We pick things up at equation (3.42). At this point, we have to average the expression of equation (3.42) over the pdf of A_n. Thus,

$$\begin{aligned}\mathscr{R}_{RR}(t_1,t_2) &= \frac{1}{N}E\left\{\sum_{n=1}^{N}\cos\left[\omega_c(t_1-t_2)+\omega_m(t_1-t_2)\cos A_n\right]\right\}\\ &= \frac{1}{N}\cos[\omega_c(t_1-t_2)]E\left\{\sum_{n=1}^{N}\cos[\omega_m(t_1-t_2)\cos A_n]\right\}\\ &\quad -\frac{1}{N}\sin[\omega_c(t_1-t_2)]E\left\{\sum_{n=1}^{N}\sin[\omega_m(t_1-t_2)\cos A_n]\right\},\end{aligned} \tag{3.52}$$

where we have used the well-known trigonometric identity

$$\cos(x+y)=\cos x\cos y-\sin x\sin y.$$

As well, we have moved the deterministic factors $\cos\omega_c t$ and $\sin\omega_c t$ outside the expectation operator.

The next step is to compute the expectations in equation (3.52) as appropriate integrals

$$\begin{aligned}\mathscr{R}_{RR}(t_1,t_2) &= \frac{1}{N}\cos[\omega_c(t_1-t_2)]\sum_{n=1}^{N}\int_0^{2\pi}\frac{1}{2\pi}\cos[\omega_m(t_1-t_2)\cos\alpha_n]d\alpha_n\\ &\quad -\frac{1}{N}\sin[\omega_c(t_1-t_2)]\sum_{n=1}^{N}\int_0^{2\pi}\frac{1}{2\pi}\sin[\omega_m(t_1-t_2)\cos\alpha_n]d\alpha_n.\end{aligned} \tag{3.53}$$

From [36, eq. 3.715.13] with $n=0$ we have

$$\int_{-\pi}^{\pi}\sin(z\cos x)dx=0. \tag{3.54}$$

Thus, substituting equation (3.10) and equation (3.54) in equation (3.53) yields the desired answer, namely

$$\mathscr{R}_{RR}(t_1,t_2)=\cos[\omega_c(t_1-t_2)]J_0(\omega_m(t_1-t_2)). \tag{3.55}$$

We note that the fading process defined in equation (2.6) is indeed wide-sense stationary, so that we may write

$$\mathscr{R}_R(\tau)=\cos(\omega_c\tau)J_0(\omega_m\tau). \tag{3.56}$$

The result of equation (3.56) is the same as that of equation (3.51), except for a factor of 3 in the latter. This difference occurs because in Gans' work, the effect, i.e., the gain, of the

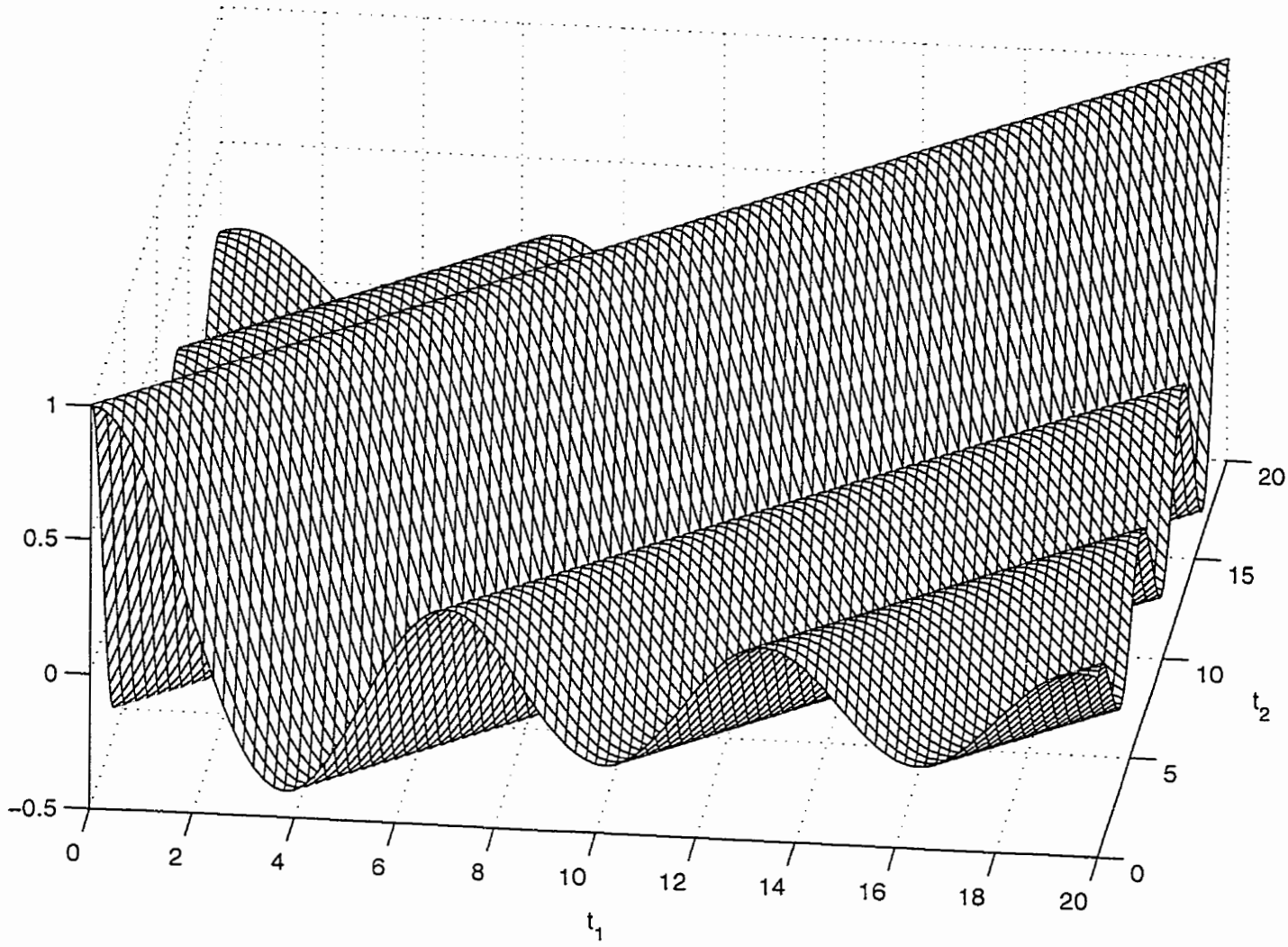

Figure 3.6. Lowpass equivalent form of the autocorrelation function of $R(t)$, for $N = 34$, $\omega_m = 1$.

antenna is also included. As it happens, the gain of an omnidirectional antenna, the type used by Gans in his analysis, is $\frac{3}{2}$. Also, inclusion of both negative and positive frequencies introduces a factor of two. We conclude, then, that the two results are identical up to the inclusion of antenna gains.

A plot of the lowpass equivalent form of the autocorrelation function given by equation (3.42) is shown in Figure 3.6. From this diagram, the independence of the autocorrelation function of time origin is obvious. In particular, the surface can be readily obtained by translating a slice parallel to either axis along the line $t_1 = t_2$. This is generally true of

wide-sense stationary processes.

3.2.2 Non-stationarity of Jakes' simulator

In this subsection, we compute the autocorrelation function $\mathscr{R}_{\tilde{R}\tilde{R}}(t_1,t_2)$ of the signal produced by Jakes' fading channel simulator $\tilde{R}(t)$, a second order statistical property. As well, we compute the mean function $\mu_{\tilde{R}}(t)$ of $\tilde{R}(t)$, paralleling the developments of the previous subsection.

For ease of reference, we copy equations (2.11) of Section 2.2 here

$$\tilde{R}(t) = \tilde{X}_c(t)\cos(\omega_c t) + \tilde{X}_s(t)\sin(\omega_c t) \tag{3.57}$$

where the in-phase and quadrature components, $\tilde{X}_c(t)$ and $\tilde{X}_s(t)$ are given by equations (2.12a) and (2.12b)

$$\tilde{X}_c(t) = \frac{2\sqrt{2}}{\sqrt{N}}\cos B_{M+1}\cos\omega_m t + \frac{4}{\sqrt{N}}\sum_{n=1}^{M}\cos B_n\cos\omega_n t, \tag{3.58a}$$

and

$$\tilde{X}_s(t) = \frac{2\sqrt{2}}{\sqrt{N}}\sin B_{M+1}\cos\omega_m t + \frac{4}{\sqrt{N}}\sum_{n=1}^{M}\sin B_n\cos\omega_n t. \tag{3.58b}$$

We recall that the purpose of Jakes' fading channel simulator is to efficiently generate the fading signal of equation (2.6)

$$R(t) = \sqrt{\frac{2}{N}}\sum_{n=1}^{N}\cos(\omega_c t + \omega_m t\cos\frac{2\pi n}{N} + \Phi_n). \tag{3.59}$$

We begin with the computation of the mean function $\mu_{\tilde{R}}(t)$. From Subsection 2.2.1, we have that $B_1,\ldots,B_{M+1}$ are uniform i.i.d. over $[0,2\pi]$. Knowledge of these pdf's allows us to compute the expectations

$$E\{\cos B_n\} = E\{\sin B_n\} = 0, \quad n = 1,\ldots,M+1. \tag{3.60}$$

We can now compute

$$E\{\tilde{X}_c(t)\} = E\left\{\frac{2\sqrt{2}}{\sqrt{N}}\cos B_{M+1}\cos\omega_m t + \frac{4}{\sqrt{N}}\sum_{n=1}^{M}\cos B_n\cos\omega_n t\right\}$$

$$= \frac{2\sqrt{2}}{\sqrt{N}} E\{\cos B_{M+1}\} \cos \omega_m t + \frac{4}{\sqrt{N}} \sum_{n=1}^{M} E\{\cos B_n\} \cos \omega_n t$$
$$= 0. \tag{3.61}$$

Similarly, we obtain $E\{\tilde{X}_s(t)\} = 0$. Therefore,

$$\begin{aligned} \tilde{\mu}(t) &= E\{\tilde{R}(t)\} \\ &= \cos \omega_c t E\{\tilde{X}_c(t)\} + \sin \omega_c t E\{\tilde{X}_s(t)\} \\ &= 0. \end{aligned} \tag{3.62}$$

To make the derivation of the autocorrelation function simpler, we re-write the signal produced by the Jakes' simulator by expanding the expressions for the quadrature terms. That is,

$$\begin{aligned} \tilde{R}(t) &= \left(\frac{2\sqrt{2}}{\sqrt{N}} \cos B_{M+1} \cos \omega_m t + \frac{4}{\sqrt{N}} \sum_{n=1}^{M} \cos B_n \cos \omega_n t \right) \cos \omega_c t \\ &\quad + \left(\frac{2\sqrt{2}}{\sqrt{N}} \sin B_{M+1} \cos \omega_m t + \frac{4}{\sqrt{N}} \sum_{n=1}^{M} \sin B_n \cos \omega_n t \right) \sin \omega_c t \\ &= \frac{2\sqrt{2}}{\sqrt{N}} \cos B_{M+1} \cos \omega_m t \cos \omega_c t + \frac{4}{\sqrt{N}} \sum_{n=1}^{M} \cos B_n \cos \omega_n t \cos \omega_c t \\ &\quad + \frac{2\sqrt{2}}{\sqrt{N}} \sin B_{M+1} \cos \omega_m t \sin \omega_c t + \frac{4}{\sqrt{N}} \sum_{n=1}^{M} \sin B_n \cos \omega_n t \sin \omega_c t. \end{aligned} \tag{3.63}$$

We can further simplify equation (3.63) by grouping the deterministic terms and making the substitutions

$$\cos \omega_m t \cos \omega_c t = a_{M+1}(t), \tag{3.64a}$$

$$\cos \omega_n t \cos \omega_c t = a_n(t), \quad n = 1, \ldots, M, \tag{3.64b}$$

and

$$\cos \omega_m t \sin \omega_c t = b_{M+1}(t), \tag{3.64c}$$

$$\cos \omega_n t \sin \omega_c t = b_n(t), \quad n = 1, \ldots, M. \tag{3.64d}$$

Substituting equations (3.64a) – (3.64d) in equation (3.63) yields

$$\begin{aligned}\tilde{R}(t) &= \frac{2\sqrt{2}}{\sqrt{N}}a_{M+1}(t)\cos B_{M+1} + \frac{4}{\sqrt{N}}\sum_{n=1}^{M} a_n(t)\cos B_n \\ &\quad + \frac{2\sqrt{2}}{\sqrt{N}}b_{M+1}(t)\sin B_{M+1} + \frac{4}{\sqrt{N}}\sum_{n=1}^{M} b_n(t)\sin B_n. \end{aligned} \tag{3.65}$$

Next, we determine the autocorrelation function according to the definition [29, eq. (10-8)]. We have

$$\begin{aligned}&\mathscr{R}_{\tilde{R}\tilde{R}}(t_1,t_2) = E\{\tilde{R}(t_1)\tilde{R}(t_2)\} \\ &= E\Bigg\{\Big[\frac{2\sqrt{2}}{\sqrt{N}}a_{M+1}(t_1)\cos B_{M+1} + \frac{4}{\sqrt{N}}\sum_{n=1}^{M} a_n(t_1)\cos B_n + \frac{2\sqrt{2}}{\sqrt{N}}b_{M+1}(t_1)\sin B_{M+1} \\ &\quad + \frac{4}{\sqrt{N}}\sum_{n=1}^{M} b_n(t_1)\sin B_n\Big] \times \Big[\frac{2\sqrt{2}}{\sqrt{N}}a_{M+1}(t_2)\cos B_{M+1} + \frac{4}{\sqrt{N}}\sum_{k=1}^{M} a_k(t_2)\cos B_k \\ &\quad + \frac{2\sqrt{2}}{\sqrt{N}}b_{M+1}(t_2)\sin B_{M+1} + \frac{4}{\sqrt{N}}\sum_{k=1}^{M} b_k(t_2)\sin B_k\Big]\Bigg\}. \end{aligned} \tag{3.66}$$

To simplify the result of equation (3.66) we use the linearity of the expectation operator to move it inside the summation signs. To further simplify the result of equation (3.66) we make use of the following equalities, readily obtainable by noting that the rv's $B_1, \ldots, B_{M+1}$ are uniform i.i.d. over $[0, 2\pi]$. This allows us to compute

$$\begin{aligned}&E\{\cos B_n \sin B_k\} = 0, \\ &E\{\cos B_n \cos B_k\} = E\{\sin B_n \sin B_k\} = \begin{cases} \frac{1}{2}, & \text{if } n = k, \\ 0, & \text{otherwise,} \end{cases}\end{aligned}$$

for $1 \le n, k \le M+1$. Thus, we may simplify equation (3.66) to

$$\begin{aligned}&\mathscr{R}_{\tilde{R}\tilde{R}}(t_1,t_2) \\ &= \frac{8}{N}a_{M+1}(t_1)a_{M+1}(t_2)E\{\cos^2 B_{M+1}\} + \frac{8}{N}b_{M+1}(t_1)b_{M+1}(t_2)E\{\sin^2 B_{M+1}\} \\ &\quad + \frac{16}{N}\sum_{n=1}^{M} a_n(t_1)a_n(t_2)E\{\cos^2 B_n\} + \frac{16}{N}\sum_{n=1}^{M} b_n(t_1)b_n(t_2)E\{\sin^2 B_n\}. \end{aligned} \tag{3.67}$$

Back-substituting equations (3.64a) – (3.64d) in equation (3.67) yields

$$\begin{aligned}
&\mathscr{R}_{\tilde{R}\tilde{R}}(t_1,t_2) \\
&= \frac{4}{N}\left(\cos\omega_m t_1 \cos\omega_c t_1 \cos\omega_m t_2 \cos\omega_c t_2 + \cos\omega_m t_1 \sin\omega_c t_1 \cos\omega_m t_2 \sin\omega_c t_2\right) \\
&\quad + \frac{8}{N}\sum_{n=1}^{M}\left(\cos\omega_n t_1 \cos\omega_c t_1 \cos\omega_n t_2 \cos\omega_c t_2 + \cos\omega_n t_1 \sin\omega_c t_1 \cos\omega_n t_2 \sin\omega_c t_2\right).
\end{aligned} \tag{3.68}$$

We now use the well-known trigonometric identity

$$\cos(x-y) = \cos x \cos y + \sin x \sin y$$

in equation (3.68) to obtain

$$\begin{aligned}
&\mathscr{R}_{\tilde{R}\tilde{R}}(t_1,t_2) = \\
&= \frac{4}{N}\cos\omega_m t_1 \cos\omega_m t_2 \cos\omega_c(t_2-t_1) + \frac{8}{N}\sum_{n=1}^{M}\cos\omega_n t_1 \cos\omega_n t_2 \cos\omega_c(t_2-t_1) \\
&= \frac{4}{N}\left(\cos\omega_m t_1 \cos\omega_m t_2 + 2\sum_{n=1}^{M}\cos\omega_n t_1 \cos\omega_n t_2\right)\cos\omega_c(t_2-t_1).
\end{aligned} \tag{3.69}$$

We can re-write the autocorrelation obtained above in a slightly different form, by using the trigonometric identity of equation (3.41), to obtain

$$\begin{aligned}
&\mathscr{R}_{\tilde{R}\tilde{R}}(t_1,t_2) = E\{\tilde{R}(t_1)\tilde{R}(t_2)\} \\
&= \frac{2}{N}\cos\omega_c(t_2-t_1)\left[\cos\omega_m(t_2-t_1) + \cos\omega_m(t_2+t_1)\right] \\
&\quad + \frac{4}{N}\cos\omega_c(t_2-t_1)\sum_{n=1}^{M}\left[\cos\omega_n(t_2-t_1) + \cos\omega_n(t_2+t_1)\right].
\end{aligned} \tag{3.70}$$

Note that

$$\begin{aligned}
\mathscr{R}_{\tilde{R}\tilde{R}}(t,t) &= \frac{2}{N}(1+\cos 2\omega_m t) + \frac{4}{N}\sum_{n=1}^{M}(1+\cos 2\omega_n t) \\
&= \frac{4M+2}{N} + \frac{2}{N}\left(\cos 2\omega_m t + 2\sum_{n=1}^{M}\cos 2\omega_n t\right) \\
&\to 1 + J_0(2\omega_m t)
\end{aligned} \tag{3.71}$$

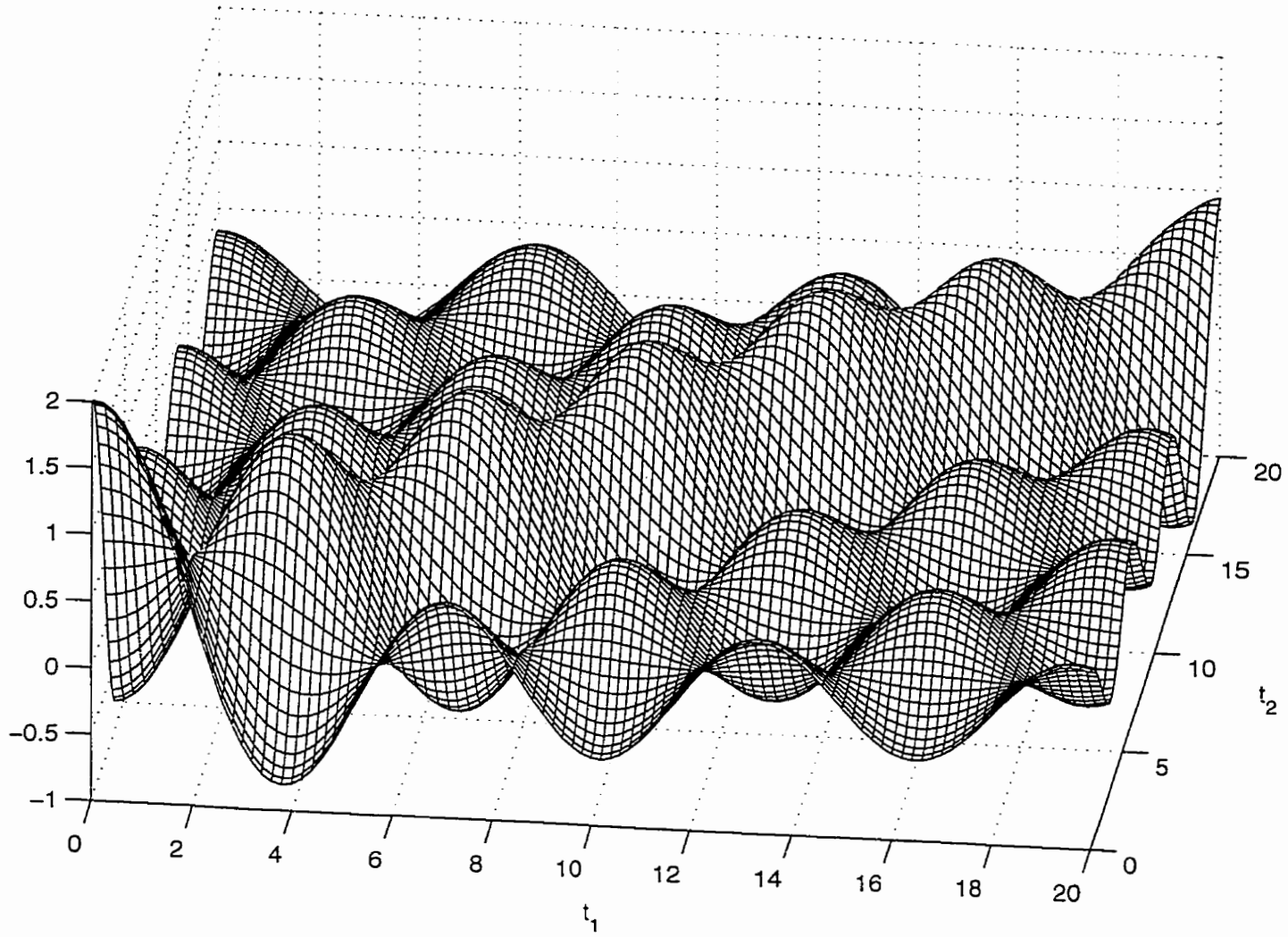

Figure 3.7. Lowpass equivalent form of the autocorrelation function of $\tilde{R}(t)$, for $M = 8$ corresponding to $N = 34$ in Figure 3.6, and $\omega_m = 1$.

as $N \to \infty$, or equivalently $M \to \infty$, where we have used [23, eq. (1.7-10)] to determine the limit of the sum. That is, the variance of the stochastic process $\tilde{R}(t)$ is time-variant, as already observed in Subsection 3.1.2.

A plot of the lowpass equivalent form of the autocorrelation function produced by Jakes' simulator is given in Figure 3.7. Upon comparing Figure 3.6 and Figure 3.7, the non-stationary character of the signal produced by Jakes' simulator is readily obvious. In particular, note that unlike the autocorrelation of Figure 3.6, the autocorrelation depicted in Figure 3.7 does not exhibit translational invariance along the line $t_1 = t_2$.

Furthermore, the form of equation (3.70) emphasizes the dependence of the autocorrelation function of the signal generated by Jakes' simulator $\tilde{R}(t)$ on both the difference $t_2 - t_1$ and the sum $t_2 + t_1$. From this, we are forced to conclude the signal produced by Jakes' simulator is not stationary. Indeed, it is not even wide-sense stationary. Observe that the signal will, in general, not be cyclostationary either, as the frequencies in the fading signal $\tilde{R}(t)$ are incommensurate.

3.2.3 Ergodicity of the fading signal

In this section we analyze some of Pätzold's work and determine whether the fading signals produced by Clarke's model and Jakes' simulator possess ergodicity of the mean and autocorrelation.

A common problem facing the wireless engineer is that of estimating some statistic, i.e., average, of a stochastic process given a small number, usually one, of sample functions. In other words, one uses time averages to estimate statistical ones. In particular, it is of interest to know when time averages are equal to corresponding statistical averages; this is the topic of ergodic theorems [32], [33].

A theorem due to Birkhoff and Khinchin [33, p. 177] states that for ergodic and stationary stochastic processes the sample, i.e., time, averages converge to the statistical averages with probability one. The difficulty in applying this theorem lies in the verification of the ergodicity and stationarity properties. It would seem appropriate that stationarity, in some sense, is required to apply this theorem, and in general, ergodic theorems. That is, averaging over time removes dependence on a time origin. Similarly, the statistics of stationary stochastic processes do not depend on time origin. The ergodicity property is required to ensure that all convergent samples, i.e., time, averages converge to a constant and not to a random variable.

Due to the technical difficulties[5] encountered in the verification of the ergodicity and

[5] Arguments about the ergodicity and stationarity of processes are most easily handled via measure theory. For an excellent treatment of the subject, though outside the scope of this thesis, the reader is directed to [32].

stationarity properties, the wireless engineer is forced to resort to weaker requirements, such as wide-sense stationarity instead of strict stationarity. Correspondingly, the statements one would be able to make would be weaker. Another common approach, often followed in electrical engineering fields, is to classify stochastic processes as possessing ergodicity of nth order if the nth order time average is equal to the nth order statistical average in some sense. For example, stochastic processes whose sample, time-average, mean is equal to the statistical mean are said to possess ergodicity of the mean. Similarly, stochastic processes whose sample, time-average, autocorrelation is equal to the statistical autocorrelation are said to possess ergodicity of the autocorrelation.

In this simpler case, conditions exist which help one determine whether a signal possesses either type of ergodicity. Slutsky's theorem [29, p. 430], for example, states that for wide-sense stationary processes, ergodicity of the mean is guaranteed if the autocorrelation function is bounded and its average value tends to zero. Unfortunately, simple conditions under which ergodicity of the autocorrelation exists are not given; usually, this requires knowledge of fourth-order statistics. In the case of normal processes, however, knowledge of the autocorrelation function is sufficient. This usually means that one has to compute both the statistical autocorrelation and the time-average one to determine whether they are equal. We still need to determine in what sense the time-average autocorrelation converges to the statistical autocorrelation, i.e., we may need to determine the variance of this estimator if its use is to be of any relevance.

Unfortunately, common practice among some wireless engineers is to assume a given stochastic process, such as that representing a multipath fading signal, is both stationary and ergodic. This assumption then serves as justification for replacing statistical averages by time averages. The flaw in this approach is illustrated by Jakes [23] and later by Pätzold [9]. The latter author states that pseudo-random processes can be studied on the basis of time averages providing no explanation why this approach might work. We have already

Also, an excellent introductory text is [33].

shown the signal of Jakes' simulator to be not wide-sense stationary. As such, we would not expect to be able to make any statements about the statistical autocorrelation of the signal produced by the simulator based on a single sample signal.

We begin by determining whether the signal generated by Clarke's model exhibits ergodicity of either the mean or autocorrelation. We have already determined the statistical autocorrelation function for this signal. From equation (3.42) we have

$$\mathscr{R}_R(\tau) = \frac{1}{N}\sum_{n=1}^{N}\cos(\omega_c\tau + \omega_m\tau\cos\alpha_n). \tag{3.72}$$

That is, the fading signal

$$R(t) = \sqrt{\frac{2}{N}}\sum_{n=1}^{N}\cos(\omega_c t + \omega_m t\cos\alpha_n + \Phi_n) \tag{3.73}$$

is at least wide-sense stationary. We also note that

$$\frac{1}{T}\int_0^T \mathscr{R}_R(\tau)d\tau \to 0$$

as $T \to \infty$. Thus, $R(t)$ satisfies Slutsky's theorem [29, eq. (13-7)] and we conclude that $R(t)$ exhibits ergodicity of the mean.

To determine whether $R(t)$ also exhibits ergodicity of the autocorrelation, we need to compute the time-average autocorrelation. To condense the formulae, we make the substitution $\omega_n = \omega_m\cos\alpha_n$. Starting with the definition of the time-average autocorrelation, we have successively

$$\begin{aligned}
\langle R(t)R(t+\tau)\rangle &= \lim_{T\to\infty}\frac{1}{2T}\int_{-T}^{T} R(t)R(t+\tau)dt \\
&= \lim_{T\to\infty}\frac{1}{NT}\int_{-T}^{T}\sum_{n=1}^{N}\sum_{k=1}^{N}\left\{\cos(\omega_c t+\omega_n t+\phi_n)\cos[\omega_c(t+\tau)+\omega_k(t+\tau)+\phi_k)]\right\}dt \\
&= \lim_{T\to\infty}\frac{1}{NT}\int_{-T}^{T}\sum_{n=1}^{N}\sum_{k=1}^{N}\{[\cos\phi_n\cos(\omega_c+\omega_n)t - \sin\phi_n\sin(\omega_c+\omega_n)t] \\
&\quad\times\left[\cos\phi_k\cos(\omega_c+\omega_k)(t+\tau) - \sin\phi_k\sin(\omega_c+\omega_k)(t+\tau)\right]\}dt \\
&= \lim_{T\to\infty}\frac{1}{NT}\int_{-T}^{T}\sum_{n=1}^{N}\sum_{k=1}^{N}\{\cos\phi_n\cos\phi_k\cos[(\omega_c+\omega_n)t]\cos[(\omega_c+\omega_k)(t+\tau)] \\
&\quad+\sin\phi_n\sin\phi_k\sin[(\omega_c+\omega_n)t]\sin[(\omega_c+\omega_k)(t+\tau)]
\end{aligned}$$

$$
\begin{aligned}
&- \sin\phi_n \cos\phi_k \sin[(\omega_c+\omega_n)t]\cos[(\omega_c+\omega_k)(t+\tau)] \\
&- \cos\phi_n \sin\phi_k \cos[(\omega_c+\omega_n)t]\sin[(\omega_c+\omega_k)(t+\tau)]\}dt \\
&= \lim_{T\to\infty}\frac{1}{NT}\int_{-T}^{T}\sum_{n=1}^{N}\sum_{k=1}^{N}\frac{1}{2}\{(\cos\phi_n\cos\phi_k-\sin\phi_n\sin\phi_k) \\
&\times\cos[(\omega_c+\omega_n)t+(\omega_c+\omega_k)(t+\tau)] \\
&+(\cos\phi_n\cos\phi_k+\sin\phi_n\sin\phi_k)\cos[(\omega_c+\omega_n)t-(\omega_c+\omega_k)(t+\tau)] \\
&-(\sin\phi_n\cos\phi_k+\cos\phi_n\sin\phi_k)\sin[(\omega_c+\omega_n)t+(\omega_c+\omega_k)(t+\tau)] \\
&-(\sin\phi_n\cos\phi_k-\cos\phi_n\sin\phi_k)\sin[(\omega_c+\omega_n)t-(\omega_c+\omega_k)(t+\tau)]\}dt \\
&= \frac{1}{N}\lim_{T\to\infty}\frac{1}{2T}\int_{-T}^{T}\sum_{n=1}^{N}\sum_{k=1}^{N}\{(\cos\phi_n\cos\phi_k-\sin\phi_n\sin\phi_k) \\
&\times\cos[(\omega_c+\omega_k)\tau]\cos[(2\omega_c+\omega_n+\omega_k)t] \\
&-(\cos\phi_n\cos\phi_k-\sin\phi_n\sin\phi_k)\sin[(\omega_c+\omega_k)\tau]\sin[(2\omega_c+\omega_n+\omega_k)t] \\
&+(\cos\phi_n\cos\phi_k+\sin\phi_n\sin\phi_k)\cos[(\omega_c+\omega_k)\tau]\cos[(\omega_n-\omega_k)t] \\
&+(\cos\phi_n\cos\phi_k+\sin\phi_n\sin\phi_k)\sin[(\omega_c+\omega_k)\tau]\sin[(\omega_n-\omega_k)t] \\
&-(\sin\phi_n\cos\phi_k+\cos\phi_n\sin\phi_k)\cos[(\omega_c+\omega_k)\tau]\sin[(2\omega_c+\omega_n+\omega_k)t] \\
&-(\sin\phi_n\cos\phi_k+\cos\phi_n\sin\phi_k)\sin[(\omega_c+\omega_k)\tau]\cos[(2\omega_c+\omega_n+\omega_k)t] \\
&-(\sin\phi_n\cos\phi_k-\cos\phi_n\sin\phi_k)\cos[(\omega_c+\omega_k)\tau]\sin[(\omega_n-\omega_k)t] \\
&+(\sin\phi_n\cos\phi_k-\cos\phi_n\sin\phi_k)\sin[(\omega_c+\omega_k)\tau]\cos[(\omega_n-\omega_k)t]\}dt. \qquad (3.74)
\end{aligned}
$$

We recognize we are dealing with integrals of the form

$$
\lim_{T\to\infty}\frac{1}{2T}\int_{-T}^{T}a\cos btdt=\begin{cases}0 & \text{if } b\neq 0,\\ a & \text{if } b=0,\end{cases} \qquad (3.75a)
$$

and

$$
\lim_{T\to\infty}\frac{1}{2T}\int_{-T}^{T}a\sin btdt=0. \qquad (3.75b)
$$

The second integral is always zero because it is the integral of an odd function, $\sin(\cdot)$, over an interval symmetric about 0.

Substituting the identities of equations (3.75a) and (3.75b) into equation (3.74), we note the only terms which remain are those which contain only $\cos[(\omega_n-\omega_k)t]$, and for which

$k = n$. Thus, we have

$$\begin{aligned}
&\langle R(t)R(t+\tau)\rangle \\
&= \frac{1}{N}\sum_{n=1}^{N}\left\{(\cos^2\phi_n + \sin^2\phi_n)\cos[(\omega_c+\omega_n)\tau]\right. \\
&\quad \left. + (\sin\phi_n\cos\phi_n - \cos\phi_n\sin\phi_n)\sin[(\omega_c+\omega_n)\tau]\right\} \\
&= \frac{1}{N}\sum_{n=1}^{N}\cos[(\omega_c+\omega_n)\tau]. \qquad (3.76)
\end{aligned}$$

Upon comparison of equation (3.42) and equation (3.76), and observing that $t_2 - t_1 = \tau$ and $\omega_n = \omega_m \cos\alpha_n$, we note the two averages are equal, i.e.

$$\langle R(t)R(t+\tau)\rangle = \mathscr{R}_R(\tau).$$

Note that we have made no attempt to compute the variance of the time-average autocorrelation.

We may attempt to simplify equation (3.76) in a manner similar to the simplification of equation (3.42). Recall that the α_n's represent the angles of arrivals of the components of the multipath signal and that in the case of Jakes' simulator they are uniformly spaced around the unit circle, i.e.

$$\alpha_n = \frac{2\pi n}{N}, \quad n = 1,\ldots,N.$$

From equation (3.43) it follows that summations of the form

$$\sum_{n=1}^{N}\sin(\omega_m\tau\cos 2\pi n/N) = 0$$

for N even. For N odd, the sum is approximately 0 for $0 \le \omega_m\tau \le N/2$. Thus, for N even, we may simplify equation (3.76) to

$$\begin{aligned}
&\langle R(t)R(t+\tau)\rangle = \\
&= \frac{1}{N}\left\{\left[\sum_{n=1}^{N}\cos(\omega_m\tau\cos\alpha_n)\right]\cos\omega_c\tau - \left[\sum_{n=1}^{N}\sin(\omega_m\tau\cos\alpha_n)\right]\sin\omega_c\tau\right\} \\
&= \frac{1}{N}\left[\sum_{n=1}^{N}\cos(\omega_m\tau\cos\alpha_n)\right]\cos(\omega_c\tau). \qquad (3.77)
\end{aligned}$$

Jakes [23] notes that the summation appearing in equation (3.77), inside the square brackets, is an approximation to the $J_0(\omega_m \tau)$ encountered in the theoretical model. Note that the approximation of equation (3.48) is identical to the approximation of equation (3.77).

We now turn our attention to the case of Jakes' simulator. We have already computed the statistical autocorrelation of the signal produced by Jakes' simulator. From equation (3.70) we have

$$\begin{aligned}
&\mathscr{R}_{\tilde{R}\tilde{R}}(t_1, t_2) = \\
&= \frac{2}{N} \cos \omega_c (t_2 - t_1) \left[\cos \omega_m (t_2 - t_1) + \cos \omega_m (t_2 + t_1) \right] \\
&\quad + \frac{4}{N} \cos \omega_c (t_2 - t_1) \sum_{n=1}^{M} \left[\cos \omega_n (t_2 - t_1) + \cos \omega_n (t_2 + t_1) \right],
\end{aligned}$$

showing that the signal produced by Jakes' simulator is not wide-sense stationary. At this point, we note that the wide-sense stationarity condition required to establish ergodicity of the mean or autocorrelation is not met. It may well be that the sample, i.e., time averages, converge to some value, possibly a random variable, but they may not be reliable estimators for the appropriate statistical averages. This is made obvious in the case of the autocorrelation. Note that the statistical autocorrelation $\mathscr{R}_{\tilde{R}\tilde{R}}(t_1, t_2)$ is a function of two variables, while the time-average autocorrelation is a function of only one.

For the sake of completeness, we give below the time-average mean and autocorrelation functions. It is readily observed that

$$\begin{aligned}
\langle \tilde{R}(t) \rangle &= \frac{2}{\sqrt{N}} \lim_{T \to \infty} \int_{-T}^{T} \tilde{R}(t) dt \\
&= \lim_{T \to \infty} \int_{-T}^{T} \cos \omega_c t \left(\sqrt{2} \cos B_{M+1} \cos \omega_m t + 2 \sum_{n=1}^{M} \cos B_n \cos \omega_n t \right) \\
&\quad + \sin \omega_c t \left(\sqrt{2} \sin B_{M+1} \cos \omega_m t + 2 \sum_{n=1}^{M} \sin B_n \cos \omega_n t \right) dt \\
&= 0.
\end{aligned}$$

Pätzold [9], determines the time-average autocorrelation for the fading signal generated by Jakes' simulator. First, he obtains the time-average autocorrelation of the in-phase and

quadrature components

$$\langle \tilde{X}_c(t)\tilde{X}_c(t+\tau)\rangle^{LP} = \frac{4}{N}\left(\frac{\cos^2\beta_{M+1}}{2}\cos\omega_m\tau + \sum_{n=1}^{M}\cos^2\beta_n\cos\omega_n\tau\right), \tag{3.78}$$

and

$$\langle \tilde{X}_s(t)\tilde{X}_s(t+\tau)\rangle^{LP} = \frac{4}{N}\left(\frac{\sin^2\beta_{M+1}}{2}\cos\omega_m\tau + \sum_{n=1}^{M}\sin^2\beta_n\cos\omega_n\tau\right). \tag{3.79}$$

Here the superscript *LP* is used to emphasize the autocorrelations under consideration are in lowpass equivalent form. To obtain the time-average autocorrelation of the fading signal, Pätzold observes

$$\begin{aligned}\langle \tilde{R}(t)\tilde{R}(t+\tau)\rangle^{LP} &= \langle \tilde{X}_c(t)\tilde{X}_c(t+\tau)\rangle^{LP} + \langle \tilde{X}_s(t)\tilde{X}_s(t+\tau)\rangle^{LP} \\ &= \frac{2}{N}\cos\omega_m\tau + \frac{4}{N}\sum_{n=1}^{M}\cos\omega_n\tau,\end{aligned} \tag{3.80}$$

where $\tau = t_2 - t_1$. The autocorrelation of equation (3.80) is the lowpass equivalent form of the time-average autocorrelation. The corresponding bandpass equivalent is

$$\langle \tilde{R}(t)\tilde{R}(t+\tau)\rangle = \frac{2}{N}\cos\omega_c\tau\left(\cos\omega_m\tau + 2\sum_{n=1}^{M}\cos\omega_n\tau\right). \tag{3.81}$$

Comparing the statistical average autocorrelation of equation (3.70), to the time-average autocorrelation of equation (3.81), it is immediately obvious that the two averages do not agree. This illustrates that, in general, one can not study the statistical nature of a (pseudo)random process based upon time averages. In other words, one can not readily substitute time averages for statistical ones.

In the introduction, we made a passing remark that some authors [5], [9] have argued Jakes' simulator does not work properly because the in-phase and quadrature components are correlated. Such arguments are based on showing that the time-average cross-correlation of the two components is non-zero. We have already discussed that in the case of Jakes' simulator replacement of statistical averages by time averages is not warranted. To further illustrate this point, we compute the statistical cross-correlation below. Starting

with the definition, we have

$$\begin{aligned}
\mathcal{R}_{\tilde{X}_c\tilde{X}_s}(t_1,t_2) &= E\{\tilde{X}_c(t_1)\tilde{X}_s(t_2)\} \\
&= \frac{4}{N}E\left\{\left(\sqrt{2}\cos B_{M+1}\cos\omega_m t_1 + 2\sum_{n=1}^{M}\cos B_n\cos\omega_n t_1\right)\right. \\
&\quad \left.\times\left(\sqrt{2}\sin B_{M+1}\cos\omega_m t_2 + 2\sum_{n=1}^{M}\sin B_n\cos\omega_n t_2\right)\right\} \\
&= 0,
\end{aligned}$$

where we have used the fact

$$E\{\cos B_n \sin B_k\} = 0, \quad 1 \le k,n \le M+1.$$

In conclusion, we found that the signal produced by Clarke's model exhibits ergodicity of the mean and may also exhibit ergodicity of the autocorrelation, although this is not explicitly shown in this thesis. We also found that the signal produced by Jakes' simulator does not exhibit ergodicity of either mean or autocorrelation; this is due to the non-stationary nature of the signal produced by Jakes' simulator. Note, however, that despite the fact that the signal is not wide-sense stationary, the sample average still converges to a constant, and may be used as an estimate to the statistical average.

3.3 Summary

In this chapter we have analyzed the statistical properties of sum-of-sinusoids models and simulators. We have derived a result which may be used to compute the envelope and phase pdf's of sum-of-sinusoids simulators. The derivation is based on determining the pdf of the sum of independent two-dimensional random vectors. We then applied this result to obtain the first order pdf's for the signals produced by Clarke's model and Jakes' simulator, i.e., the envelope and phase pdf's.

We have found that as long as the fading signal produced by the model or simulator can be written as a sum of circularly symmetric vectors, the phase pdf is uniform over

$[0, 2\pi]$. This result contradicts the one given by Pätzold in [9]. The flaw in Pätzold's work lies in the fact that he substitutes time averages for statistical averages seemingly without justification. Furthermore, we have found that the envelope pdf of the signal produced by Clarke's model does not evolve with time, while the envelope pdf of the signal produced by Jakes' simulator does.

We then turned our attention to the computation of the statistical autocorrelations of the signals produced by Clarke's model and Jakes' simulator. As expected, we have found that the signal produced by Clarke's model is wide-sense stationary, whereas that produced by Jakes' simulator is not.

The chapter ends with a discussion of ergodicity and whether it applies in either the case of Clarke's model or Jakes' simulator. We note that, in general, substitution of time averages for statistical ones requires the stochastic process be at least wide-sense stationary. The flaw in Pätzold's work is made obvious at this point: he does not check whether the signal produced by Jakes' simulator is wide-sense stationary. We found that the signal produced by Clarke's model exhibits ergodicity of mean and autocorrelation. The signal produced by Jakes' simulator does not exhibit ergodicity of either mean or autocorrelation. However, the sample average of the signal produced by Jakes' simulator does equal the statistical average. As such, the sample average may be used as an estimator for the statistical average.

We conclude by observing that Jakes' simulator does not reproduce the fading signal of Clarke's model. We attribute this shortcoming of the simulator to design flaws. In the next chapter, we attempt to obtain a better understanding of these flaws as well as possibly improve the simulator's performance.

Chapter 4

Improving Jakes' Simulator

We have seen in Section 3.2.2 that the simulator developed by Jakes in [23] provides a non-stationary fading signal. In turn, this makes estimation of statistical parameters through time averages meaningless, as illustrated in Subsection 3.2.3. In this chapter, we try to implement some simple modifications to Jakes' simulator in order to improve its performance. The improvement is based on generating a wide-sense stationary fading signal. We will see that, in general, a reduction of terms as performed by Jakes, will always lead to stationarity problems. However, in cases where the angles of arrival are spaced uniformly and symmetrically around the unit circle, the number of low-frequency oscillators required is reduced. This reduction is a direct consequence of the periodicity and symmetry of the $\cos(\cdot)$ function. The phase shifts of the N waves, however, will all need to be included as appropriate gains for each low-frequency oscillator. This procedure is outlined in the last section of this chapter.

4.1 Understanding Jakes' assumptions

In Subsection 3.2.2 we have seen that the signal generated by Jakes' fading channel simulator is not wide-sense stationary. An obvious question to ask is whether the simulator can be slightly modified such that the signal becomes wide-sense stationary. Then, Jakes approach would have merit in that it would provide the wireless engineer with an efficient method for generating fading waveforms. The efficiency is achieved by needing to

use fewer low-frequency oscillators than Clarke's model, i.e., the simulator would need roughly $N/4$ sinusoids, whereas the model contains N.

In general, the fading signal can be written as

$$R(t) = \sqrt{2} \sum_{n=1}^{N} C_n \cos(\omega_c t + \omega_m t \cos A_n + \Phi_n), \tag{4.1}$$

where the C_n's, A_n's, and Φ_n's are random variables, i.e., the model possesses $3N$ degrees of freedom. This is the same signal as that of equation (2.6); we copy it here for ease of reference. A physical interpretation of equation (4.1) is that the received signal is a superposition of N cosine waves. We recall that the C_n can be interpreted as the signal attenuation experienced by the nth signal component, the A_n as the direction of the arrival of the nth component, and the Φ_n as the phase shift of the nth component. In its most general form, the expression for $R(t)$ can not be further simplified without losing some degrees of freedom. If we assume, as Jakes did, that there is some symmetry to the problem, we may be able to simplify the above expression; however, we would still incur a loss of degrees of freedom. Observe that the model of equation (4.1) may be sufficient to model any fading signal. However, we are interested in modelling flat fading signals; it might be the case that for such models, we require fewer than $3N$ degrees of freedom.

We follow Gilbert [2] and assume first that the A_n's are equally spaced around the unit circle. Next, we select the C_n's equal and time-invariant. Gilbert notes that the choice of path attenuation is not unique. Thus, one might wish to select the C_n's from a Rayleigh distribution. The limiting result, Gilbert points out, is the same regardless of the distribution of the C_n's. The choice of equal and time-invariant path attenuations may be justified on physical grounds. For example, it may be the case that the environment surrounding the transmitter and receiver is similar, i.e., same building density and similar building materials. Furthermore, the nature of the flat fading channel dictates that the channel parameters, including the path attenuations, do not change over the duration of the message. It should also be noted that the results obtained in this thesis can be easily generalized for other

distributions of C_n. These two assumptions taken together state that the received energy density at the mobile is constant, an earmark of Rayleigh flat fading channels. In addition, as we have seen in Section 2.2, Jakes makes similar assumptions, i.e., he selects C_n and A_n according to

$$C_n = \frac{1}{\sqrt{N}} \tag{4.2}$$

and

$$A_n = \frac{2\pi n}{N}. \tag{4.3}$$

While the restrictions above reduce the number and type of fading signals we may model, the set of reduced signals still includes flat fading. Otherwise put, Rayleigh flat fading channels are characterized by uniform power density around the receiver.

With these assumptions in hand, we may re-write the fading signal (4.1) as

$$R(t) = \sqrt{\frac{2}{N}} \sum_{n=1}^{N} \cos(\omega_c t + \omega_m t \cos \frac{2\pi n}{N} + \Phi_n). \tag{4.4}$$

We note that we have gone from a signal with $3N$ degrees of freedom, the general case, to one with N degrees of freedom, a smaller class of signals still including flat fading. We did not make any assumptions about the phase shifts Φ_n.

A further assumption made by Jakes, is that N is of the form $4M+2$; this forces a certain symmetry and therefore allows for the reduction in the number of low-frequency oscillators needed. That is, the arriving rays are symmetric about both the x- and y-axes. Essentially, this assumption limits the number of distinct Doppler frequency shifts from N values to $M+1$. This will become a little more obvious in the development of the following formulae.

We start by decomposing $R(t)$ into orthogonal components

$$\begin{aligned} R(t) &= \sqrt{\frac{2}{N}} \sum_{n=1}^{N} \cos(\omega_c t + \omega_m t \cos \frac{2\pi n}{N} + \Phi_n) \\ &= \cos \omega_c t \sqrt{\frac{2}{N}} \sum_{n=1}^{N} \cos(\omega_m t \cos \frac{2\pi n}{N} + \Phi_n) \end{aligned}$$

$$
\begin{aligned}
&\quad - \sin\omega_c t \sqrt{\frac{2}{N}} \sum_{n=1}^{N} \sin(\omega_m t \cos\frac{2\pi n}{N} + \Phi_n) \\
&= X_c(t)\cos\omega_c t - X_s(t)\sin\omega_c t. \qquad (4.5)
\end{aligned}
$$

We now look at each of the in-phase and quadrature components. Starting with the in-phase one, we have

$$
\begin{aligned}
X_c(t) &= \sqrt{\frac{2}{N}} \sum_{n=1}^{N} \cos(\omega_m t \cos\frac{2\pi n}{N} + \Phi_n) \\
&= \sqrt{\frac{2}{N}} \sum_{n=1}^{N} \left[\cos(\omega_m t \cos\frac{2\pi n}{N})\cos\Phi_n - \sin(\omega_m t \cos\frac{2\pi n}{N})\sin\Phi_n\right] \\
&= \sqrt{\frac{2}{N}} \sum_{n=1}^{M} \left[\cos(\omega_m t \cos\frac{2\pi n}{N})\cos\Phi_n\right] \\
&\quad - \sqrt{\frac{2}{N}} \sum_{n=1}^{M} \left[\sin(\omega_m t \cos\frac{2\pi n}{N})\sin\Phi_n\right] \\
&\quad + \sqrt{\frac{2}{N}} \sum_{n=1}^{M} \left[\cos(\omega_m t \cos\frac{2\pi(2M+1-n)}{N})\cos\Phi_{2M+1-n}\right] \\
&\quad - \sqrt{\frac{2}{N}} \sum_{n=1}^{M} \left[\sin(\omega_m t \cos\frac{2\pi(2M+1-n)}{N})\sin\Phi_{2M+1-n}\right] \\
&\quad + \sqrt{\frac{2}{N}} \left[\cos(\omega_m t \cos\pi)\cos\Phi_{2M+1} - \sin(\omega_m t \cos\pi)\sin\Phi_{2M+1}\right] \\
&\quad + \sqrt{\frac{2}{N}} \sum_{n=1}^{M} \left[\cos(\omega_m t \cos\frac{2\pi(2M+1+n)}{N})\cos\Phi_{2M+1+n}\right] \\
&\quad - \sqrt{\frac{2}{N}} \sum_{n=1}^{M} \left[\sin(\omega_m t \cos\frac{2\pi(2M+1+n)}{N})\sin\Phi_{2M+1+n}\right] \\
&\quad + \sqrt{\frac{2}{N}} \sum_{n=1}^{M} \left[\cos(\omega_m t \cos\frac{2\pi(4M+2-n)}{N})\cos\Phi_{4M+2-n}\right] \\
&\quad - \sqrt{\frac{2}{N}} \sum_{n=1}^{M} \left[\sin(\omega_m t \cos\frac{2\pi(4M+2-n)}{N})\sin\Phi_{4M+2-n}\right] \\
&\quad + \sqrt{\frac{2}{N}} \left[\cos(\omega_m t \cos 2\pi)\cos\Phi_{4M+2} - \sin(\omega_m t \cos 2\pi)\sin\Phi_{4M+2}\right]. \qquad (4.6)
\end{aligned}
$$

We can make use of the following identities, which follow from the periodicity properties of the $\cos(\cdot)$ function

$$
\cos\frac{2\pi(2M+1-n)}{4M+2} = -\cos\frac{2\pi n}{N},
$$

$$\cos\frac{2\pi(2M+1+n)}{4M+2} = -\cos\frac{2\pi n}{N},$$

and

$$\cos\frac{2\pi(4M+2-n)}{4M+2} = \cos\frac{2\pi n}{N},$$

to further simplify the expression for $X_c(t)$. With these identities, we can simplify equation (4.6) to

$$\begin{aligned}
X_c(t) = & \sqrt{\frac{2}{N}}\sum_{n=1}^{M}\left[\cos(\omega_m t\cos\frac{2\pi n}{N})\cos\Phi_n - \sin(\omega_m t\cos\frac{2\pi n}{N})\sin\Phi_n\right] \\
& + \sqrt{\frac{2}{N}}\sum_{n=1}^{M}\left[\cos(\omega_m t\cos\frac{2\pi n}{N})\cos\Phi_{2M+1-n} + \sin(\omega_m t\cos\frac{2\pi n}{N})\sin\Phi_{2M+1-n}\right] \\
& + \sqrt{\frac{2}{N}}\sum_{n=1}^{M}\left[\cos(\omega_m t\cos\frac{2\pi n}{N})\cos\Phi_{2M+1+n} + \sin(\omega_m t\cos\frac{2\pi n}{N})\sin\Phi_{2M+1+n}\right] \\
& + \sqrt{\frac{2}{N}}\sum_{n=1}^{M}\left[\cos(\omega_m t\cos\frac{2\pi n}{N})\cos\Phi_{4M+2-n} - \sin(\omega_m t\cos\frac{2\pi n}{N})\sin\Phi_{4M+2-n}\right] \\
& + \sqrt{\frac{2}{N}}\cos(\omega_m t)\cos\Phi_{2M+1} + \sqrt{\frac{2}{N}}\sin(\omega_m t)\sin\Phi_{2M+1} \\
& + \sqrt{\frac{2}{N}}\cos(\omega_m t)\cos\Phi_{4M+2} - \sqrt{\frac{2}{N}}\sin(\omega_m t)\sin\Phi_{4M+2}. \qquad (4.7)
\end{aligned}$$

Substituting $\omega_n = \omega_m \cos\frac{2\pi n}{N}$ in equation (4.7) yields

$$\begin{aligned}
X_c(t) = & \sqrt{\frac{2}{N}}\sum_{n=1}^{M}\left(\cos\Phi_n + \cos\Phi_{2M+1-n} + \cos\Phi_{2M+1+n} + \cos\Phi_{4M+2-n}\right)\cos\omega_n t \\
& - \sqrt{\frac{2}{N}}\sum_{n=1}^{M}\left(\sin\Phi_n - \sin\Phi_{2M+1-n} - \sin\Phi_{2M+1+n} + \sin\Phi_{4M+2-n}\right)\sin\omega_n t \\
& + \sqrt{\frac{2}{N}}(\cos\Phi_{2M+1} + \cos\Phi_{4M+2})\cos\omega_m t \\
& + \sqrt{\frac{2}{N}}(\sin\Phi_{2M+1} - \sin\Phi_{4M+2})\sin\omega_m t. \qquad (4.8)
\end{aligned}$$

Similarly, for $X_s(t)$ we can write

$$\begin{aligned}
X_s(t) &= \sqrt{\frac{2}{N}}\sum_{n=1}^{N}\sin(\omega_m t\cos\frac{2\pi n}{N} + \Phi_n) \\
&= \sqrt{\frac{2}{N}}\sum_{n=1}^{N}\left[\sin(\omega_m t\cos\frac{2\pi n}{N})\cos\Phi_n + \cos(\omega_m t\cos\frac{2\pi n}{N})\sin\Phi_n\right]
\end{aligned}$$

$$= \sqrt{\frac{2}{N}} \sum_{n=1}^{M} \left(\cos\Phi_n - \cos\Phi_{2M+1-n} - \cos\Phi_{2M+1+n} + \cos\Phi_{4M+2-n}\right) \sin\omega_n t$$
$$+ \sqrt{\frac{2}{N}} \sum_{n=1}^{M} \left(\sin\Phi_n + \sin\Phi_{2M+1-n} + \sin\Phi_{2M+1+n} + \sin\Phi_{4M+2-n}\right) \cos\omega_n t$$
$$- \sqrt{\frac{2}{N}} (\cos\Phi_{2M+1} - \cos\Phi_{4M+2}) \sin\omega_m t$$
$$+ \sqrt{\frac{2}{N}} (\sin\Phi_{2M+1} + \sin\Phi_{4M+2}) \cos\omega_m t. \tag{4.9}$$

It is interesting to note that if we substitute

$$\Phi_n = \Phi_{2M+1-n} = \Phi_{2M+1+n} = \Phi_{4M+2-n} = B_n, \quad \text{for } n = 1, \ldots, M, \tag{4.10a}$$

and

$$\Phi_{2M+1} = \Phi_{4M+2} = B_{M+1}, \tag{4.10b}$$

in equations (4.8) and (4.9), we end up with a simulator similar to Jakes' fading channel simulator. That is, $X_c(t)$ reduces to

$$X_c(t) = \frac{2\sqrt{2}}{\sqrt{N}} \cos\Phi_{4M+2} \cos\omega_m t + \frac{4\sqrt{2}}{\sqrt{N}} \sum_{n=1}^{M} \cos\Phi_n \cos\omega_n t. \tag{4.11a}$$

The corresponding in-phase component generated by Jakes' simulator is

$$\tilde{X}_c(t) = \frac{2\sqrt{2}}{\sqrt{N}} \cos B_{M+1} \cos\omega_m t + \frac{4}{\sqrt{N}} \sum_{n=1}^{M} \cos B_n \cos\omega_n t. \tag{4.11b}$$

Similarly, $X_s(t)$ reduces to

$$X_s(t) = \frac{2\sqrt{2}}{\sqrt{N}} \sin\Phi_{4M+2} \cos\omega_m t + \frac{4\sqrt{2}}{\sqrt{N}} \sum_{n=1}^{M} \sin\Phi_n \cos\omega_n t, \tag{4.12a}$$

The corresponding quadrature component generated by Jakes' simulator is

$$\tilde{X}_s(t) = \frac{2\sqrt{2}}{\sqrt{N}} \sin B_{M+1} \cos\omega_m t + \frac{4}{\sqrt{N}} \sum_{n=1}^{M} \sin B_n \cos\omega_n t. \tag{4.12b}$$

Comparing equations (4.11a) and (4.11b) and equations (4.12a) and (4.12b), we observe a discrepancy in the oscillator gains. This is easily explained if we observe that Jakes' development culminating with equations (4.11b) and (4.12b) was carried out under the constraint that the simplified signal have unity power. There was no such constraint placed on the development leading to equations (4.11a) and (4.12a).

4.2 A first attempt at improving Jakes' simulator

The first fix we propose is the introduction of sine terms, as illustrated in Figure 4.1. The interested reader might want to compare this to the block diagram of Figure 2.3.

We justify this choice by observing the fading signal

$$\begin{aligned} R(t) &= \sqrt{\frac{2}{N}} \sum_{n=1}^{N} \cos(\omega_c t + \omega_m t \cos\alpha_n + \Phi_n) \\ &= \sqrt{\frac{2}{N}} \left\{ \cos(\omega_c t) \sum_{n=1}^{N} \cos(\omega_n t + \Phi_n) - \sin(\omega_c t) \sum_{n=1}^{N} \sin(\omega_n t + \Phi_n) \right\}. \end{aligned} \tag{4.13}$$

That is, the lowpass equivalent signal

$$\begin{aligned} R^{LP}(t) &= \sqrt{\frac{2}{N}} \sum_{n=1}^{N} \cos(\omega_m t \cos\alpha_n + \Phi_n) \\ &= \sqrt{\frac{2}{N}} \left\{ \sum_{n=1}^{N} \cos\Phi_n \cos\omega_n t - \sum_{n=1}^{N} \sin\Phi_n \sin\omega_n t \right\}, \end{aligned} \tag{4.14}$$

includes both sine and cosine terms.

From Figure 4.1, we can write the new simulator signal, subject to the constraint that it have unit power, as

$$\begin{aligned} \tilde{R}_1(t) &= \cos(\omega_c t)\tilde{X}_{1c}(t) + \sin(\omega_c t)\tilde{X}_{1s}(t) \\ &= \frac{2}{\sqrt{N}} \cos\omega_c t \left(\sqrt{2}\cos B_{M+1} \cos\omega_m t + 2\sum_{n=1}^{M} \cos B_n \cos\omega_n t \right) \\ &\quad + \frac{2}{\sqrt{N}} \sin\omega_c t \left(\sqrt{2}\sin B_{M+1} \sin\omega_m t + 2\sum_{n=1}^{M} \sin B_n \sin\omega_n t \right), \end{aligned} \tag{4.15}$$

where $\omega_n = \omega_m \cos\alpha_n$.

We are interested in determining whether the new signal $\tilde{R}_1(t)$ is wide-sense stationary. As we have seen previously, we can proceed in at least two ways. We can compute the pdf of the envelope of $\tilde{R}_1(t)$ and determine whether this is a function of time. Or we can compute the autocorrelation function $E\{\tilde{R}_1(t_1)\tilde{R}_1(t_2)\}$ and show that this is a function of only $t_2 - t_1$. Here we choose the second method as it is easier.

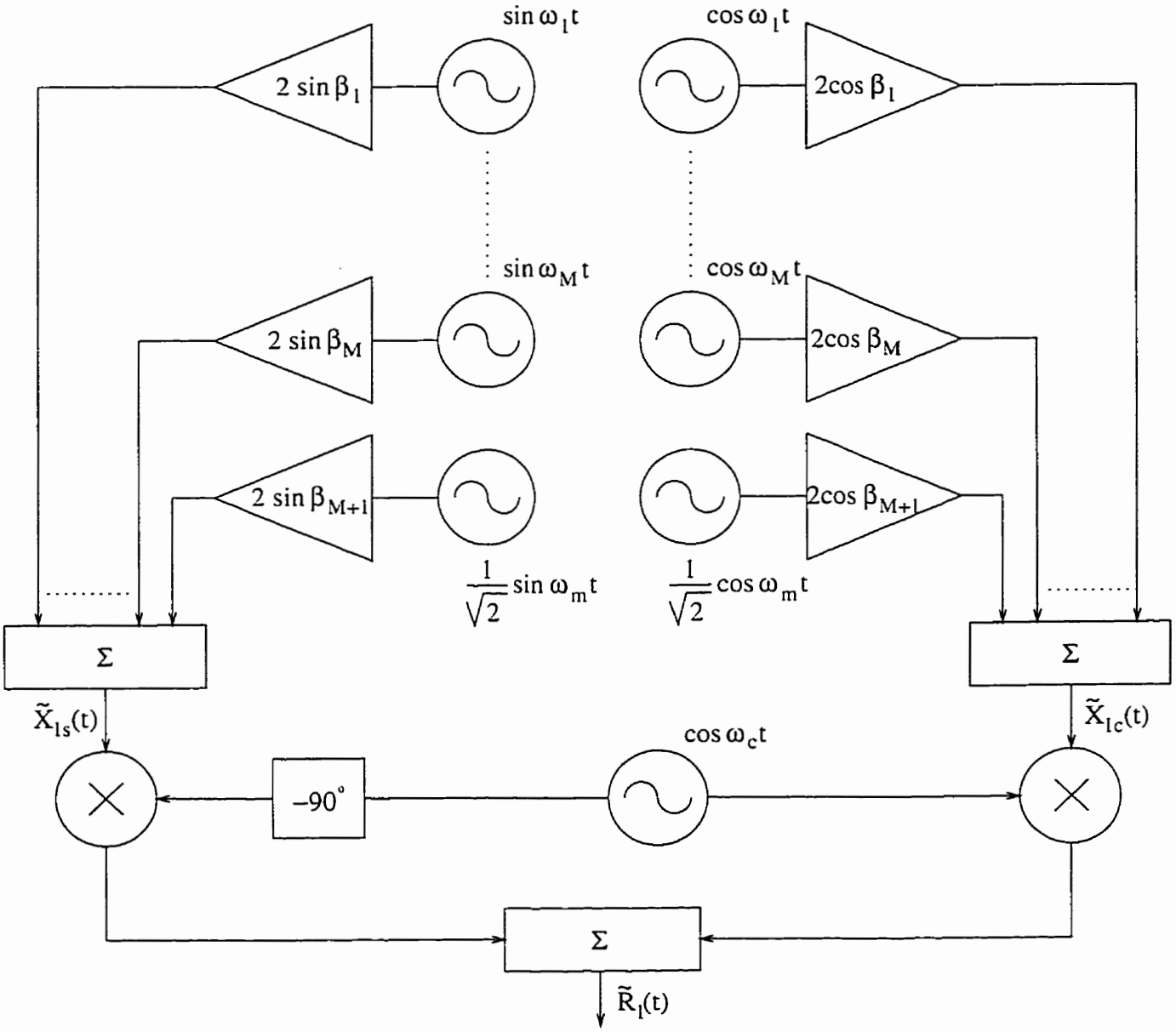

Figure 4.1. Improving Jakes' simulator by the introduction of sine terms.

We note that the random variables $B_1, \ldots, B_{M+1}$, are uniform i.i.d. over $[0, 2\pi]$ as shown in Subsection 2.2.1. We proceed below with the computation of the autocorrelation function, starting from the definition. We have

$$\begin{aligned}
&\mathscr{R}_{\tilde{R}_1\tilde{R}_1}(t_1,t_2) = E\left\{\tilde{R}_1(t_1)\tilde{R}_1(t_2)\right\} \\
&= E\left\{\frac{2}{\sqrt{N}}\left[\cos\omega_c t_1\left(\sqrt{2}\cos B_{M+1}\cos\omega_m t_1 + 2\sum_{n=1}^{M}\cos B_n\cos\omega_n t_1\right)\right.\right. \\
&\quad \left.+\sin\omega_c t_1\left(\sqrt{2}\sin B_{M+1}\sin\omega_m t_1 + 2\sum_{n=1}^{M}\sin B_n\sin\omega_n t_1\right)\right] \\
&\quad \times\frac{2}{\sqrt{N}}\left[\cos\omega_c t_2\left(\sqrt{2}\cos B_{M+1}\cos\omega_m t_2 + 2\sum_{k=1}^{M}\cos B_k\cos\omega_k t_2\right)\right. \\
&\quad \left.\left.+\sin\omega_c t_2\left(\sqrt{2}\sin B_{M+1}\sin\omega_m t_2 + 2\sum_{k=1}^{M}\sin B_k\sin\omega_k t_2\right)\right]\right\}. \qquad (4.16)
\end{aligned}$$

We pause here to compute the required expectations, readily obtainable by direct computation. We have

$$E\{\cos B_n\} = E\{\sin B_n\} = 0, \qquad (4.17)$$

$$E\{\cos B_n \sin B_k\} = 0, \qquad (4.18)$$

$$E\{\cos B_n\cos B_k\} = E\{\sin B_n\sin B_k\} = \begin{cases} \frac{1}{2}, & \text{if } n = k, \\ 0, & \text{otherwise.} \end{cases} \qquad (4.19)$$

With these equalities in hand, we note that the only terms which will appear in the autocorrelation function will be those in which the random variables $B_1, \ldots, B_{M+1}$ appear in terms of the form $\cos^2(\cdot)$ or $\sin^2(\cdot)$. Expanding the brackets in equation (4.16) and then substituting the identities of equations (4.17) – (4.19) yields

$$\begin{aligned}
&\mathscr{R}_{\tilde{R}_1\tilde{R}_1}(t_1,t_2) \\
&= \frac{8}{N}\cos\omega_m t_1\cos\omega_c t_1\cos\omega_m t_2\cos\omega_c t_2 E\{\cos^2 B_{M+1}\} \\
&\quad + \frac{16}{N}\sum_{n=1}^{M}\cos\omega_n t_1\cos\omega_c t_1\cos\omega_n t_2\cos\omega_c t_2 E\{\cos^2 B_n\} \\
&\quad + \frac{8}{N}\sin\omega_m t_1\sin\omega_c t_1\sin\omega_m t_2\sin\omega_c t_2 E\{\sin^2 B_{M+1}\}
\end{aligned}$$

$$
\begin{aligned}
&+\frac{16}{N}\sum_{n=1}^{M}\sin\omega_n t_1\sin\omega_c t_1\sin\omega_n t_2\sin\omega_c t_2 E\{\sin^2 B_n\}\\
&=\frac{4}{N}\cos\omega_m t_1\cos\omega_c t_1\cos\omega_m t_2\cos\omega_c t_2\\
&+\frac{8}{N}\sum_{n=1}^{M}\cos\omega_n t_1\cos\omega_c t_1\cos\omega_n t_2\cos\omega_c t_2\\
&+\frac{4}{N}\sin\omega_m t_1\sin\omega_c t_1\sin\omega_m t_2\sin\omega_c t_2\\
&+\frac{8}{N}\sum_{n=1}^{M}\sin\omega_n t_1\sin\omega_c t_1\sin\omega_n t_2\sin\omega_c t_2\\
&=\frac{2}{N}\left[\cos\omega_m(t_2-t_1)+2\sum_{n=1}^{M}\cos\omega_n(t_2-t_1)\right]\cos\omega_c(t_2-t_1)\\
&+\frac{2}{N}\left[\cos\omega_m(t_2+t_1)+2\sum_{n=1}^{M}\cos\omega_n(t_2+t_1)\right]\cos\omega_c(t_2+t_1). \qquad (4.20)
\end{aligned}
$$

For comparison purposes, we also give the autocorrelation of the signal produced by Jakes' simulator. It is

$$
\begin{aligned}
&\mathscr{R}_{\tilde{R}\tilde{R}}(t_1,t_2)=E\{\tilde{R}(t_1)\tilde{R}(t_2)\}\\
&=\frac{2}{N}\left[\cos\omega_m(t_2-t_1)+\cos\omega_m(t_2+t_1)\right]\cos\omega_c(t_2-t_1)\\
&+\frac{4}{N}\sum_{n=1}^{M}\left[\cos\omega_n(t_2-t_1)+\cos\omega_n(t_2+t_1)\right]\cos\omega_c(t_2-t_1)\\
&=\frac{2}{N}\left[\cos\omega_m(t_2-t_1)+2\sum_{n=1}^{M}\cos\omega_n(t_2-t_1)\right]\cos\omega_c(t_2-t_1)\\
&+\frac{2}{N}\left[\cos\omega_m(t_2+t_1)+2\sum_{n=1}^{M}\cos\omega_n(t_2+t_1)\right]\cos\omega_c(t_2-t_1). \qquad (4.21)
\end{aligned}
$$

We observe that the signal $\tilde{R}_1(t)$, like the signal produced by Jakes' simulator, is not wide-sense stationary. We conclude that the introduction of only sine terms, as illustrated in Figure 4.1, is not sufficient to produce a wide-sense stationary signal. We note in passing that the first term in the autocorrelation of equation (4.20) depends only on the time difference t_2-t_1, while the second term depends only on the the time sum t_2+t_1.

4.3 A second attempt at improving Jakes' simulator

The second method we propose to improve Jakes simulator is the introduction of random phases in the low-frequency oscillators, as illustrated in Figure 4.2. This method has been suggested and used by some authors, with some degree of success; see, for example, [8, pp. 263-264], or [31, p. 97].

Justification for using this method is the fact that for small values of time t, the values produced by the low-frequency oscillators are highly correlated; they are equal at $t = 0$. By adding the random phases, the correlation is destroyed.

The signal produced by this simulator can be written, upon analysis of Figure 4.2, again, under the constraint that it have unit power, as

$$\begin{aligned}\tilde{R}_2(t) &= \cos\omega_c t\tilde{X}_{2c}(t) + \sin\omega_c t\tilde{X}_{2s}(t) \\ &= \frac{2}{\sqrt{N}}\cos\omega_c t\left[\sqrt{2}\cos B_{M+1}\cos(\omega_m t + \Psi_{M+1}) + 2\sum_{n=1}^{M}\cos B_n\cos(\omega_n t + \Psi_n)\right] \\ &\quad + \frac{2}{\sqrt{N}}\sin\omega_c t\left[\sqrt{2}\sin B_{M+1}\cos(\omega_m t + \Psi_{M+1}) + 2\sum_{n=1}^{M}\sin B_n\cos(\omega_n t + \Psi_n)\right],\end{aligned} \tag{4.22}$$

where $\Psi_1, \ldots, \Psi_{M+1}$ are uniform i.i.d. random variables over $[0, 2\pi]$.

As in the case of the first fix, we need to determine whether the signal $\tilde{R}_2(t)$ produced by the simulator of Figure 4.2 is wide-sense stationary. We proceed by computing the autocorrelation function, in a manner similar to that of the previous section. We start with the definition of the autocorrelation function. We then have

$$\begin{aligned}\mathscr{R}_{\tilde{R}_2\tilde{R}_2}(t_1, t_2) &= E\left\{\tilde{R}_2(t_1)\tilde{R}_2(t_2)\right\} \\ &= E\left\{\frac{2}{\sqrt{N}}\left[\cos\omega_c t_1\left(\sqrt{2}\cos B_{M+1}\cos(\omega_m t_1 + \Psi_{M+1}) + 2\sum_{n=1}^{M}\cos B_n\cos(\omega_n t_1 + \Psi_n)\right)\right.\right. \\ &\quad \left.\left. + \sin\omega_c t_1\left(\sqrt{2}\sin B_{M+1}\cos(\omega_m t_1 + \Psi_{M+1}) + 2\sum_{n=1}^{M}\sin B_n\cos(\omega_n t_1 + \Psi_n)\right)\right] \right. \\ &\quad \left. \times\frac{2}{\sqrt{N}}\left[\cos\omega_c t_2\left(\sqrt{2}\cos B_{M+1}\cos(\omega_m t_2 + \Psi_{M+1}) + 2\sum_{k=1}^{M}\cos B_k\cos(\omega_k t_2 + \Psi_k)\right)\right.\right.\end{aligned}$$

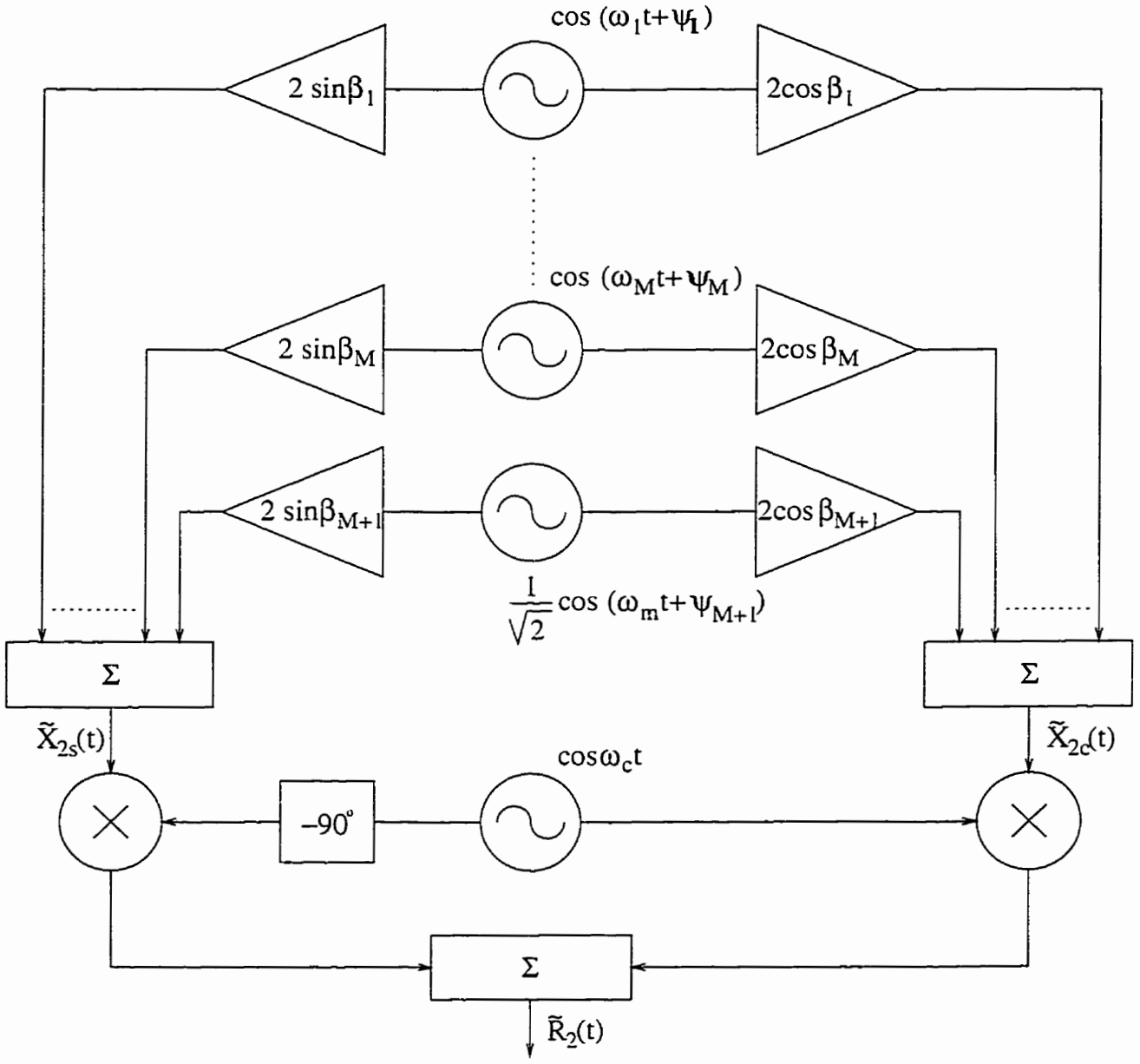

Figure 4.2. Improving Jakes' simulator by the introduction of random phases in the low-frequency oscillators.

$$+ \sin\omega_c t_2 \left(\sqrt{2}\sin B_{M+1}\cos(\omega_m t_2 + \Psi_{M+1}) + 2\sum_{k=1}^{M} \sin B_k \cos(\omega_k t_2 + \Psi_k) \right) \Bigg] \Bigg\}. \tag{4.23}$$

We note that the random variables $B_1, \ldots, B_{M+1}$, and $\Psi_1, \ldots, \Psi_{M+1}$, are uniform i.i.d. over $[0, 2\pi]$. Following a procedure similar to that in Section 4.2, we obtain successively

$$\begin{aligned}
&\mathscr{R}_{\tilde{R}_2\tilde{R}_2}(t_1, t_2) \\
&= \frac{8}{N}\cos\omega_m t_1 \cos\omega_c t_1 \cos\omega_m t_2 \cos\omega_c t_2 E\{\cos^2 B_{M+1}\cos^2\Psi_{M+1}\} \\
&\quad + \frac{8}{N}\sin\omega_m t_1 \cos\omega_c t_1 \sin\omega_m t_2 \cos\omega_c t_2 E\{\cos^2 B_{M+1}\sin^2\Psi_{M+1}\} \\
&\quad + \frac{16}{N}\sum_{n=1}^{M} \cos\omega_n t_1 \cos\omega_c t_1 \cos\omega_n t_2 \cos\omega_c t_2 E\{\cos^2 B_n \cos^2\Psi_n\} \\
&\quad + \frac{16}{N}\sum_{n=1}^{M} \sin\omega_n t_1 \cos\omega_c t_1 \sin\omega_n t_2 \cos\omega_c t_2 E\{\cos^2 B_n \sin^2\Psi_n\} \\
&\quad + \frac{8}{N}\cos\omega_m t_1 \sin\omega_c t_1 \cos\omega_m t_2 \sin\omega_c t_2 E\{\sin^2 B_{M+1}\cos^2\Psi_{M+1}\} \\
&\quad + \frac{8}{N}\sin\omega_m t_1 \sin\omega_c t_1 \sin\omega_m t_2 \sin\omega_c t_2 E\{\sin^2 B_{M+1}\sin^2\Psi_{M+1}\} \\
&\quad + \frac{16}{N}\sum_{n=1}^{M} \cos\omega_n t_1 \sin\omega_c t_1 \cos\omega_n t_2 \sin\omega_c t_2 E\{\sin^2 B_n \cos^2\Psi_n\} \\
&\quad + \frac{16}{N}\sum_{n=1}^{M} \sin\omega_n t_1 \sin\omega_c t_1 \sin\omega_n t_2 \sin\omega_c t_2 E\{\sin^2 B_n \sin^2\Psi_n\} \\
&= \frac{2}{N}\cos\omega_m t_1 \cos\omega_c t_1 \cos\omega_m t_2 \cos\omega_c t_2 + \frac{2}{N}\sin\omega_m t_1 \cos\omega_c t_1 \sin\omega_m t_2 \cos\omega_c t_2 \\
&\quad + \frac{4}{N}\sum_{n=1}^{M} \cos\omega_n t_1 \cos\omega_c t_1 \cos\omega_n t_2 \cos\omega_c t_2 + \frac{4}{N}\sum_{n=1}^{M} \sin\omega_n t_1 \cos\omega_c t_1 \sin\omega_n t_2 \cos\omega_c t_2 \\
&\quad + \frac{2}{N}\cos\omega_m t_1 \sin\omega_c t_1 \cos\omega_m t_2 \sin\omega_c t_2 + \frac{2}{N}\sin\omega_m t_1 \sin\omega_c t_1 \sin\omega_m t_2 \sin\omega_c t_2 \\
&\quad + \frac{4}{N}\sum_{n=1}^{M} \cos\omega_n t_1 \sin\omega_c t_1 \cos\omega_n t_2 \sin\omega_c t_2 + \frac{4}{N}\sum_{n=1}^{M} \sin\omega_n t_1 \sin\omega_c t_1 \sin\omega_n t_2 \sin\omega_c t_2 \\
&= \frac{2}{N}\left[\cos\omega_m(t_2 - t_1) + 2\sum_{n=1}^{M} \cos\omega_n(t_2 - t_1)\right] \cos\omega_c(t_2 - t_1).
\end{aligned} \tag{4.24}$$

We observe that the signal produced by this second simulator is wide-sense stationary,

i.e., its autocorrelation function depends only on the time difference $\tau = t_2 - t_1$

$$\mathscr{R}_{\tilde{R}_2}(\tau) = \frac{2}{N}\cos\omega_c\tau\left(\cos\omega_m\tau + 2\sum_{n=1}^{M}\cos\omega_n\tau\right). \tag{4.25}$$

One has to conclude that the introduction of the random phases $\Psi_1,\ldots,\Psi_{M+1}$ destroys the correlation observed earlier between the low-frequency oscillators, and thus leads to the generation of a wide-sense stationary signal.

Since

$$\frac{1}{T}\int_0^T \mathscr{R}_{\tilde{R}_2}(\tau)d\tau \to 0$$

as $T \to \infty$ holds, i.e., the signal $\tilde{R}_2(t)$ meets the requirements of Slutsky's theorem [29, eq. (13-7)], we conclude that $\tilde{R}_2(t)$ exhibits ergodicity of the mean.

With some effort, it may be shown that the time-average autocorrelation is

$$\langle\tilde{R}_2(t)\tilde{R}_2(t+\tau)\rangle = \frac{2}{N}\cos\omega_c\tau\left(\cos\omega_m\tau + 2\sum_{n=1}^{M}\cos\omega_n\tau\right). \tag{4.26}$$

We observe that the statistical average autocorrelation is equal to the time-average one

$$\mathscr{R}_{\tilde{R}_2}(\tau) = \langle\tilde{R}_2(t)\tilde{R}_2(t+\tau)\rangle.$$

We conclude that $\tilde{R}_2(t)$ may also possess ergodicity of the autocorrelation.

We would like to determine the envelope and phase pdf's of the fading signal produced by this simulator $\tilde{R}_2(t)$. Comparing to the sum of independent random vectors model developed in Section 3.1 we note

$$\begin{aligned} R_n &= \frac{4}{\sqrt{N}}\cos(\omega_n t + \Psi_n), \quad n = 1,\ldots,M \\ R_{M+1} &= \frac{2\sqrt{2}}{\sqrt{N}}\cos(\omega_m t + \Psi_{M+1}) \end{aligned} \tag{4.27}$$

and

$$\Theta_n = B_n, \quad n = 1,\ldots,M+1. \tag{4.28}$$

As in the case of Jakes' simulator, studied in Subsection 3.1.2, we note that R_n is in general a function of C_n, A_n, and Ψ_n, while Θ_n is a function of B_n, and hence Φ_n only. Since

C_n, A_n, Ψ_n, and Φ_n are independent random variables, it follows that R_n and Θ_n are also independent. This verifies the requirement of Section 3.1, and thus we may use the results developed in that section. The rv's $\Theta_1, \ldots, \Theta_{M+1}$ are uniform i.i.d. over $[0, 2\pi]$, as required.

Using equation [29, eq. (5-13)], we obtain the pdf's of the random vector lengths

$$f_{R_n}(r) = \frac{2}{\pi\sqrt{16/N - r^2}}, \quad 0 \le r \le \frac{4}{\sqrt{N}} \tag{4.29}$$

for $n = 1, \ldots, M$, and

$$f_{R_{M+1}}(r) = \frac{2}{\pi\sqrt{8/N - r^2}}, \quad 0 \le r \le \frac{2\sqrt{2}}{\sqrt{N}}. \tag{4.30}$$

Note that the choice of pdf's above for the R_n's ensures that we have no negative lengths.

To compute the characteristic functions, we make use of [36, eq. (6.552.4)] to obtain

$$\begin{aligned} \Phi_n(\omega_1, \omega_2) &= \int_0^{\infty} \frac{2}{\pi\sqrt{16/N - r_n^2}} J_0\left(r_n\sqrt{\omega_1^2 + \omega_2^2}\right) dr_n \\ &= J_0^2\left(\frac{2q}{\sqrt{N}}\right), \end{aligned} \tag{4.31}$$

and similarly,

$$\Phi_{M+1}(\omega_1, \omega_2) = J_0^2\left(\frac{\sqrt{2}q}{\sqrt{N}}\right), \tag{4.32}$$

where $q = \sqrt{\omega_1^2 + \omega_2^2}$. Thus, the envelope pdf is given by

$$f_{\bar{R}_2}(r) = r\int_0^{\infty} \left[J_0\left(\frac{\sqrt{2}q}{\sqrt{N}}\right) J_0^{2M}\left(\frac{2q}{\sqrt{N}}\right)\right] J_0(rq) q\, dq, \quad r \ge 0. \tag{4.33}$$

As expected, the envelope pdf does not depend on time.

The phase pdf is given by

$$f_{\bar{\Theta}_2}(\theta) = \frac{1}{2\pi}, \quad 0 \le \theta \le 2\pi. \tag{4.34}$$

Thus far, we have seen that introduction of random phases in the low-frequency oscillators leads to the generation of a wide-sense stationary signal. The only question remaining to be answered is whether the addition of the random phases $\Psi_1, \ldots, \Psi_{M+1}$ has changed

the content of the signal. To determine whether the signal $\tilde{R}_2(t)$ still approximates $R(t)$ we return to equation (4.22) and attempt to re-write it in a more insightful form. We have successively

$$\begin{aligned}
\tilde{R}_2(t) &= \frac{2}{\sqrt{N}}\cos\omega_c t\left[\sqrt{2}\cos B_{M+1}\cos(\omega_m t+\Psi_{M+1})+2\sum_{n=1}^{M}\cos B_n\cos(\omega_n t+\Psi_n)\right] \\
&\quad +\frac{2}{\sqrt{N}}\sin\omega_c t\left[\sqrt{2}\sin B_{M+1}\cos(\omega_m t+\Psi_{M+1})+2\sum_{n=1}^{M}\sin B_n\cos(\omega_n t+\Psi_n)\right\} \\
&= \frac{2\sqrt{2}}{\sqrt{N}}\cos(\omega_c t-B_{M+1})\cos(\omega_m t+\Psi_{M+1})+\frac{4}{\sqrt{N}}\sum_{n=1}^{M}\cos(\omega_c t-B_n)\cos(\omega_n t+\Psi_n) \\
&= \sqrt{\frac{2}{N}}\left[\cos(\omega_c t-\omega_m t-B_{M+1}-\Psi_{M+1})+\cos(\omega_c t+\omega_m t-B_{M+1}+\Psi_{M+1})\right] \\
&\quad +\frac{2}{\sqrt{N}}\sum_{n=1}^{M}\left[\cos(\omega_c t-\omega_n t-B_n-\Psi_n)+\cos(\omega_c t+\omega_n t-B_n+\Psi_n)\right]. \qquad (4.35)
\end{aligned}$$

Recall that the phase shifts $\Phi_1,\ldots,\Phi_N$ in the fading signal $R(t)$ are uniform i.i.d. over $[0,2\pi]$. In the case of the simulator of Figure 4.2 the phase shifts are represented by the random variables $B_1+\Psi_1,\ldots,B_{M+1}+\Psi_{M+1}$, and $B_1-\Psi_1,\ldots,B_{M+1}-\Psi_{M+1}$. It is interesting to note that in the case of $\tilde{R}_2(t)$, the phase shifts are no longer independent, as was the case with the phase shifts Φ_n of $R(t)$. In particular, we note that the phases $B_n+\Psi_n$ and $B_n-\Psi_n$ are dependent, for $n=1,\ldots,M+1$; however, they are uncorrelated. Note that the envelope pdf of the signal generated by Clarke's model is not the same as the envelope pdf of the signal generated by this improved simulator; they do, however, converge to the same pdf, the standard Rayleigh. Despite the fact that the mean and autocorrelation function of Clarke's model are identical to the mean and autocorrelation function of the improved simulator, we conclude that this improved model does not completely represent the fading signal of equation (2.6).

4.4 A closer look at Clarke's formula

Now that we have taken a look at some fixes, we go back to Clarke's model given in equation (2.6). We try to obtain a different perspective on why these improvements would

work or not. Recall that the fading signal we want to simulate may be expressed as

$$R(t) = \sqrt{\frac{2}{N}} \sum_{n=1}^{N} \cos(\omega_c t + \omega_m t \cos A_n + \Phi_n), \tag{4.36}$$

where A_n and Φ_n are i.i.d. random variables over $[0, 2\pi]$. This is the signal of equation (4.1) with $C_n = \frac{1}{\sqrt{N}}$.

One way to interpret the above equation is that there are $2N$ degrees of freedom, i.e., the random variables $A_1, \ldots, A_N$ and $\Phi_n, \ldots, \Phi_N$. In the method Jakes outlines, the A_n are chosen in a symmetric manner, according to the formula

$$A_n = \frac{2\pi n}{N}. \tag{4.37}$$

This has the effect of removing N degrees of freedom. Furthermore, Jakes reduces the number of low-frequency oscillators and their corresponding phase shifts from N to $M+1$, where N is assumed to be of the form $N = 4M+2$. This has the effect of further reducing the number of degrees of freedom. As shown in Subsection 2.2.1, this last reduction leads to waves of different frequencies becoming correlated, and the simulator signal becoming non-stationary. From this point of view, we would expect the signal generated by the simulator to differ from the signal it was intended to reproduce, i.e., the signal of equation (4.36). To summarize, the loss of phase shift information, i.e., number of degrees of freedom relating to the phase shifts, leads to the generation of a non-stationary signal.

A more insightful interpretation is obtained by re-writing equation (4.36) in terms of quadrature components

$$\begin{aligned} R(t) \;=\; & \sqrt{\frac{2}{N}} \cos \omega_c t \left[\sum_{n=1}^{N} (\cos \Phi_n \cos \Omega_n t - \sin \Phi_n \sin \Omega_n t) \right] \\ & - \sqrt{\frac{2}{N}} \sin \omega_c t \left[\sum_{n=1}^{N} (\sin \Phi_n \cos \Omega_n t + \cos \Phi_n \sin \Omega_n t) \right]. \end{aligned} \tag{4.38}$$

From this equation we derive the simulator structure of Figure 4.3.

Note that Jakes' simulator does not contain the branches corresponding to the $\sin(\Omega_n t)$ terms. This comes about because the restrictions Jakes imposes on the random variables

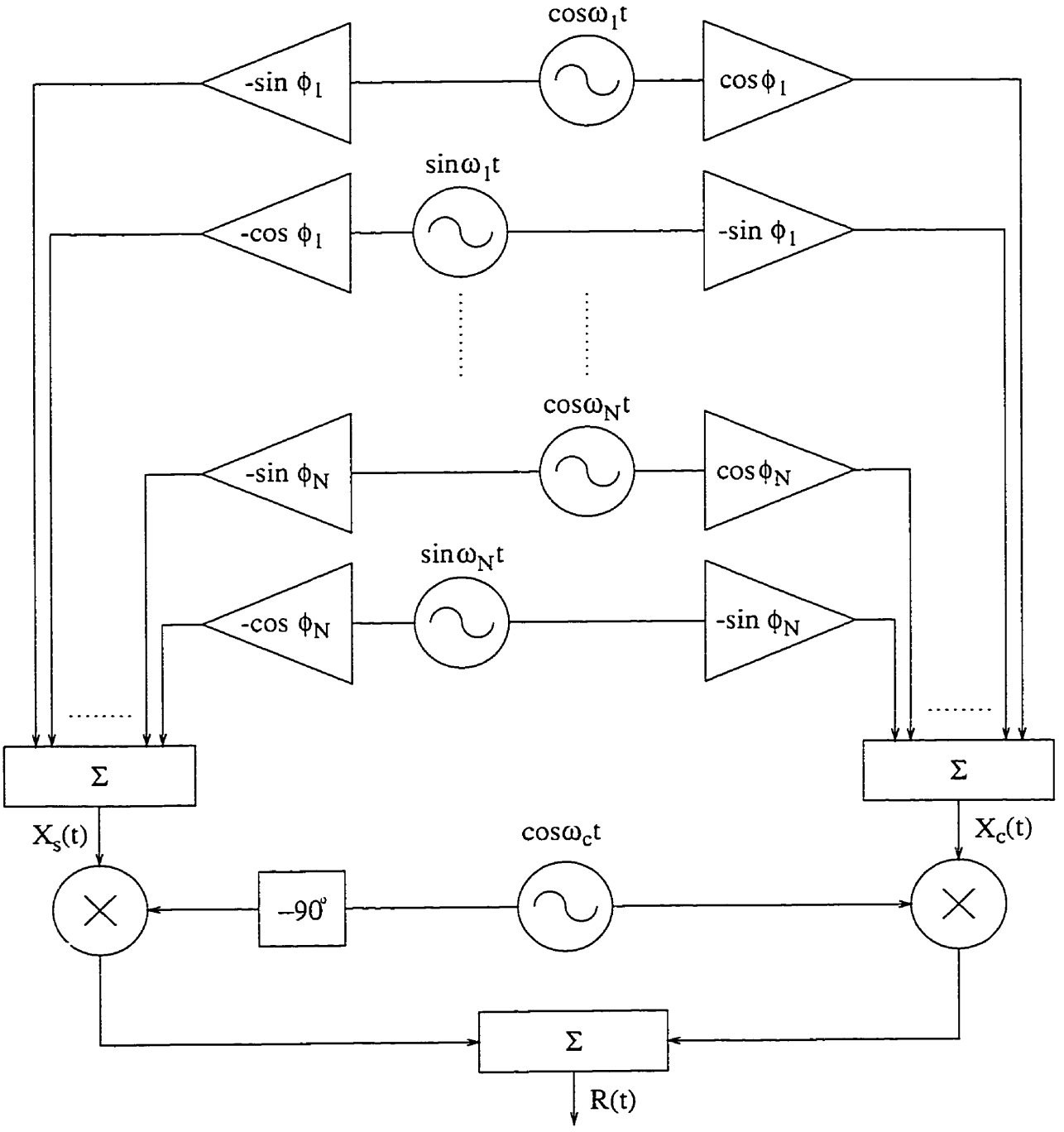

Figure 4.3. Complete simulator of fading channel.

A_n and Φ_n force the sums of the terms coming from the $\sin(\Omega_n t)$ branches to be (approximately) zero. In addition to the missing sine branches, the Jakes simulator reduces the number of cosine oscillators from N to $M+1$, through the choice of A_n, which in turn determine the value of the Doppler shift frequencies $\Omega_n = \omega_m \cos A_n$.

Also, by analyzing Figure 4.1 and Figure 4.3 it becomes obvious why the first fix did not work. Namely, in the former case, we observe the $\sin B_n \sin \Omega_n t$ terms occur in the quadrature branch. In the latter case, however, the same $\sin B_n \sin \Omega_n t$ terms occur in the in-phase branch. Since the two simulators are different, we would not expect the simulator in Figure 4.1 to reproduce, or even approximate the signal of simulator in Figure 4.3.

Note that, in general, the restrictions on the phase shifts given by equations (4.10a) and (4.10b) are not true. Hence, we will not be able to reduce the expressions for $X_c(t)$ and $X_s(t)$ as was done in Section 4.1. That is, we will have to keep all N phase shifts $\Phi_1, \ldots, \Phi_N$. In some cases, in particular when the angles of arrival are symmetrically and equally spaced around the unit circle, we reduce the number of low-frequency oscillators, but we still must ensure inclusion of all N phase shifts. We illustrate this idea for the case $N = 4M+2$.

The angles of arrival are given, as usual, by

$$A_n = \frac{2\pi n}{N}, \quad n = 1, \ldots, N.$$

Recalling equation (4.8),we write the in-phase component of the fading signal as

$$\begin{aligned} X_c(t) \;=\; & \sqrt{\frac{2}{N}} \sum_{n=1}^{M} \left(\cos\Phi_n + \cos\Phi_{2M+1-n} + \cos\Phi_{2M+1+n} + \cos\Phi_{4M+2-n}\right) \cos\omega_n t \\ & - \sqrt{\frac{2}{N}} \sum_{n=1}^{M} \left(\sin\Phi_n - \sin\Phi_{2M+1-n} - \sin\Phi_{2M+1+n} + \sin\Phi_{4M+2-n}\right) \sin\omega_n t \\ & + \sqrt{\frac{2}{N}} (\cos\Phi_{2M+1} + \cos\Phi_{4M+2}) \cos\omega_m t \\ & + \sqrt{\frac{2}{N}} (\sin\Phi_{2M+1} - \sin\Phi_{4M+2}) \sin\omega_m t, \end{aligned} \tag{4.39}$$

and, recalling equation (4.9), the quadrature component as

$$X_s(t) \;=\; \sqrt{\frac{2}{N}} \sum_{n=1}^{M} \left(\cos\Phi_n - \cos\Phi_{2M+1-n} - \cos\Phi_{2M+1+n} + \cos\Phi_{4M+2-n}\right) \sin\omega_n t$$

$$+\sqrt{\frac{2}{N}}\sum_{n=1}^{M}\left(\sin\Phi_n+\sin\Phi_{2M+1-n}+\sin\Phi_{2M+1+n}+\sin\Phi_{4M+2-n}\right)\cos\omega_n t$$
$$-\sqrt{\frac{2}{N}}(\cos\Phi_{2M+1}-\cos\Phi_{4M+2})\sin\omega_m t$$
$$+\sqrt{\frac{2}{N}}(\sin\Phi_{2M+1}+\sin\Phi_{4M+2})\cos\omega_m t. \tag{4.40}$$

The simulator derived based on the simplified equations for $X_c(t)$ and $X_s(t)$ is shown in Figure 4.4. The gains corresponding to each sinusoid, or oscillator, in equations (4.39) and (4.40) are too cumbersome to include in a block diagram. Thus, we make the substitutions

$$P_n^c = \cos\Phi_n+\cos\Phi_{2M+1-n}+\cos\Phi_{2M+1+n}+\cos\Phi_{4M+2-n}, \tag{4.41}$$
$$P_n^s = \sin\Phi_n-\sin\Phi_{2M+1-n}-\sin\Phi_{2M+1+n}+\sin\Phi_{4M+2-n}, \tag{4.42}$$
$$Q_n^c = \sin\Phi_n+\sin\Phi_{2M+1-n}+\sin\Phi_{2M+1+n}+\sin\Phi_{4M+2-n}, \tag{4.43}$$
$$Q_n^s = \cos\Phi_n-\cos\Phi_{2M+1-n}-\cos\Phi_{2M+1+n}-\cos\Phi_{4M+2-n}, \tag{4.44}$$
$$P_{M+1}^c = \cos\Phi_{2M+1}+\cos\Phi_{4M+2}, \tag{4.45}$$
$$P_{M+1}^s = \sin\Phi_{2M+1}-\sin\Phi_{4M+2}, \tag{4.46}$$
$$Q_{M+1}^c = \sin\Phi_{2M+1}+\sin\Phi_{4M+2}, \tag{4.47}$$
$$Q_{M+1}^s = \cos\Phi_{2M+1}-\cos\Phi_{4M+2}. \tag{4.48}$$

We note that the low-frequency oscillators generate the various Doppler frequency shifts. In particular, one low-frequency oscillator corresponds to two Doppler frequency shifts of the appropriate magnitude. Analyzing Figure 2.2 we note that each Doppler frequency magnitude corresponds to four waves arriving at the receiver, except for the waves arriving from directly ahead and behind at the receiver. In this latter case, the Doppler frequency magnitude corresponds to just two waves. From this it is apparent that for $N = 4M+2$ each Doppler frequency magnitude should have four phase shifts associated with it; two phase shifts associated with the maximum Doppler frequency shift. This is what is illustrated by equations (4.41) – (4.48) and Figure 4.4. To conclude, the savings

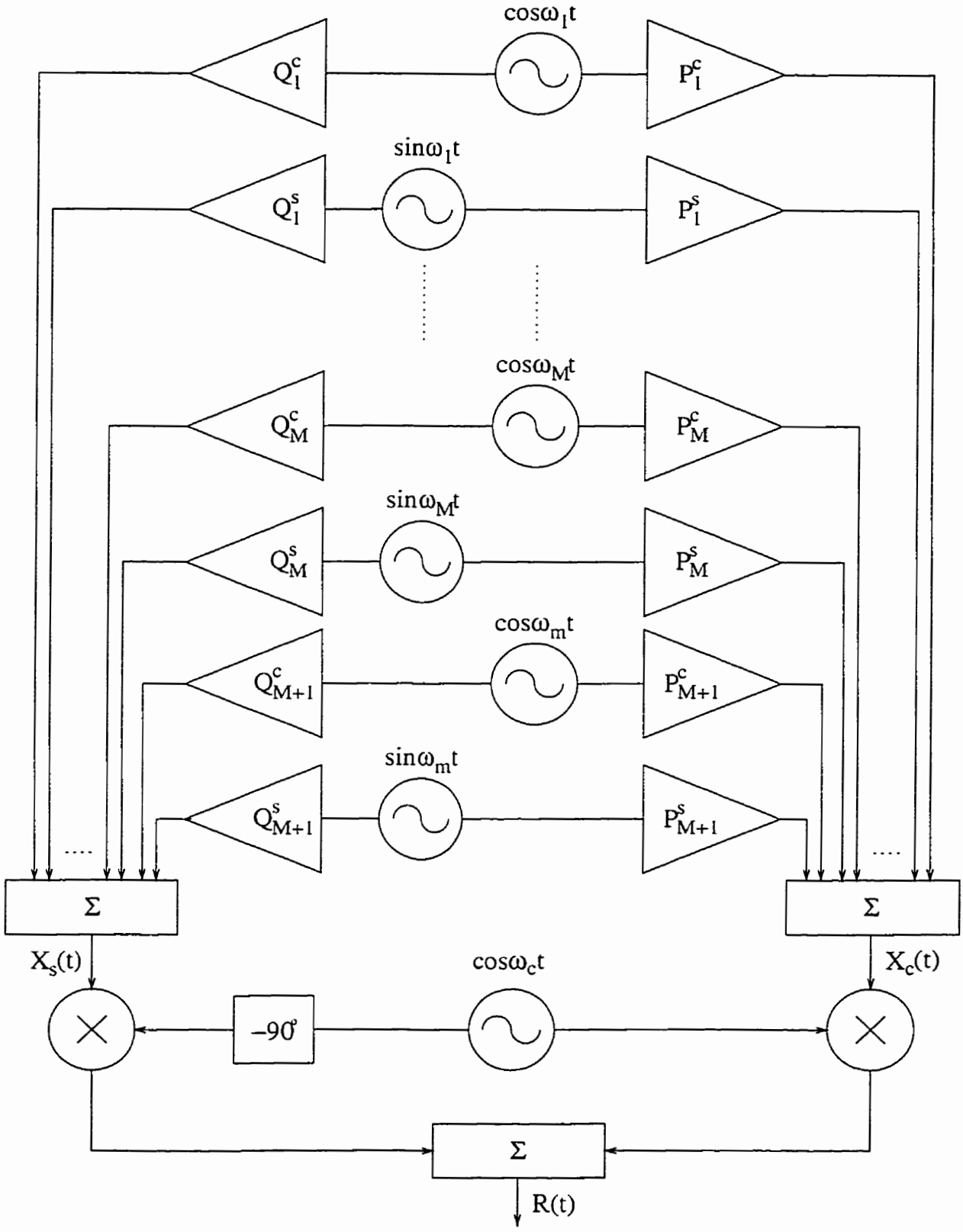

Figure 4.4. Simplified simulator obtained for the case $N = 4M + 2$ and $\alpha_n = \frac{2\pi n}{N}$, $n = 1, \ldots, N$. The gains are defined in equations (4.41) – (4.48).

incurred by forcing the angles of arrival to be symmetric about the x- and y-axes, as in Jakes' work, occur through the inclusion of only the least number of different Doppler frequency shifts. However, we must include the appropriate phase shifts corresponding to each Doppler frequency magnitude. Failure to do so leads to stationarity problems, as was illustrated in Subsection 3.2.2 for Jakes' simulator.

Chapter 5

Quantifying the Inaccuracies in Clarke's Model

As mentioned in the introduction to this thesis, an inherent drawback in the use of simulators is that the signal produced is an approximation to the phenomenon observed in nature. In our case, the problem derives from the fact that the continuum of angles of arrival which exists in the natural fading channel is replaced by N arriving waves uniformly spaced around the unit circle. We can view this process as some sort of quantization. Of interest, then, is how much error this quantization process introduces in the statistics of the fading signal. Various authors have proposed solutions; these solutions usually stem from some theoretical consideration (see, for example, [9]). However, when the simulators are implemented in practice, the number of oscillators used is usually larger by at least an order of magnitude than the theoretical solutions proposed, as in the case of [12]. In this section, we seek to quantify the quantization error. The derivation of our results is based on the knowledge of the approximating function, whether it be probability density, cumulative distribution, or autocorrelation. We arrive at our conclusions via examples.

An important point to note is that the use for which the simulator is intended will often dictate the choice of quality measure. The measures used in this section are generally indicative of the performance of a simulator; they also illustrate how the results obtained earlier in this thesis can be used to determine other quality measures.

5.1 First order statistics

In Subsection 3.1.1 we developed a formula to compute the pdf of the envelope of the signal produced by Clarke's model. In this section, we obtain a measure of the quality of the model based on how close the envelope pdf is to the desired Rayleigh pdf. There are many ways such a comparison can be made, and the approach below is only an example. Such comparisons can be based, for example, on computation of the maximum absolute error between the envelope pdf of the signal produced by the model and the standard Rayleigh pdf, i.e., between the approximating signal pdf and the theoretical, desired signal pdf. It is this approach that we take below. Of course, one could choose mean square error, comparison of variances, or other quality measures such as those proposed by Young [22]. Note that different applications of the simulator may require different quality measures for proper evaluation.

The pdf of the envelope of the signal produced by Clarke's model is given by equation (3.29). For convenience, we re-write this equation below. The envelope pdf is

$$f_R^{app}(r) = r\int_0^\infty J_0^N\left(q\sqrt{\frac{2}{N}}\right)J_0(qr)qdq, \quad r>0.$$

The superscript app is used to emphasize that the pdf is an approximation to the standard Rayleigh, the desired result.

The standard Rayleigh pdf is given by

$$f_R(r) = re^{-r^2/2}. \tag{5.1}$$

This result is readily available from a number of probability texts; see, for example, [29, p. 96][1].

As mentioned above, the quality measure we choose to compute is the maximum absolute error between the two pdf's $|f_R(r) - f_R^{app}(r)|$. The error is computed for various values of N and then plotted in Figure 5.1. The graph is plotted for values of $N \geq 6$, as $N = 6$ is the smallest number of oscillators suggested in the literature.

[1] See also [29, Table 4.1].

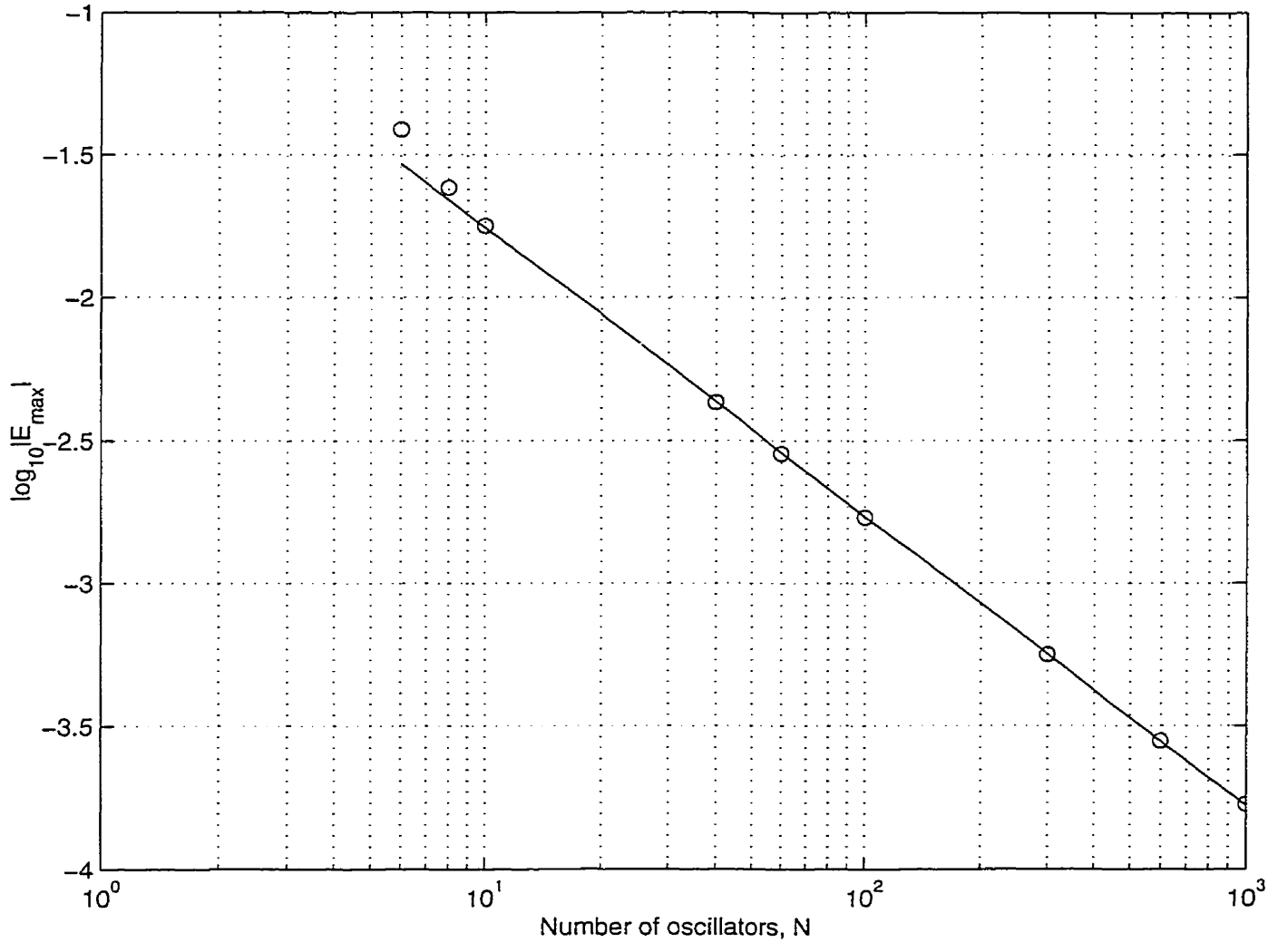

Figure 5.1. Variation of maximum absolute error of the envelope pdf with the number of oscillators N in Clarke's model.

Upon inspection of Figure 5.1 a simple rule of thumb becomes apparent. To reduce the maximum error in the envelope pdf by an order of magnitude, the number of oscillators N must be increased by an order of magnitude. That is, approximately 20 oscillators are needed to reduce the maximum error to 0.01, while 200 oscillators would be needed to further decrease the maximum error to 0.001.

The equation for the fit line is given by

$$\log_{10} Error_{pdf} \approx -1.0 \log_{10} N - 0.75. \tag{5.2}$$

Equation (5.2) can be re-written as

$$Error_{pdf} \times N \approx 0.18, \tag{5.3}$$

showing that the product of the error and the number of oscillators tends to remain constant. Analyzing Figure 5.1 one may conclude that this relationship becomes more accurate as N increases, with the relationship being less accurate for small N. Again, the reader is reminded that this approach is provided only as an example, and that other quality measures exist. Ultimately, the use of the simulator will dictate the choice of quality measure.

Of course, we are not limited to quality measures relating only to the pdf. We can also apply these measures to the cdf. Equation (3.25) gives the cdf of the envelope of the signal produced by Clarke's model. For convenience, we re-write this equation below. The envelope cdf is

$$F_R^{app}(r) = r \int_0^\infty J_1(rq) \prod_{n=1}^{N} J_0\left(q\sqrt{\frac{2}{N}}\right) dq.$$

Again, the superscript *app* indicates the cdf is an approximation to the theoretical one.

The standard Rayleigh cdf is easily obtainable either by consulting a probability text, such as [29], or by integrating the standard Rayleigh pdf of equation (5.1). Either method produces

$$F_R(r) = 1 - e^{-r^2/2}. \tag{5.4}$$

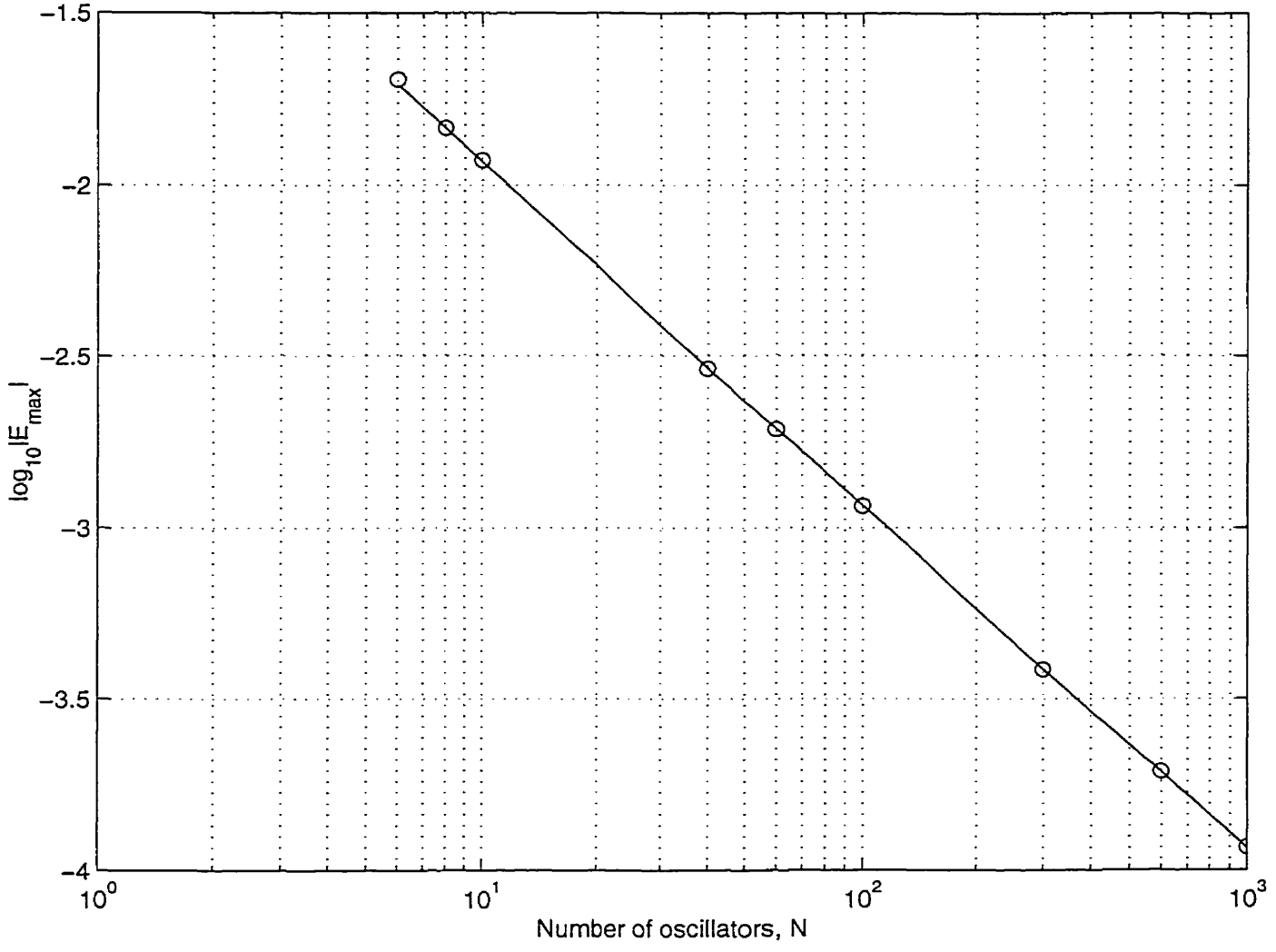

Figure 5.2. Variation of maximum absolute error in the envelope cdf of the signal produced by Clarke's model with the number of oscillators N.

As before, our quality measure will be the maximum error between the approximating cdf and the standard Rayleigh cdf $|F_R(r) - F_R^{app}(r)|$. The error is computed for various values of N and the results are plotted in Figure 5.2, again, for $N \geq 6$.

Similar to the case of the pdf's discussed above, we observe the same rule of thumb. To reduce the maximum error in the envelope cdf by an order of magnitude, the number of oscillators N must be increased by an order of magnitude. For example, we require approximately 12 oscillators to reduce the maximum absolute error in the cdf to 0.01, while we require 120 oscillators to reduce the same error to 0.001.

The equation of the fit line in this case is given by

$$\log_{10} Error_{cdf} \approx -1.0 \log_{10} N - 0.93. \tag{5.5}$$

As done for equation (5.2) we rewrite equation (5.5) as

$$Error_{cdf} \times N \approx 0.12 \tag{5.6}$$

and observe that in this case, too, the product of the error and number of oscillators tends to remain constant. As before, we note from Figure 5.2 that the approximation in equation (5.5) is best for large values of N.

The reader is reminded that the phase pdf of the signal produced by Clarke's model is equal to the desired pdf, i.e, uniform pdf over $[0, 2\pi]$, regardless of the value of N. Quality measures based on the phase pdf would, therefore, reveal little about the performance of sum-of-sinusoids simulators.

Another common way of assessing the quality of a random variate generator is through the use of probability plots. Such plots emphasize deviations from the desired behaviour at the extremes, i.e., tails, of the distribution. In most communication applications, it is these pdf or cdf tail regions which are of importance. This method entails plotting the cdf of the generated random variate versus the desired cdf. On such a plot, the desired cdf would appear as a straight line. A ready measure then, would be how close to a straight line the approximating cdf appears. In our case, we are plotting $F_R^{app}(r)$ versus $F_R(r)$; this is done in Figure 5.3.

A close-up of the right tail is given in Figure 5.4. We justify this by observing that cumulative cdf values on the order of 10^{-6} or less are common. In other words, we are interested in knowing the cdf in the neighbourhood of values such as $1 - 10^{-6}$. Such applications may be found in analysis of error performance.

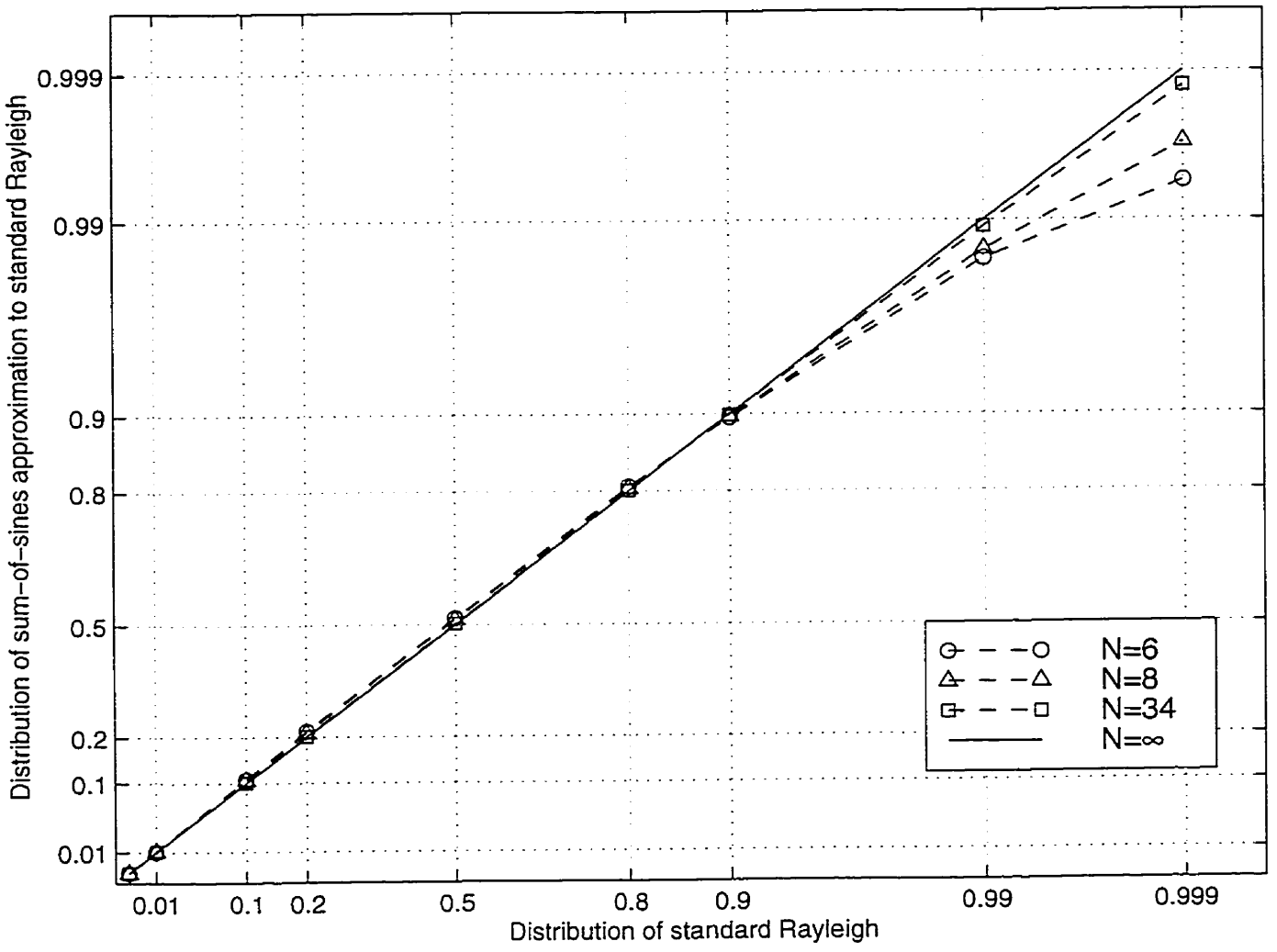

Figure 5.3. Probability plot for the envelope cdf of the signal produced by Clarke's model for various N.

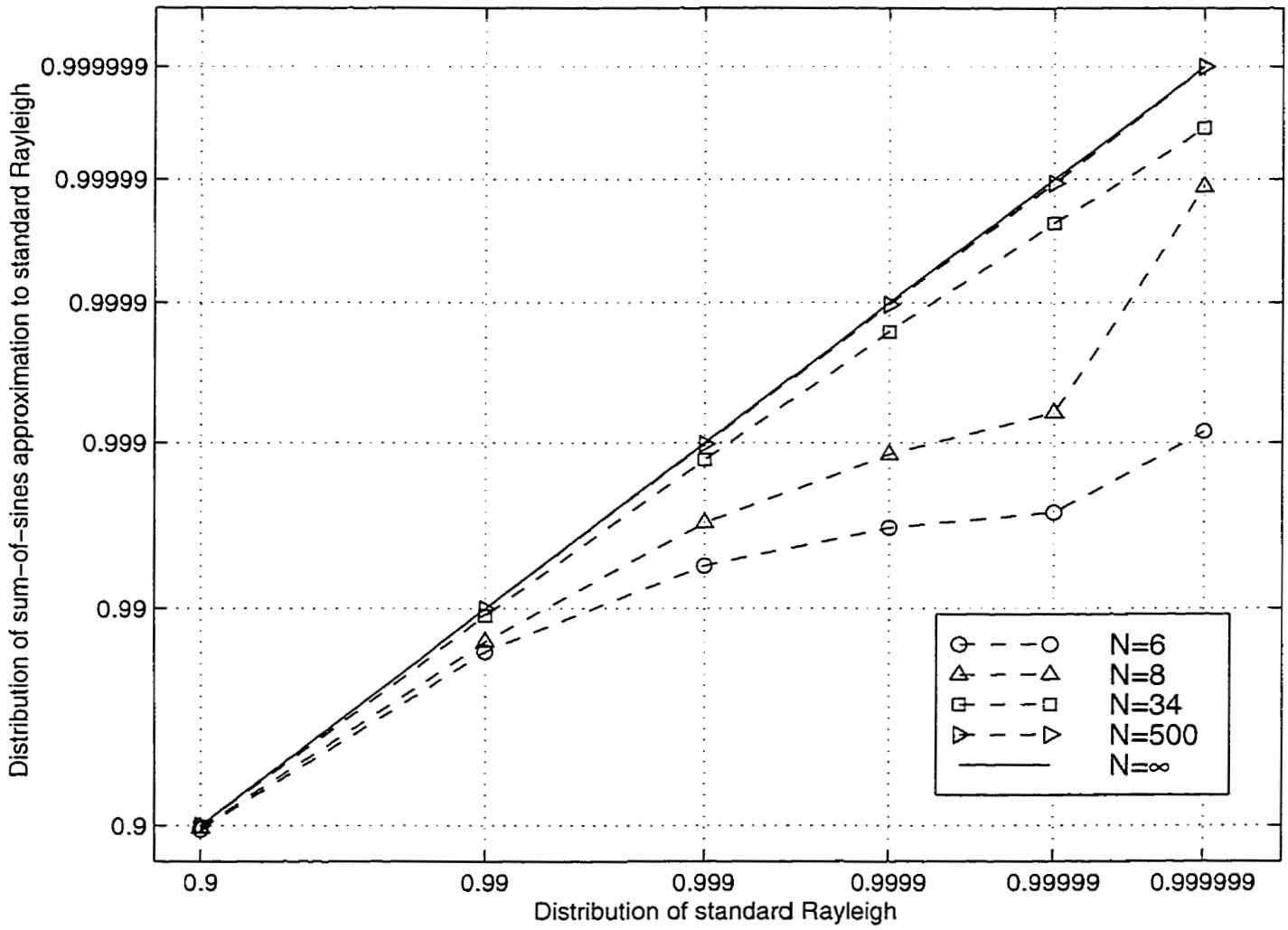

Figure 5.4. Close-up of probability plot for the envelope cdf of the signal produced by Clarke's model for various N.

5.2 Second order statistics

In Subsection 3.2.1 we determined the autocorrelation function of the fading signal $R(t)$ to be

$$\mathscr{R}_{RR}(t_1,t_2) = \frac{1}{N}\sum_{n=1}^{N}\cos[\omega_c(t_1-t_2)+\omega_m(t_1-t_2)\cos\frac{2\pi n}{N}]. \tag{5.7}$$

For even N, the autocorrelation function $\mathscr{R}_{RR}(t_1,t_2)$ simplifies to

$$\mathscr{R}_{RR}(t_1,t_2) = \frac{1}{N}\cos[\omega_c(t_1-t_2)]\sum_{n=1}^{N}\cos[\omega_m(t_1-t_2)\cos\frac{2\pi n}{N}], \tag{5.8}$$

as seen in Subsection 3.2.1. Here we are interested in the low-frequency term

$$\mathscr{R}_R^{LP}(\tau) = \frac{1}{N}\sum_{n=1}^{N}\cos\left(\omega_m\tau\cos\frac{2\pi n}{N}\right), \tag{5.9}$$

where $\tau = t_1 - t_2$, and the superscript LP is used to emphasize we are using the lowpass equivalent form.

In the particular case chosen by Jakes, $N = 4M+2$, and equation (5.9) simplifies to

$$\mathscr{R}_R^{LP}(\tau) = \frac{1}{2M+1}\cos(\omega_m\tau) + \frac{2}{2M+1}\sum_{n=1}^{M}\cos\left(\omega_m\tau\cos\frac{2\pi n}{4M+2}\right). \tag{5.10}$$

Jakes [23] notes that (5.10) is an approximation to the Bessel function of order zero, the autocorrelation one observes in practice. He also notes this approximation breaks down for large enough lag values $\tau = t_2 - t_1$. In this section, we investigate why this breakdown occurs. We also attempt to determine the lag value τ_{max} beyond which the autocorrelation function diverges from the reference model, and how this point varies with the number of oscillators N, or equivalently the number of distinct Doppler frequency shifts $M+1$.

We begin by recalling that one can define the Bessel function of order zero [36, eq. 8.411.4] as

$$J_0(x) = \frac{2}{\pi}\int_0^{\frac{\pi}{2}}\cos(x\cos u)du. \tag{5.11}$$

We can compute the above integral through a Riemann sum. Let

$$g(u) = \frac{2}{\pi}\cos(x\cos u).$$

We divide the interval $[0, \frac{\pi}{2}]$ in $2M+1$ intervals of length $\frac{\pi}{4M+2}$. We label every other point, starting with $u = 0$. Thus, the nth point along the axis is given by

$$u_n = \frac{\pi n}{2M+1}, \quad n = 0, 1, \ldots, M. \tag{5.12}$$

Then, the integral in equation (5.11) can be approximated through the finite sum

$$\begin{aligned} J_0(x) &\approx \frac{\frac{\pi}{2}}{2M+1} g(u_0) + \sum_{n=1}^{M} \frac{\pi}{2M+1} g(u_n) \\ &= \frac{1}{2M+1} \cos x + \frac{2}{2M+1} \sum_{n=1}^{M} \cos\left(x \cos \frac{\pi n}{2M+1}\right). \end{aligned} \tag{5.13}$$

The process of approximating the integral in equation (5.11) by the Riemann sum of equation (5.13) is illustrated in Figure 5.5.

We are interested in finding a relationship between the error level

$$E_{level} = \left| J_0(x_{max}) - \left[\frac{1}{2M+1} \cos x_{max} + \frac{2}{2M+1} \sum_{n=1}^{M} \cos\left(x_{max} \cos \frac{\pi n}{2M+1}\right) \right] \right|, \tag{5.14}$$

the number of low-frequency oscillators $M+1$, and the breakpoint[2] x_{max} beyond which the approximation to the Bessel function deviates significantly from the desired value. We have already noted that we are attempting to compute $J_0(x)$ as an integral. We evaluate the integral in question via the midpoint rule. Thus, one relationship between E_{level}, M, and x_{max} is provided by the error bound on the midpoint rule [34, eq. (7-32)]

$$|E_{level}| \leq \frac{(b-a)^3 g''_{max}}{24n^2}, \tag{5.15}$$

where

- g''_{max} is the maximum absolute value[3] of the second derivative of $g(u)$, i.e., $|g''(u)| \leq g''_{max}$ for $a \leq u \leq b$,
- b is the right end point of the interval of integration, in our case $b = \frac{\pi}{2}$,

[2]Note that $x_{max} = \omega_m \tau_{max}$ in the autocorrelation function.

[3]One may use an optimization routine, such as that provided by Maple, to determine the maximum value. In our case, $g(u) = \cos(x \cos u)$, and we find $g''_{max} = x^2$ for $u = \frac{\pi}{2}$.

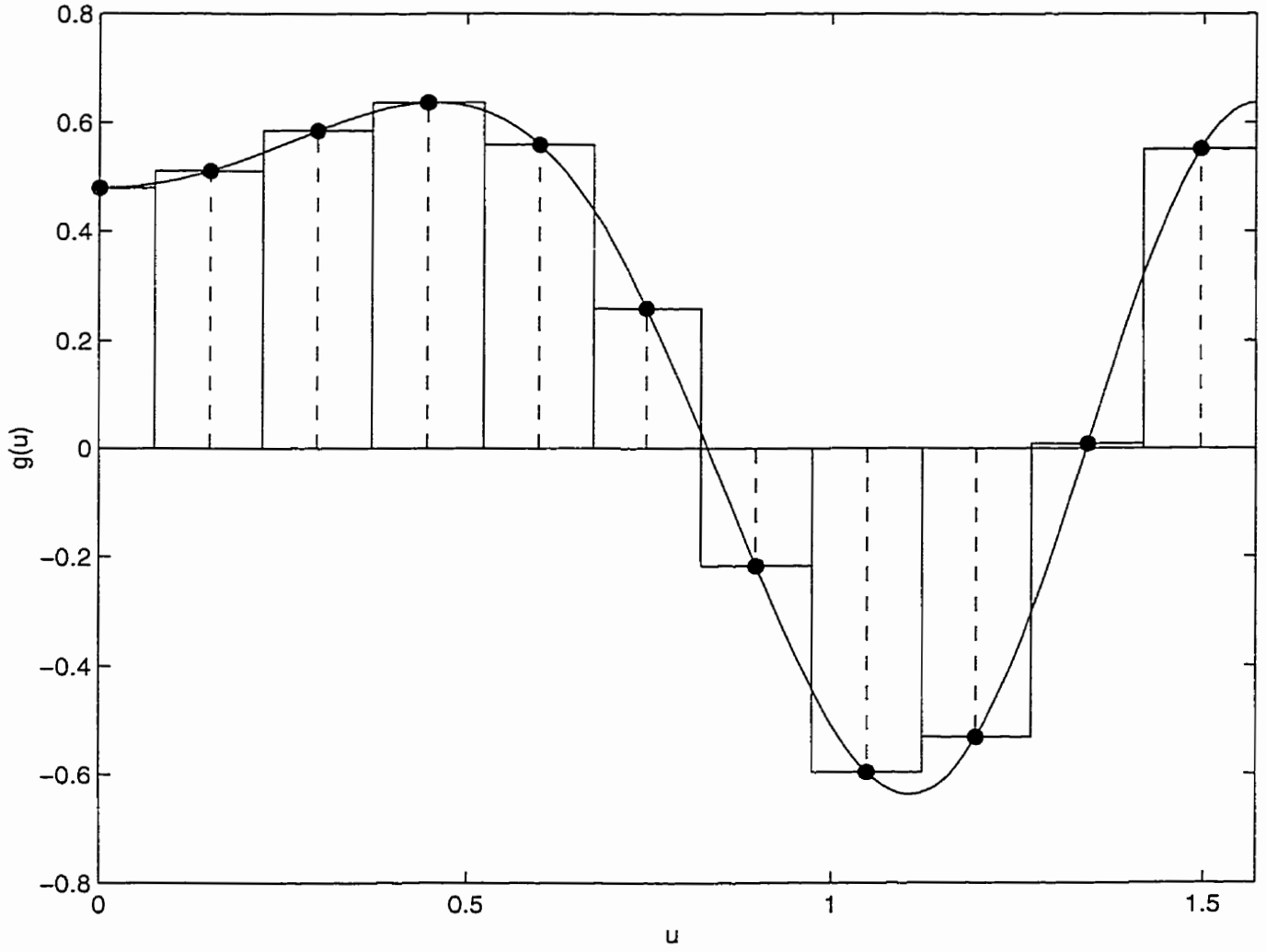

Figure 5.5. Approximating $J_0(x)$ via the midpoint rule, $x = 7$ and $M = 10$. Here, $g(u) = \frac{2}{\pi}\cos(x\cos u)$.

- a is the left end point of the interval of integration, in our case $a = 0$, and
- n is the number of panels used in the integration process, in our case $n = M + \frac{1}{2}$; the $\frac{1}{2}$ comes about because the panel at origin is half as wide as the other ones.

Thus, equation (5.15) specializes to

$$|E_{level}| \leq \frac{\left(\frac{\pi}{2}\right)^3 x_{max}^2}{24\left(M + \frac{1}{2}\right)^2}. \tag{5.16}$$

However, we found the bound of equation (5.16) to be weak, and thus the relationship between E_{level}, M, and x_{max} is also weak. An alternate approach is needed.

We observe that all quantities in equation (5.14) can be readily computed. We begin by choosing an error level, and a number of low-frequency oscillators to be included in a sum-of-sinusoids simulator. Next, we use a search algorithm to determine the smallest value of x_{max} for which equation (5.14) holds. We then plot the points (M, x_{max}) for each error level. Using this procedure, we obtain the family of lines of Figure 5.6. Observe that a small increase in the number of oscillators can drastically reduce the error in the autocorrelation function. We exploit this a little later, in order to derive a rule-of-thumb relating the number of low-frequency oscillators M to the breakpoint τ_{max} in the autocorrelation function.

To illustrate the use of Figure 5.6 consider the following scenario. Suppose we would like to design a sum-of-sinusoids simulator whose autocorrelation function is within 10^{-3} of the desired value up to a time lag of 200 s. Also, take $\omega_m = 1\ rad/s$. Choosing the line in Figure 5.6, i.e., the line corresponding to $E_{level} = 10^{-3}$, we find the point corresponding to $x_{max} = \omega_m \tau_{max} = 200$; on the x-axis we read the corresponding number of low-frequency oscillators we need. In this case, $M = 54$. Note that the number of low frequencies needed, or equivalently, the number of distinct Doppler shifts, we need is $M + 1$, or 55 here.

In some cases, we are interested in using a small number of oscillators. To this end, we enlarge the lower-left hand corner of Figure 5.6 and present the result in Figure 5.7.

Upon analysis of Figures 5.6 and 5.7, we observe that the breakpoint τ_{max} in the autocorrelation function depends almost linearly on the number of oscillators. Thus, one

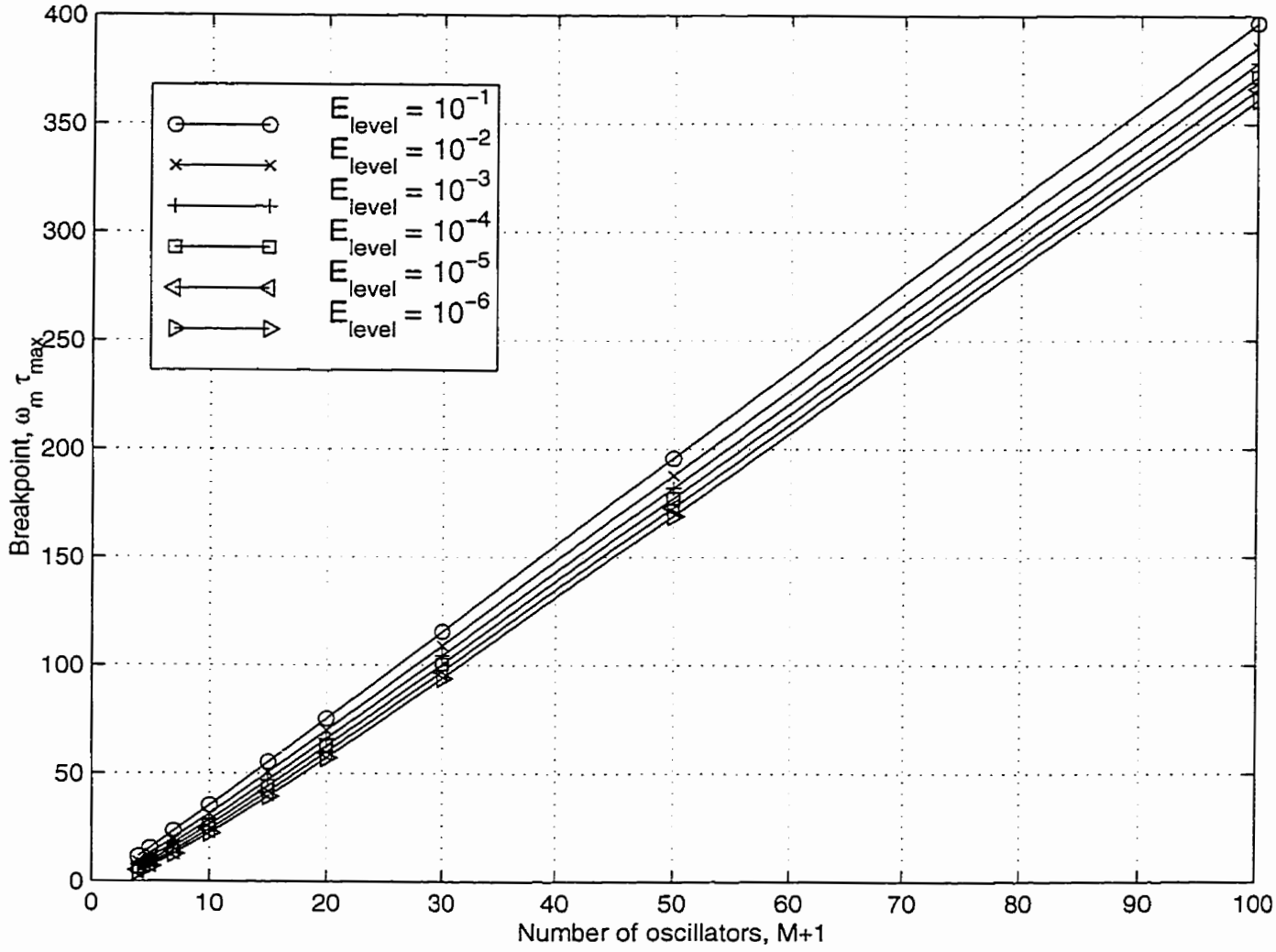

Figure 5.6. Variation of autocorrelation function breakpoint with the number of low-frequency oscillators (number of distinct Doppler frequency shifts M) and the error level E_{level}.

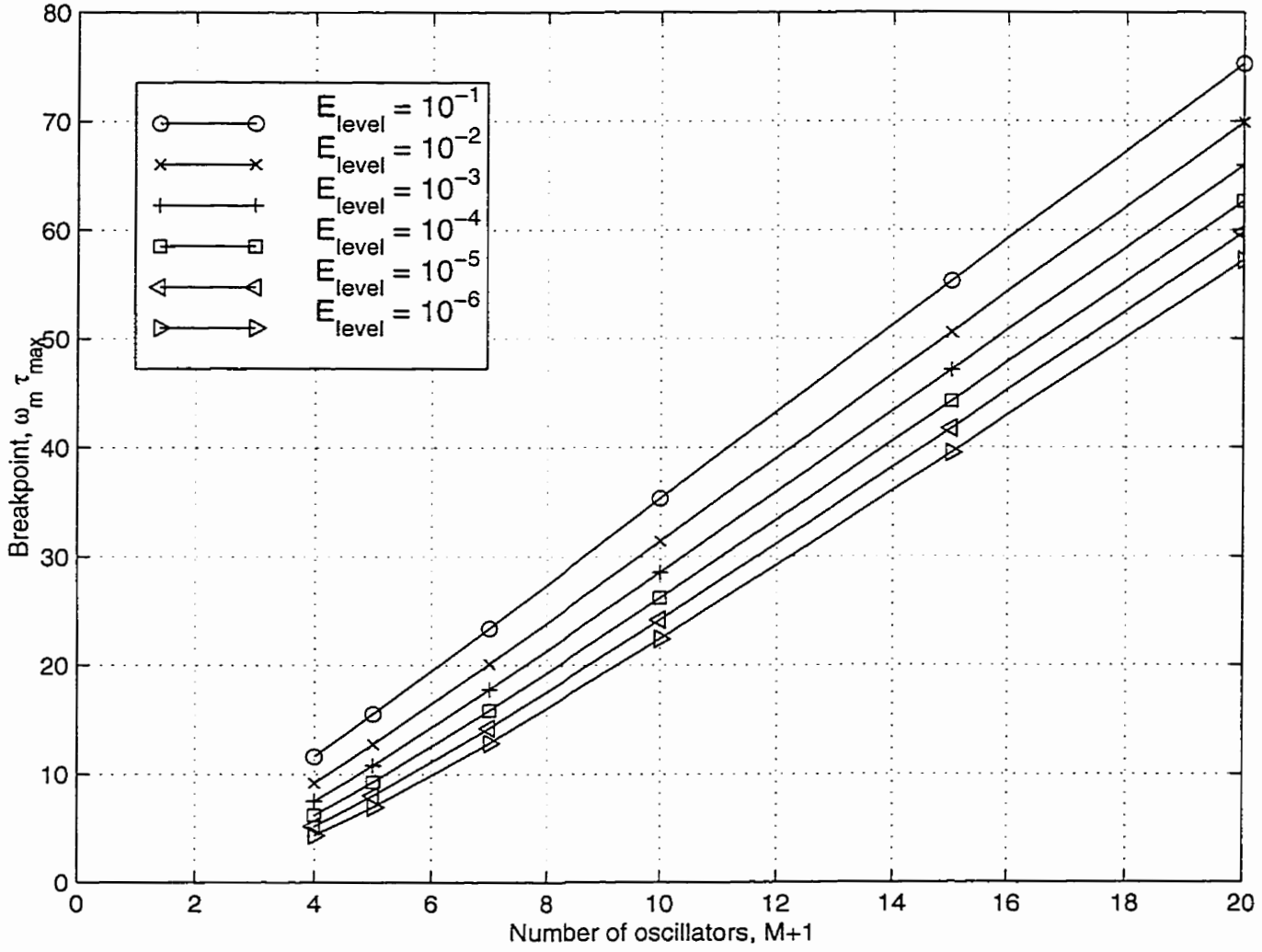

Figure 5.7. Detail of Figure 5.6.

may derive some approximate relationships between the error level, the breakpoint, and the number of oscillators. To illustrate this process, we choose to quantify the relationship between τ_{max} and M for $E_{level} = 10^{-2}$. Analysis of Figure 5.7 reveals the slope of the line corresponding to this error level is approximately 3.5, while the x-axis intercept is roughly 2. This yields

$$\tau_{max} = \frac{3.5(M+1) - 1.5}{\omega_m},$$

where the reader is reminded that $M+1$ is the number of distinct Doppler shifts, or equivalently, the number of low-frequency oscillators in the sum-of-sinusoids simulator.

Further analysis of Figures 5.6 and 5.7 reveals that the slopes of the family of lines lie between 2.5 for small values of the error level and few oscillators, and 4 for large values of error level and many oscillators. Also, the x-axis intercept seems to lie in the interval $[0, 3]$. This enables us to obtain the following rule of thumb

$$\tau_{max} = \frac{2.5M + 3}{\omega_m}. \tag{5.17}$$

We may use equation (5.17) to select an appropriate number of low-frequency oscillators M given we want the autocorrelation function to be close to the desired value over the interval $[0, \tau_{max}]$. Conversely, given a simulator with M low-frequency oscillators, we may use equation (5.17) to determine the value beyond which the autocorrelation deviates significantly from the desired value.

It is important to note that the breakpoint τ_{max} depends on the number of distinct Doppler frequency shifts M, rather than the number of multipath components N. To illustrate this point, we consider two scenarios. In the first, we choose $N = 17$ and in the second, $N = 18$. We still have

$$A_n = \frac{2\pi n}{N},$$

as before. Note that in the first case $N = 17$, there are nine distinct Doppler frequency shifts. In the second case $N = 18$, the number of distinct Doppler frequency shifts has decreased

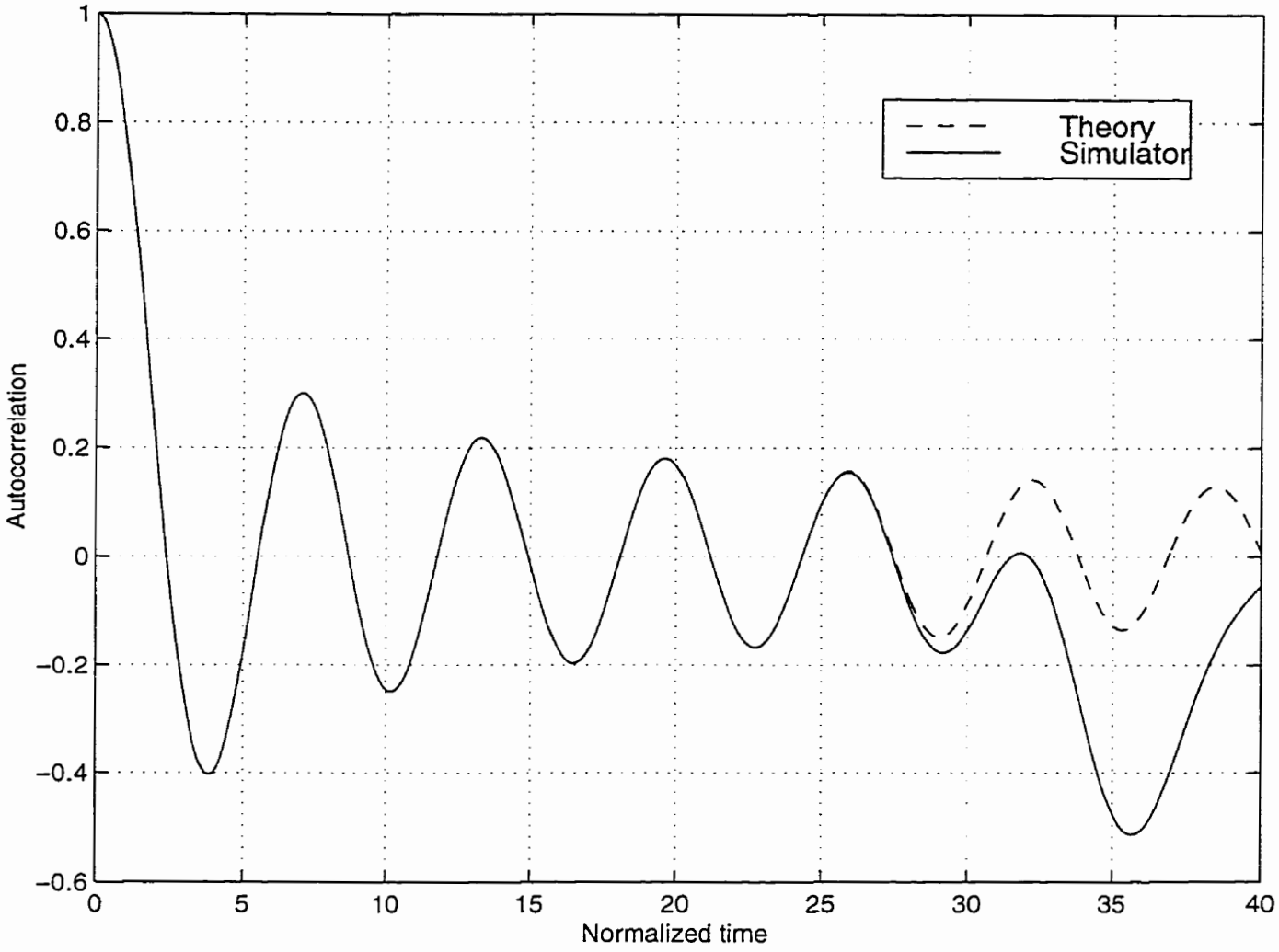

Figure 5.8. Simulator autocorrelation for $N = 17$.

to just five. Thus, based on the argument above, one would expect the simulator autocorrelation function in the first case to match the desired autocorrelation over a longer interval than in the second, despite the fact that the second simulator comprises more multipath components than the first. If $\omega_m = 1$ rad/s, then according to equation (5.17), in the first case the simulator autocorrelation should match the desired one over the interval $[0, 25.5]$, while in the second case they should match over the interval $[0, 13]$. This is readily verified from Figures 5.8 and 5.9.

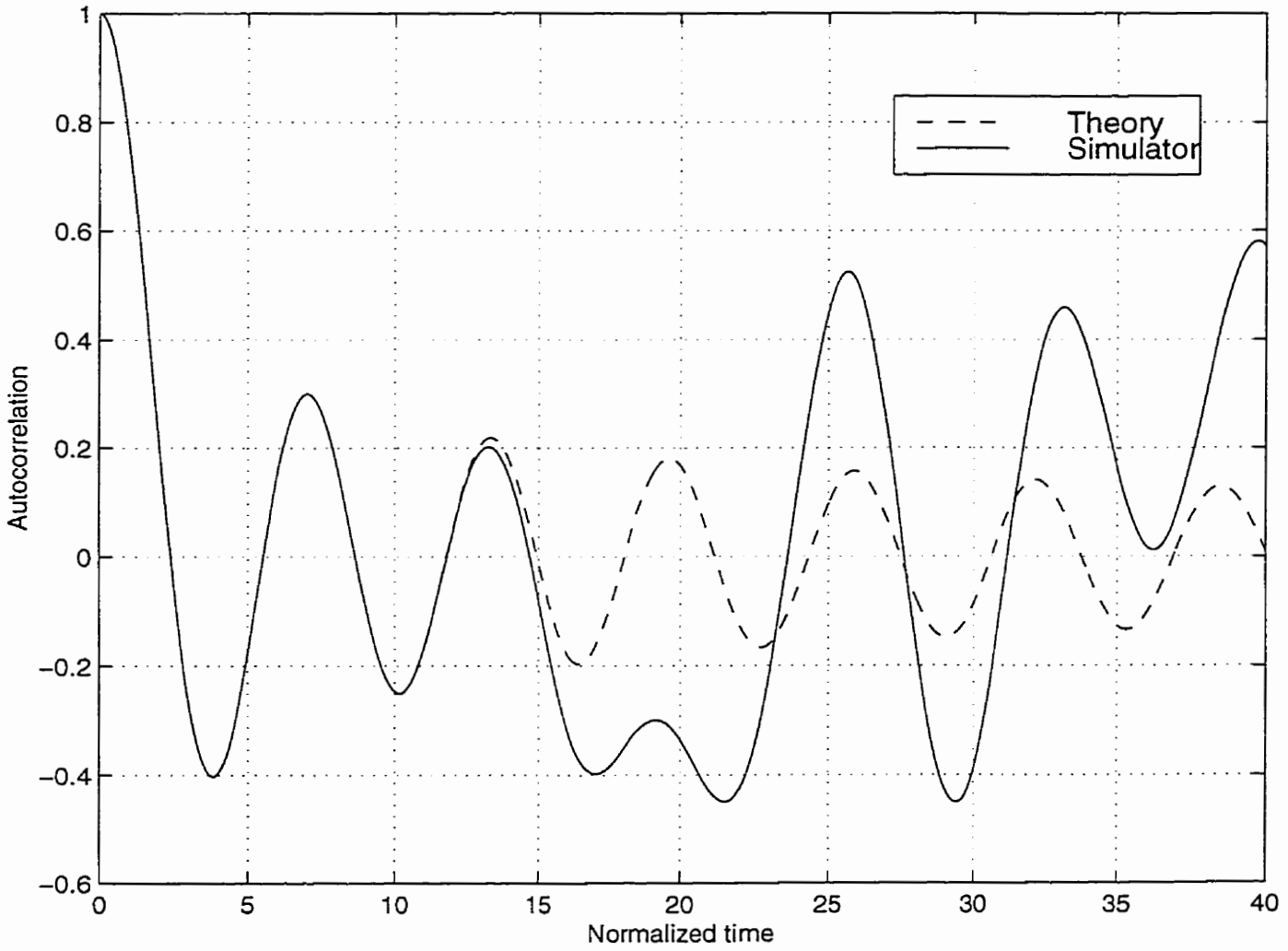

Figure 5.9. Simulator autocorrelation for $N = 18$.

5.3 Relating the number of low-frequency oscillators to the inaccuracies

In previous sections we have seen that the narrowband Rayleigh flat fading signal can be characterized by

$$R(t) = \sqrt{\frac{2}{N}} \sum_{n=1}^{N} \cos(\omega_c t + \omega_m t \cos \frac{2\pi n}{N} + \Phi_n).$$

Note that $R(t)$ represents an approximation to the fading phenomenon observed in nature. We need to obtain an estimate on how far this approximation deviates from the desired value.

Beginning with Jakes [23] many authors have stated that the number of low-frequency oscillators required to simulate the fading signal is usually small. Thus, Jakes [23] suggests that more than 6 oscillators should suffice for producing a Rayleigh flat fading signal. Pätzold et al. [7], Pätzold et al. [8], and finally Pätzold et al. [9] have also suggested that 7 oscillators is enough to generate a fading signal. In his work, Pätzold also uses 10 or 25 oscillators, without an explanation for the increase in number. More recently, Eyceoz [10] has used the Jakes' simulator with 10 oscillators to characterize the fading channel, i.e., to determine the fading coefficients and thus predict the statistics of the fading signal.

However, despite the many suggestions that a small number of oscillators is enough to generate a Rayleigh flat fading signal, some authors use much larger numbers when trying to fit simulator data to real life measurements. For example, Hoeher [12] uses 500 oscillators to model a wireless channel impulse response. While it is generally true that inclusion of more oscillators leads to a better model, it would be helpful if one knew in advance how many oscillators would be required to achieve a certain level of accuracy.

In the previous two sections, we have developed quality measures for the performance of Clarke's model. Thus, we may analyze the performance in terms of the envelope pdf, the envelope cdf, or the autocorrelation function. The phase pdf is the same as the desired pdf regardless of the number of sinusoids; for this reason, we do not use it as a quality measure.

In the former two cases, we are usually interested in generating a fading signal with pdf and cdf close to the desired value. Knowledge of the pdf is of interest, for example, in the determination of the level-crossing rate and the average fade duration.

We may also need to know the value of the autocorrelation function. Behaviour of the autocorrelation, especially at the origin, is required in the computation of the level-crossing rate and average fade duration. Furthermore, knowledge of the autocorrelation is useful in designing sampling or diversity schemes; i.e., useful in obtaining independent samples, or placing antennas at points which experience independent fading. It has been known, as early as Jakes [23], that the autocorrelation function of the simulator signal breaks down for large enough time lags. In the previous section we have determined a relationship between the number of oscillators and the interval over which the autocorrelation function is close to the desired value.

To use the results of this thesis successfully, the engineer would first have to decide which statistic is most important to his/her work. Then, using an appropriate quality measure, as illustrated in this chapter, the engineer may determine the number of oscillators required by the simulator. If, however, there is more than one statistic relevant to the project, the engineer may determine the number of oscillators required for each statistic, and simply pick the largest value for the practical implementation.

Chapter 6

Conclusion

One method of simulating the multipath fading encountered on Rayleigh flat fading narrowband wireless channels is based upon the sum-of-sinusoids model. Such simulators are readily derived from consideration of the physical phenomenon. The work of Clarke [3] summarizes the important characteristics of such simulators, and sets the stage for further developments, such as those of Jakes [23]. Clarke's model and Jakes' fading channel simulator, as well as other work in the area of sum-of-sinusoids simulators were presented in Chapter 2. In addition, we presented Pätzold's results relating to the statistical properties of Jakes' simulator.

In Chapter 3, we derived the statistical properties of sum-of-sinusoids simulators in general. The starting point of the analysis is the assumptions made by Clarke in deriving a mathematical model of multipath Rayleigh fading. We noted that this is different from the starting point in Pätzold's analysis; his analysis is based on the assumption that the quadrature components of the fading signal are approximately Gaussianly distributed and uncorrelated, and hence independent.

The results derived for the envelope and phase pdf's are applied to determine the statistics of Clarke's model and Jakes' fading channel simulator. We also compute the autocorrelation functions for the signals of the two models. The main reason for doing this is to determine whether the assumptions made by Jakes in simplifying Clarke's model are justified. We show that they are not. The signal produced by Clarke's model is shown to be

wide-sense stationary, while that produced by Jakes' simulator is shown to not be wide-sense stationary. The chapter concludes with a discussion of ergodicity and how it applies to sum-of-sinusoids models and simulators.

It is generally desired to have an efficient method for generating fading signals. Viewed in this light, Jakes' approach presents an interesting point. That is, if we are able to reduce the complexity of the model, i.e., the number of low-frequency oscillators, then the generation of the signal is more efficient. In Chapter 4, we attempt to improve the performance of Jakes' simulator through simple modifications. We found that introduction of random phase shifts in the low-frequency oscillators removes the stationarity problems; that is, the resulting signal is wide-sense stationary. However, the intuitive relationship between the physical parameters and the simulator structure is lost. Also, the phase shifts of the components of the resulting multipath fading signal are still dependent. This may have adverse effects on the determination of higher order statistics through simulation. We conclude the chapter with a note regarding the possibility of reducing the complexity of Clarke's model. We found that the least number of low-frequency oscillators required is equal to the number of distinct Doppler frequency shifts, counting positive and negative shifts as one. However, we must be careful in determining the gain of each branch for each low-frequency oscillator, i.e., we must include all phase shifts corresponding to a particular Doppler frequency shift.

Another point of interest is how accurate the statistics of the fading signal produced by the sum-of-sinusoids simulator are. In Chapter 5, we showed how the results obtained in Chapter 3 can be used to derive quality measures. Depending on the accuracy required of the simulator, the appropriate number of low-frequency oscillators, or equivalently, sinusoids, to be included in the simulator can be determined. The quality measures may be derived with respect to either the envelope pdf or cdf, or the autocorrelation function. We do not use the phase pdf as the basis of quality measures. The phase pdf is equal to the desired pdf, regardless of the number of low-frequency oscillators, and thus conveys little

information about the performance of the simulator.

To derive the quality measures, we may use criteria such as the maximum error, mean square error, variance, or an approach similar to that of Young [22]. In the event that we wish to control the accuracy of the envelope pdf, cdf, and the signal autocorrelation, we proceed as indicated for each function. Then, for the practical implementation, we select the largest number of sinusoids obtained through each of the quality measures. We conclude by noting that the interval over which the autocorrelation function closely approximates the desired autocorrelation function is directly related to the number of Doppler frequency shifts. Prior to this, we noted that the wide-sense stationarity character of the fading signal was dependent upon inclusion of all phase shifts, i.e., combining the phase shifts as an appropriate gain for waves experiencing the same Doppler shift. Failure to do so, as in Jakes' case, leads to non-stationarity problems.

During the writing of this thesis, the various methods employed and the results derived have suggested other areas which might be of interest to future researchers. For example, approaches similar to those used in this thesis may be used to derive other results of interest to the wireless engineer. In particular, the random walk in the plane may be used to derive analytical results to problems such as determination of level-crossing rates, fade duration distribution, or the variance of the average fade duration. Another area of interest is design of fading channel simulators with arbitrary arrival angles pdf. Still another area of possible interest is design of three-dimensional fading channel simulators based on sum-of-sinusoids. Such scenarios have been shown to provide better fading channel models in the case of heavily urbanized areas [6]. Future work in this area would potentially culminate with the development of a three-dimensional fading channel simulator.

References

[1] J. F. Ossanna, Jr., "A Model for Mobile Radio Fading Due to Building Reflections: Theoretical and Experimental Fading Waveform Power Spectra", *Bell Syst. Tech. J.*, pp. 2935-2971, Nov. 1964.

[2] E. N. Gilbert, "Energy Reception for Mobile Radio", *Bell Syst. Tech. J.*, pp. 1779-1803, Oct. 1965.

[3] R. H. Clarke, "A Statistical Theory of Mobile-Radio Reception", *Bell Syst. Tech. J.*, pp. 957-1000, Jul.–Aug. 1968.

[4] M. J. Gans, "A Power-spectral Theory of Propagation in the Mobile Radio Environment", *IEEE Trans. Veh. Tech.*, vol. VT-21, February 1972, pp. 27-38.

[5] P. Dent, G. E. Bottomley, and T. Croft, "Jakes' Fading Model Revisited", *Electron. Lett.*, vol. 29, no. 3, pp. 1162-1163, Jun. 1993.

[6] T. Aulin, "A Modified Model for the Fading Signal at a Mobile Radio Channel", *IEEE Trans. Veh. Tech.*, vol. VT-28, no. 3, pp. 182-203, Aug. 1979.

[7] M. Pätzold, U. Killat, and F. Laue, "A Deterministic Digital Simulation Model for Suzuki Processes with Application to a Shadowed Rayleigh Land Mobile Radio Channel", *IEEE Trans. Veh. Tech.*, vol. 45, no. 2, pp. 318-331, May 1996.

[8] M. Pätzold, U. Killat, F. Laue, and Y. Li, "On the Statistical Properties of Deterministic Simulation Models for Mobile Fading Channels", *IEEE Trans. Veh. Tech.*, vol. 47, no.1, pp. 254-269, Feb. 1998.

[9] M. Pätzold and F. Laue, "Statistical properties of Jakes' fading channel simulator", *VTC '98 Conference Record*, vol. II, pp. 712-718, Ottawa, Ontario, Canada, May 1998.

[10] T. Eyceoz, A. Duel-Hallen, and H. Hallen, "Deterministic Channel Modeling and Long Range Prediction of Fast Fading Mobile Radio Channels", *IEEE Commun. Lett.*, vol. 2, no. 9, pp. 254-256, Sep. 1998.

[11] P. A. Bello, "Characterization of Randomly Time-Variant Linear Channels", *IEEE Trans. Commun. Syst.*, vol. CS-11, pp. 360-393, Dec. 1963.

[12] P. Hoeher, "A Statistical Discrete-Time Model for the WSSUS Multipath Channel", *IEEE Trans. Veh. Tech.*, vol. 41, no. 4, pp. 461-468, Nov. 1992.

[13] G. A. Arredondo and J. I. Smith, "Voice and Data Transmission in a Mobile Radio Channel at 850 MHz", *IEEE Trans. Veh. Tech.*, vol. VT-26, no. 1, pp. 88-93, Feb. 1977

[14] S. O. Rice, "Mathematical Analysis of Random Noise", *Bell Syst. Tech. J.*, vol. 23, pp. 282-332, Jul. 1944.

[15] S. O. Rice, "Mathematical Analysis of Random Noise", *Bell Syst. Tech. J.*, vol. 24, pp. 46-156, Jan. 1945.

[16] S. O. Rice, "Distribution of the Extreme Values of the Sum of n Sine Waves Phased at Random", *Quart. Appl. Math.*, vol. XII, no. 4, pp. 375-381, Jan. 1955.

[17] J. Goldman, "Statistical Properties of a Sum of Sinusoids and Gaussian Noise and its Generalization to Higher Dimensions", *Bell Syst. Tech. J.*, vol. 53, no. 4, pp. 557-580, Apr. 1974.

[18] S. O. Rice, "Probability Distributions for Noise Plus Several Sine Waves – The Problem of Computation", *IEEE Trans. Commun.*, vol. COM-22, pp. 851-853, Jun. 1974.

[19] C. W. Helstrom, "Computing the Distribution of Sums of Random Sine Waves and of Rayleigh-Distributed Random Variables by Saddle-Point Integration", *IEEE Trans. Commun.*, vol. 45, no. 11, pp. 1487-1494, Nov. 1997.

[20] M. Slack, "The Probability Distribution of Sinusoidal Oscillations Combined in Random Phase", *Proc. IEE*, vol. 93, pt. C, no. 22, pp. 76-86, Mar. 1946.

[21] W. R. Bennett, "Distribution of the Sum of Randomly Phased Components", *Quart. Appl. Math.*", vol. 5, pp. 385-393, Jan. 1948.

[22] D. J. Young, "The Generation of Correlated Rayleigh Random Variates By Discrete Fourier Transform and Quality Measures for Random Variate Generation", M. Sc. Thesis, Queen's University, Kingston, Canada, 1997.

[23] W. C. Jakes, *Microwave Mobile Communications*, IEEE edition, IEEE Press, New York, 1994.

[24] G. L. Stüber, *Principles of Mobile Communication*, Kluwer Academic Publishers, Boston, 1996.

[25] T. S. Rappaport, *Wireless Communications: Principles and Practice*, Prentice Hall PTR, Upper Saddle River, New Jersey, 1996.

[26] G. N. Watson, *A Treatise on the Theory of Bessel Functions*, Cambridge Mathematical Library edition, Cambridge University Press, New York, 1995.

[27] S. Bochner, *Lectures on Fourier Integrals*, Annals of Mathematics Studies, Study 42, Princeton University Press, Princeton, New Jersey, 1959.

[28] R. E. Ziemer and W. H. Tranter, *Principles of Communications: Systems, Modulation, and Noise*, 4th ed., John Wiley & Sons, Inc., New York, 1995.

[29] A. Papoulis, *Probability, Random Variables, and Stochastic Processes*, 3rd ed., McGraw-Hill, Inc., Toronto, 1991.

[30] J. G. Proakis, *Digital Communications*, 3rd ed., McGraw-Hill, Inc., New York, 1995.

[31] W. A. Gardner, *Introduction to Random Processes: With Applications to Signals and Systems*, Macmillan Publishing Company, New York, 1985.

[32] J. L. Doob *Stochastic Processes*, 3rd printing, John Wiley & Sons, Inc., New York, 1960.

[33] R. M. Gray and L. D. Davisson, *Random Processes: A Mathematical Approach for Engineers*, Prentice-Hall, Inc., Englewood Cliffs, New Jersey, 1986.

[34] J. Stewart, *Calculus: Early Transcedentals*, 2nd ed., Brooks/Cole Publishing Company, Pacific Grove, CA, 1991.

[35] R. Bracewell, *The Fourier Transform and Its Application*, McGraw-Hill Book Company, New York, 1965.

[36] I. S. Gradshteyn and I. M. Ryzhik; Allan Jeffrey, editor, *Table of integrals, series, and products*, 5th edition, Academic Press, Inc., New York, 1994.

[37] M. Abramowitz and I. A. Stegun, *Handbook of Mathematical Functions with Formulas, Graphs, and Mathematical Tables*, 10th printing, U. S. Government Printing Office, Washington, D. C., 1972.

[38] F. Oberhettinger, *Fourier Transforms of Distributions and Their Inverses: A Collection of Tables*, Academic Press, New York, 1973.